AN ABSTRACT OF THE THESIS OF

Nicholas T. Dosch for the degree of Master of Science in Water Resources Engineering presented on September 12, 2014.

Title: Spatiotemporal Dynamics and Drivers of Stream pCO_2 in a Headwater Catchment in the Western Cascade Mountains, Oregon

Abstract approved:

_____

Roy D. Haggerty

We examined the spatial and temporal variability of stream carbon dioxide (CO_2) and the drivers of these variations in a headwater catchment. To examine temporal variation and drivers, we measured stream and hyporheic pCO_2 at high temporal resolution over 11 months in a 95.9-ha forested headwater catchment in the Western Cascades of Central Oregon, USA. Stream and hyporheic pCO_2 showed high seasonal and event-scale variability with distinct stream and hyporheic dynamics during storm discharge events. Hyporheic exchange flow exported 37.5 kg-C yr^{-1} per watershed hectare (confidence interval 4.0–122.3 kg-C ha^{-1} yr^{-1}) from the riparian zone to the stream. Summing CO_2 evasion and downstream advection suggests that one third of inorganic carbon export originated in the hyporheic zone. Hyporheic exchange flow had greatest influence over stream pCO_2 during low and high baseflow, while CO_2 evasion had greatest influence during storm discharge events. These findings suggest that the hyporheic zone actively participates in carbon cycling in this headwater stream and continuously replenishes stream CO_2.

To examine spatial variation and drivers, we measured stream CO_2 at monthly intervals from July 2013 through July 2014 at 38 locations across the 6400-ha HJ Andrews Experimental Forest. Stream pCO_2 was consistently supersaturated with respect to atmospheric concentrations. Stream pCO_2 ranged from atmospheric (~400 µatm) to 20 times atmospheric concentrations (8150 µatm) and exhibited strong spatial and temporal variability. The distribution of pCO_2 over the study period was different in small and large streams within the drainage network. At the watershed scale, pCO_2 decreased with distance downstream. At the reach scale, we did not detect clear patterns in the downstream direction. However, individual transects displayed persistent profile shape, with consistent high and low pCO_2 locations. We found negative relationships between stream pCO_2 and stream discharge, mean velocity and the carbon dioxide gas transfer velocity. Stream pCO_2 exhibited changes over short distances, with large changes in pCO_2 over less than 50 m. Longitudinal variability indicates spatial variability of in-stream controls on pCO_2 at this scale. Stream pCO_2 shows generally higher concentrations during the summer and lower concentrations in the winter, with considerable intrannual variability.

Spatiotemporal Dynamics and Drivers of Stream pCO_2 in a Headwater Mountain Catchment in the Cascade Mountains, Oregon

by
Nicholas T. Dosch

A THESIS

submitted to

Oregon State University

in partial fulfillment of
the requirements for the
degree of

Master of Science

Presented September 12, 2014
Commencement June 2015

Master of Science thesis of Nicholas T. Dosch presented on September 12, 2014.

APPROVED:

Major Professor, representing Water Resources Engineering

Director of the Water Resources Graduate Program

Dean of the Graduate School

I understand that my thesis will become part of the permanent collection of Oregon State University libraries. My signature below authorizes release of my thesis to any reader upon request.

Nicholas T. Dosch, Author

ACKNOWLEDGEMENTS

I would like to thank my major advisor Dr. Roy Haggerty for his continual support, enthusiasm, and boundless insight. Thank you for asking the hard questions and pushing me to do the same. I have been very lucky to have had the opportunity to work with and have been advised by you. I would also like to thank my committee members Dr. Steve Wondzell and Dr. Alba Argerich. Your knowledgeable advice has greatly contributed to this research. I am grateful for the help of Kathty Motter and Cam Jones at the IWW Collaboratory, whose continual assistance helped me accomplish some of the largest tasks of this work. I would like to thank all of the folks involved at H.J. Andrews Experimental Forest, with a special thanks to Mark Schulze, Kathy Keable, and John Moreau. Their help with coordinating and conducting field work (and the occasional recue towing) was greatly helpful and deeply appreciated. I would like to thank Dr. John Bailey for his willingness to serve as my graduate representative on such short notice. I would also like to thank John Hammond and Will L'Hommedieu for lending a hand with fieldwork, seemingly always in the worst possible conditions. I am forever grateful to my family for their constant support and encouragement through this endeavor. Finally, I want to thank Hayley Corson-Rikert, for her help with field work, lab work, data interpretation, and for always being source for support and stability. Thank you all.

CONTRIBUTION OF AUTHORS

Manuscript 1: Dr. Roy Haggerty assisted in the development of this project, contributed stream CO_2 evasion data, and provided feedback and insight throughout. Dr. Steve M. Wondzell assisted in the development of the hyporheic DIC export model and provided hyporheic residence time distribution data. Hayley A. Corson-Rikert provided DIC data from the WS01 well network which was used for model calibration.

Manuscript 2: Dr. Roy Haggerty helped in the development of this project and provided guidance and feedback throughout.

TABLE OF CONTENTS

TABLE OF CONTENTS (CONTINUED)

LIST OF FIGURES

Figure Page

LIST OF TABLES

Table Page

LIST OF APPENDIX FIGURES

Figure Page

LIST OF APPENDIX FIGURES (CONTINUED)

Figure Page

LIST OF APPENDIX TABLES

Table Page

1 Introduction

Recent work has established that streams and rivers play a disproportionately large role in the global carbon cycle relative to their size on the on the landscape [e.g., *Richey et al*., 2002; *Raymond et al.*, 2008; *Tranvik et al.*, 2009]. Despite making up only ~1% of terrestrial surface area, carbon fluxes per unit area in streams and rivers often surpass that of the landscape that makes up their watershed [*Cole et al.,* 2007; *Aufdenkampe et al*., 2011]. Headwater streams in particular may play an important role because they are a major component of terrestrial drainage networks. First and second order streams make up ~75% total river length and ~30% of total stream and river surface area worldwide [*Leopold et al.,* 1964; *Downing et al.,* 2012].

Inputs of terrestrial organic matter to headwater streams from adjacent ecosystems fuel high rates of microbial respiration that exceed in-stream production, causing most headwater systems to be heterotrophic [*Vannote et al.,* 1980; *Dawson et al.,* 2001]. This high metabolic rate is driven by the delivery of organic matter, nutrients, and oxygen to subsurface microbial communities via hyporheic exchange, which occurs at proportionally higher rates in headwater streams than in larger streams and rivers [*Battin et al.,* 2008; *Wondzell,* 2011]. Because headwater streams are typically heterotrophic, they are often supersaturated with carbon dioxide (CO_2) with respect to atmospheric concentrations [e.g., *Cole and Caraco,* 2001; *Richey et al*., 2002; *Humborg et a*l., 2010; *Butman and Raymond*, 2011].

Annually, ~0.9 Pg of carbon are advected downstream by rivers and delivered to the ocean [*Cole et al.,* 2007; *Battin et al.,* 2009; *Stets and Striegl*, 2012]. However, a

large fraction of stream dissolved carbon does not reside in streams long enough to be transported to the ocean. Excess CO_2 has a short residence time and is quickly evaded from the stream surface [*Fiedler et al.*, 2006; *Davidson et al.*, 2010]. A recent global estimate reported as much as ~2.1 Pg C evades from stream surfaces annually [*Raymond et al.*, 2013]. The abundance of geomorphic features that influence this gaseous flux of CO_2 can vary between geographic regions and within watersheds [*Butman and Raymond*, 2011; *Raymond et al.*, 2012]. Rates of evasion scale with stream turbulence, the ratio of surface to cross-sectional area, and the CO_2 concentration gradient across the stream surface – all of which tend to be greatest in low-order streams [*Wallin et al.*, 2010; *Raymond et al.*, 2012]. Nonetheless, research on small streams has shown that many are able to sustain elevated partial pressures of carbon dioxide (pCO_2) on both daily and seasonal time scales despite continual CO_2 loss from evasion fluxes [*Jones and Mulholland*, 1998; *Öquist et al.*, 2009; *Wallin et al.*, 2013]. Sustained stream CO_2 evasion requires continual CO_2 input. The hydrologic and ecosystem patterns and sources of that CO_2 input are not yet known [*Dinsmore et al.*, 2013*; Crawford et al.*, 2014].

The supply of CO_2 to headwater streams has been attributed primarily to inputs of CO_2-rich ground- and soil-water. However, interactions between headwater streams and adjacent riparian zones through hyporheic exchange may also represent an important mechanism for CO_2 delivery to headwater streams [*Peter et al.*, 2014]. Headwater streams support high rates of hyporheic exchange, a process where water leaves and renters the stream after following short (minutes to hours) or long (days) subsurface flowpaths [*Valett et al.*, 1993; *Bencala*, 2011; *Boano et al.*, 2014]. Stream water may enter the hyporheic repeatedly along a reach of headwater stream [*Wondzell*, 2011]. This

exchange delivers organic material, nutrients and oxygen to active subsurface microbial communities, generating a hotspot of microbial respiration [e.g., *Grim and Fisher*, 1984; *Findlay et al.*, 1993; *Sobczak and Findlay*, 2002]. The continual cycling of stream water through these zones may replenish stream CO_2 concentrations.

Research on CO_2 dynamics in stream ecosystems has demonstrated that the spatial distribution of CO_2 in streams is not uniform. In order to characterize spatial variability in stream pCO_2, studies have collected measurements at various scales. Many studies have sampled within regions, along transects or at points in a stream [e.g., *Jones and Mulholland*, 1998b; *Hope et al.*, 2001; *Striegl et al.*, 2012]. Studies focusing on regional or larger spatial scales have observed general decreasing trends in stream pCO_2 with distance downstream [e.g., *Humborg et al.*, 2010; *Butman and Raymond*, 2011]. However, studies of stream pCO_2 at smaller scales with higher spatial resolution report strong spatial stream pCO_2 variability, with no consistent downstream trend [e.g., *Dawson et al.*, 2001; *Crawford et al.*, 2014]. The spatial resolution of stream pCO_2 measurements appears to be important, with fine-scale measurements revealing patterns in stream CO_2 not discernable from coarse sampling [*Crawford et al.*, 2013]. The degree of spatial variability across a watershed and the factors that influence this variability remain uncertain.

In response to these issues, we sought to address the flowing research questions:

1. How does stream pCO_2 vary across a headwater drainage network and what factors influence variability?
2. What are the scales and magnitudes of temporal and spatial variability of stream pCO_2?

3. Does hyporheic exchange influence stream pCO_2 and overall inorganic carbon export in a headwater ecosystem?

In our first paper, *Hyporheic export of inorganic carbon responsible for elevated stream pCO_2 in a temperate forested catchment*, we investigated stream and hyporheic pCO_2 dynamics, and modeled the contribution of dissolved inorganic carbon to a headwater stream from the hyporheic zone. In the second paper, *Drainage network variations in stream pCO_2 within the Lookout Creek watershed*, we examined the magnitude and spatial scale of stream pCO_2 variability across a headwater drainage network in order to identify features and processes that drive changes in stream CO_2 concentrations.

2 Hyporheic export of inorganic carbon responsible for elevated stream pCO_2 in a temperate forested catchment

Nicholas T. Dosch, Roy Haggerty, Hayley A. Corson-Rikert, Steve M. Wondzell

For Submission to *Geophysical Research Letters*

2.1 Abstract

We measured stream and hyporheic pCO_2 at high temporal resolution over 11 months in a 95.9-ha forested headwater catchment in the Western Cascades of Central Oregon, USA. Stream and hyporheic pCO_2 showed high seasonal and event-scale variability with distinct stream and hyporheic dynamics during storm discharge events. Hyporheic exchange flow exported 37.5 kg-C yr^{-1} per watershed hectare (confidence interval 4.0–122.3 kg-C ha^{-1} yr^{-1}) from the riparian zone to the stream. Summing CO_2 evasion and downstream advection suggests that one third of inorganic carbon export originated in the hyporheic zone. Hyporheic exchange flow had greatest influence over stream pCO_2 during low and high baseflow, while CO_2 evasion had greatest influence during storm discharge events. These findings suggest that the hyporheic zone actively participates in carbon cycling in this headwater stream and continuously replenishes stream CO_2.

2.2 Introduction

Headwater streams may play an important role in global carbon cycling because they are a major component of terrestrial drainage networks, removing both water and carbon. First- and second-order streams make up ~75% total river length and ~30% of total stream and river surface area worldwide [*Leopold et al.,* 1964; *Downing et al.,*

2012]. Inputs of terrestrial organic matter to headwater streams from adjacent ecosystems fuel high rates of microbial respiration that exceed in-stream production, causing most headwater systems to be heterotrophic [*Vannote et al.,* 1980; *Dawson et al.,* 2001]. High metabolic rates in subsurface microbial communities are maintained by the delivery of organic matter, nutrients, and oxygen via hyporheic exchange, which occurs at proportionally higher rates in headwater streams than in larger streams and rivers [*Battin et al.,* 2008; *Wondzell,* 2011].

Headwater streams are typically heterotrophic and are often supersaturated with carbon dioxide (CO_2), with respect to atmospheric concentrations [e.g., *Cole and Caraco*, 2001; *Richey et al*., 2002; *Humborg et a*l., 2010; *Butman and Raymond*, 2011]. This excess CO_2 has a short residence time in streams and is quickly evaded from the stream surface [*Fiedler et al.,* 2006; *Davidson et al.,* 2010]. Rates of evasion scale with stream turbulence, the ratio of surface to cross-sectional area, and the CO_2 concentration gradient across the stream surface – all of which tend to be greatest in low order streams [*Wallin et al.,* 2010; *Raymond et al.*, 2012]. Nonetheless, research on small streams has shown that many are able to sustain elevated partial pressures of carbon dioxide (pCO_2) on both daily and seasonal time scales despite continuous CO_2 loss from evasion fluxes [*Jones and Mulholland,* 1998; *Öquist et al.,* 2009; *Wallin et al.,* 2013]. Sustained stream CO_2 evasion requires continual CO_2 input. The hydrologic and biologic patterns and sources of that CO_2 input are not yet known [*Dinsmore et al.,* 2013*; Crawford et al.,* 2014].

The supply of CO_2 to headwater streams has been attributed primarily to inputs of CO_2-rich ground- and soil-water. However, interactions between headwater streams and adjacent riparian zones through hyporheic exchange may also represent an important

mechanism for CO_2 delivery to headwater streams [*Peter et al.,* 2014]. Headwater streams support high rates of hyporheic exchange, a process where water leaves and renters the stream following along short (minutes to hours) or long (days) subsurface flowpaths [*Valett et al.,* 1993; *Bencala*, 2011; *Boano et al.*, 2014]. Stream water may enter the hyporheic zone repeatedly along a reach of headwater stream [*Wondzell,* 2011]. This exchange delivers organic material, nutrients and oxygen to active subsurface microbial communities, generating hotspots of microbial respiration [e.g., *Grim and Fisher,* 1984; *Findlay et al.,* 1993; *Sobczak and Findlay*, 2002]. The continual cycling of stream water through these zones may replenish stream CO_2 concentrations.

We sought to examine the dynamics of stream and hyporheic pCO_2 in a headwater stream with high temporal resolution at seasonal and event scales. We investigated the relative stream-hyporheic dynamics and timescales at which hyporheic exchange flow influences the stream water pCO_2. We did this by measuring and modeling hyporheic DIC and estimating the rate and magnitude of DIC contributed to a headwater stream from the hyporheic zone.

2.3 Site Description and Methods

The study was conducted in within a second-order stream reach of Watershed 1 (WS01) in the HJ Andrews Experimental Forest (HJA) (44°12’28.0’’N, 122°15’30.0’’W), in the Western Cascades of Central Oregon, USA. WS01 is a steep catchment draining 95.9 ha of temperate, second-growth conifer forest. The catchment is underlain by bedrock of exclusively volcanic origin, largely tuffs and breccias, and is free of carbonates [*Swanson and James,* 1975]. Weathering in WS01 has led to locally steep

valley walls while the valley floor is filled by colluvial deposits that rarely exceed 2 m in depth [Wondzell, 2006]. The climate consists of warm, dry summers and cool, mild winters with total annual precipitation of 2200-2600 mm, dominated by rainfall in November – March. The hydrology of surface and groundwater in WS01 has been well studied. The study reach contains a well network that has been used to observe hydraulic gradients and exchange fluxes [e.g., *Wondzel*, 2006; *Ward et al.*, 2013]. Results from these studies suggest that the WS01 hyporheic zone receives essentially all water from the stream, is dominated by down-valley gradients with no significant changes in lateral or downslope hydraulic gradients from low to high baseflow or during storms, and has a water uptake length of ~130m with all stream water cycled through the hyporheic over this distance [*Kasahara and Wondzell*, 2003; *Wondzell*, 2006; *Voltz et al.*, 2013; *Ward et al.*, 2013].

Stream and hyporheic pCO_2 were observed over 11 months from 27 August 2013 to 10 July 2014. CO_2 measurements were made using GMM220 series CO_2 probes following the method in *Johnson et al.* [2010]. Probes were sealed in gas permeable PTFE sleeves and connected to external data loggers where mole fraction pCO_2 (ppmv) was measured at 5-min intervals, averaged and recoded at 30-min intervals, and converted to partial pressure (μatm) by multiplying by atmospheric pressure. One probe was placed in the WS01 stream attached to a stryofoam float at a depth of 6 cm and another in a riparian well located 0.4 m from the stream edge at a depth of 65 cm below the water table. The median travel time to this well was determined to be 64.2 hours from a 5-day salt tracer study [*Wondzell*, unpublished data]. Stream temperature and discharge were recorded at 15-min intervals at the WS01 gauge station located 75 m downstream.

Independent measurements of hyporheic temperature, and water level were measured at monthly intervals. Synoptic measurements of stream and hyporheic DIC, pH and alkalinity were performed between June and December 2013 at monthly intervals. We used a 1 m LIDAR-based digital elevation model to create a flow accumulation raster and delineate stream length.

We delineated 13 storm discharge events from the hydrograph with flows in the 90th percentile or greater of all observed discharge measurements (> 128.3 L s^{-1}). These events were produced by precipitation, snowmelt, or a combination thereof. We defined the onset of storms as the first hour of an increasing hydrograph following baseflow. For the purpose of quantifying response times and magnitudes, two storms with clean event hydrographs and pCO_2 response were selected for this analysis. Other storms, with more complex hydrographs, displayed similar but more complex responses, and were therefore not included in this analysis.

To gauge the relative importance of hyporheic exchange flow in WS01, we modeled the difference between stream and hyporheic DIC concentrations over the study period. We chose to model DIC because it accounts for carbonate species change between the stream and hyporheic zone. This excess hyporheic DIC was modeled as a function of hyporheic travel time (τ ; hr) and stream temperature (T_s ; °K).

$$DIC_H(\tau, T_s) = DIC_{max}\left\{1 - exp\left[-\tau\lambda_0\, exp\left(\frac{E_R}{k\,T_c} - \frac{E_R}{k\,T_s}\right)\right]\right\} \qquad (1)$$

where DIC_H is the modeled 30-minute concentration of hyporheic excess DIC at a given temperature and travel time (g-C L^{-1}). DIC_{max} (g-C L^{-1}), a model parameter representing the maximum hyporheic excess DIC, and λ_o (hr^{-1}), a reaction rate constant, are fitting

parameters set to minimize model root-mean-square error (RMSE) with observed excess DIC. Stream temperature (T_C) was normalized to its mean of 281.75°K using the Boltzmann-Arrhenius relationship where E_R is the apparent activation energy for respiration in stream ecosystems, here selected to be 0.58 eV [*Yvon-Durocher et al.*, 2012].The term k is the Boltzmann constant (8.62×10^{-5} eV K^{-1}), reference and stream temperature (1) are in K. The model was calibrated using results from our 7-month dataset of hyporheic and stream DIC, water temperature, and experimentally determined travel times within the WS01 well network [*Wondzell*, unpublished data].

Export of hyporheic DIC is a function of the concentration difference between the stream and the hyporheic zone, the residence time distribution of hyporheic water, and hyporheic discharge henceforth referred to as hyporheic exchange flow (Q_{hef}). The total mass of DIC exported from the hyporheic zone in WS01 was calculated as follows:

$$Q_{hef} = 0.47\, Q_S^{\,0.87} \tag{2}$$

$$M_{DIC} = \frac{L}{100\ m} \int_0^{1\ yr} Q_{hef}(t) \int_0^{125\ h} f\,(\tau) DIC_H(\tau, t)\ d\tau\ dt \tag{3}$$

Equation 2, applied here to calculate Q_{hef} ($m^3\ s^{-1}$) in WS01, was established from a synthesis of well network and streamflow data throughout the HJA and defines Q_{hef} as a function of Q_s per 100 meters of stream [*Wondzell,* 2012]. The mass exported was calculated according to (3), where $f(\tau)$ is the hyporheic exchange flow residence time distribution function in the WS01 well network determined by *Kasahara and Wondzell* [2003]. DIC_H in (3) is modeled hyporheic excess DIC from (1). These two terms are integrated over travel times of 0 to 125 hours, with negligible amounts of flow experiencing travel times greater than 125 h, to calculate average flux-averaged

hyporheic DIC concentration. To determine WS01 hyporheic DIC export rate for each time step, the representative concentration is multiplied by Q_{hef} and is scaled to the WS01 by multiplying by the number of 100 m segments of stream in WS01, where L is the length of stream (L = 2361m). The total annual mass of DIC exported from the hyporheic zone in WS01 is calculated by integrating hyporheic export rate over 1 year (3).

We performed a Monte Carlo simulation (10,000 iterations) to constrain the total uncertainty of our estimate. We calculate the mean value of the model output and the 90 percent confidence intervals (5 and 95 percentile of Monte Carlo simulations) based on ranges of parameter uncertainty and error distribution. Confidence intervals for nonlinear terms DIC_{max} and λ_o were calculated with a first-order approximation to the parameter covariance matrix, using the sensitivity of model output to parameter estimates and model RMSE [*e.g., Bard,* 1974; *Draper and Smith*, 1981; *Haggerty et al.,* 2001]. Parameter values and 95% confidence intervals for the Monte Carlo simulations are given in Table A.1 of Appendix A.

2.4 Results

In the monitored locations Stream and hyporheic water were supersaturated with CO_2 with respect to atmospheric concentrations at all times, with hyporheic concentrations ranging from 4 to 15 times greater than stream concentrations over the study period (Figure 1). Stream and hyporheic pCO_2 displayed different seasonal patterns between summer and winter. Changeover from the summer baseflow period to winter higher flows occurred after an early October storm, delineating a shift in the hydraulic

regime. Stream hyporheic pCO_2 were greater during summer months (Aug–Sep; Jun–Jul) and lower during winter months (Oct–May) (Figure 2.1).

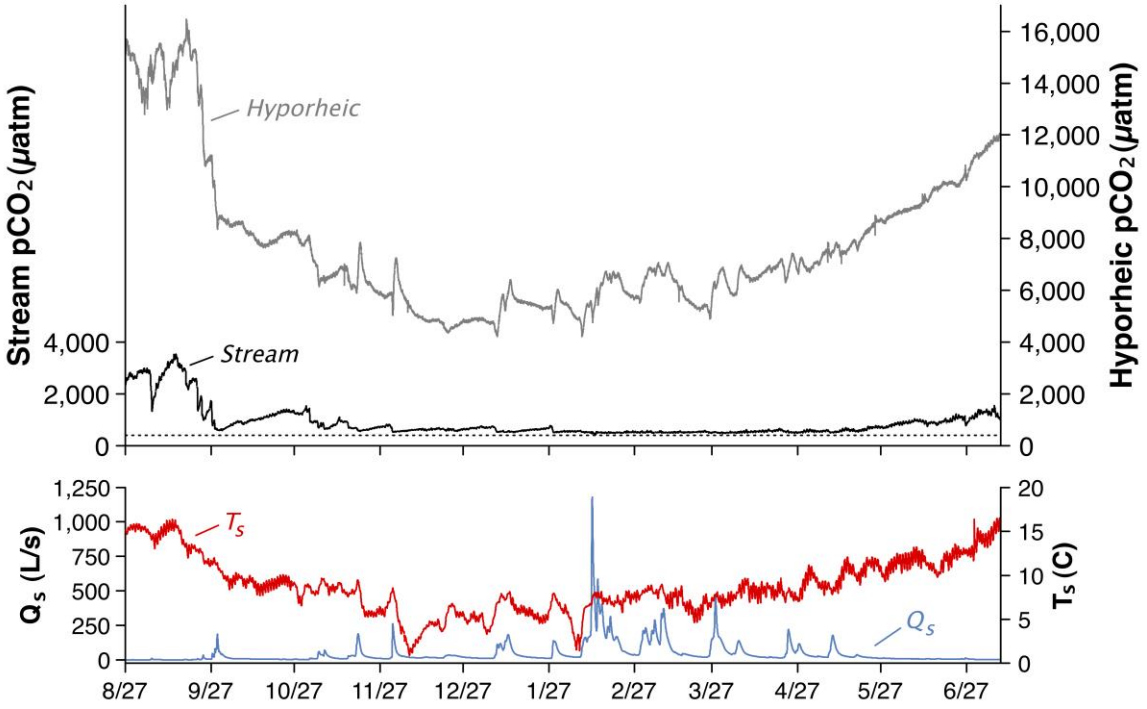

Figure 2.1 – Concentration of hyporheic and stream CO_2 (top), stream temperature and stream discharge (bottom) over the study period from late August, 2013 to July, 2014. The dotted line in the top portion shows atmospheric pCO_2.

Maximum pCO_2 occurred at the end of the summer baseflow period in late September 2013 with pCO_2 of 3,550 µatm in the stream and 16,480 µatm in the hyporheic zone. Decreases in pCO_2 in both locations occurred into the fall, with the largest drop from September to October when monthly averages of stream pCO_2 decreased 55% and hyporheic pCO_2 decreased 41%. Sustained lower pCO_2 occurred during winter months, with average stream pCO_2 of 665 µatm and average hyporheic pCO_2 of 6,444 µatm (Table 2.1). Beginning in late May, stream and hyporheic pCO_2 steadily recovered from low winter concentrations. This recovery coincided with

increasing stream temperature and decreasing discharge, and continued through the end of the study period in July, with stream pCO_2 increasing 89% and hyporheic pCO_2 increasing 40%.

Table 2.1 - Summary of measured properties and Pearson Correlation Coefficients

Property		Annual	Summer	Winter
Mean Stream pCO_2 (µatm)		889	1634	665
Mean Hyporheic pCO_2 (µatm)		7715	11896	6444
Mean Discharge (L/s)		44.8	7.0	56.3
Mean Stream Temperature (°C)		8.7	13.2	7.0
Correlation Coefficient (r) pCO_2 and Discharge	*Stream*	-0.29	-0.34	-0.36
	Hyporheic	-0.23	-0.35	-0.12
Correlation Coefficient (r) pCO_2 and Stream Temp.	*Stream*	0.73	0.73	0.26
	Hyporheic	0.89	0.72	0.80
Correlation Coefficient (r) between Stream and Hyporheic pCO_2		0.89	0.90	0.47

Hyporheic DIC export is relatively constant through the year compared with pCO_2, temperature and discharge (Figure 2.2). Although excess hyporheic DIC concentrations exhibit seasonal change, the overall export rate is moderated and largely controlled by Q_{hef}. Mean Q_{hef} was 2.4 L s^{-1}, ranging from 1.3 – 4.8 L s^{-1}, experiencing fluctuations proportionally smaller than those in Q_s. The hyporheic zone exports 37.5 kg-C yr^{-1} per watershed hectare (kg-C ha^{-1} yr^{-1}), with confidence interval (CI) of 4.0 – 122.3 kg-C ha^{-1} yr^{-1}. This represents 35% (CI = 3.6-100%) of the inorganic carbon evaded as

CO_2 or exported downstream as DIC by WS01 [based partly on data from *Argerich et al.*, manuscript in preparation, 2014].

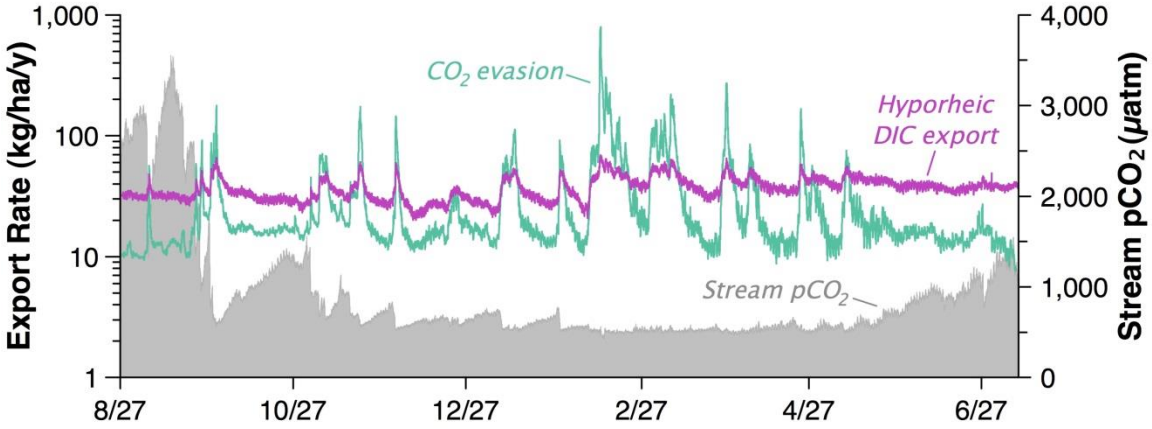

Figure 2.2 - Hyporheic CO_2 export rate, CO_2 evasion rate from Argerich et al., [manuscript in preparation, 2014] and stream pCO_2 over the study period.

Stream and hyporheic pCO_2 concentrations show a distinct response to storm discharge events (Figure 2.3). Each location responds rapidly, though distinctly, to changes in discharge. Stream pCO_2 exhibits a negative discharge-concentration relationship, with stream concentrations decreasing sharply, with no lag following storm onset, to near atmospheric concentrations (average =520 µatm) through the peak of the storm hydrograph. Recovery of stream pCO_2 changes from fall to winter to spring. In the late summer early fall, stream pCO_2 recovers quickly following discharge events, with an average recovery of 41.8 µatm day^{-1} (Figure 2.1). In the late fall and early winter, the rate of stream pCO_2 recovery decreases to 9.4 µatm day^{-1}. No identifiable recovery occurred following discharge events from February to May 2014. Hyporheic pCO_2 also responds strongly to discharge but the response is distinct from the stream. Hyporheic pCO_2 initially drops then increases sharply through the peak and falling limb of the storm

hydrograph. Hyporheic response times lag stream pCO_2 response, but only just, with the initial response lagging storm onset by an average of 2.5 hours.

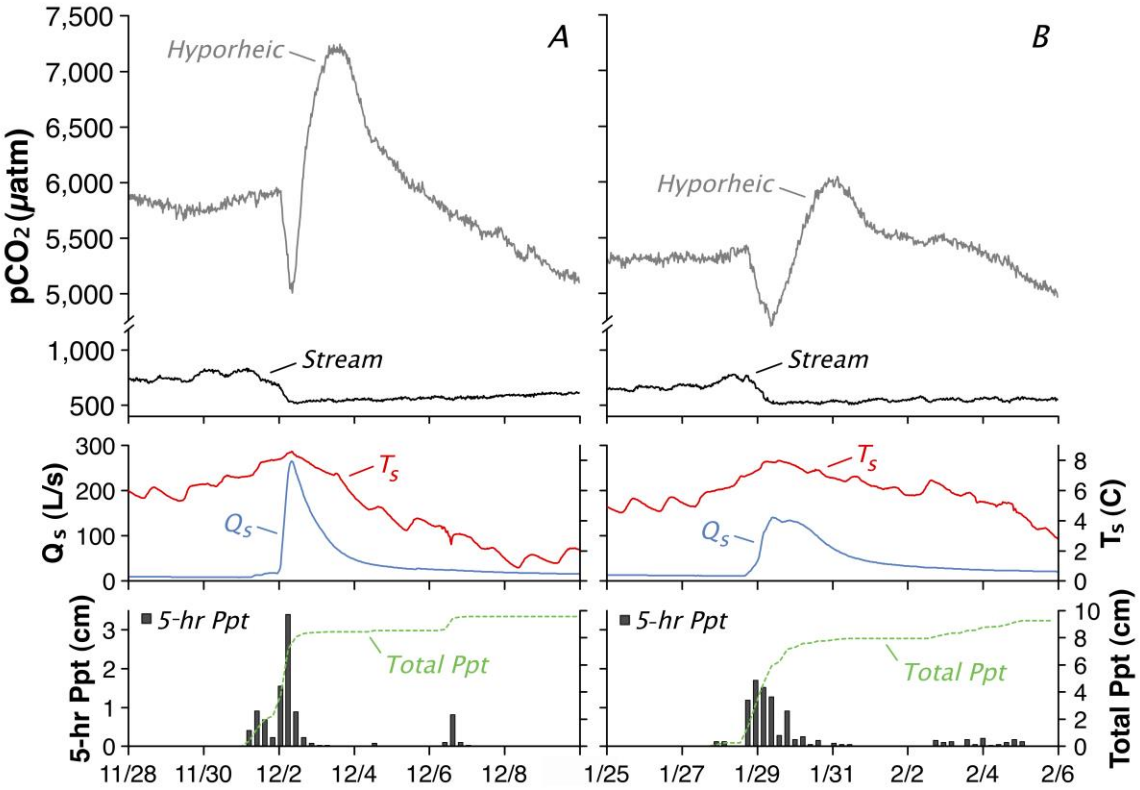

Figure 2.3 - Discharge event response: hyporheic and stream pCO_2, stream discharge, stream temperature, 5-hour precipitation (ppt) and total precipitation during (A) late November 2013 storm and (B) late January 2014 storms.

2.5 Discussion

Both stream and hyporheic pCO_2 follow seasonal patterns that reflect changes in local discharge and temperature. Changeover from summer baseflow to winter highflow has a strong influence on stream and hyporheic pCO_2. At seasonal timescales, both locations exhibit slight negative concentration-discharge correlation (Table 2.1), with lower concentrations occurring in winter when average flows were higher and storm events were frequent. Variations in stream flow affect stream-atmosphere gas transfer

rate and hydraulic flow paths through the catchment, thereby changing patterns of CO_2 delivery and export within the system [*Jones and Mulholland*, 1998]. Seasonal changes in temperature also appear to be important, with stream temperatures explaining 53 percent of the variance in stream pCO_2 and 79 percent of the variance in hyporheic pCO_2. Observed seasonal changes agree with the findings of *Peter et al.* [2014], where strong seasonal variability in stream and hyporheic pCO_2 were observed, and with those of *Dinsmore et al.* [2013], where seasonal variations were observed in an intermittent headwater stream in the Fraser Lowland of British Columbia, Canada. It is worth noting that despite concentration and seasonal differences, stream and hyporheic pCO_2 have a strong positive correlation ($r^2 = 0.78$) over the study period, which suggests interdependence between stream and hyporheic pCO_2. This relationship, however, is stronger in summer than winter, indicating a seasonal change in stream-hyporheic exchange dynamics.

Comparison of modeled hyporheic DIC export rate and CO_2 evasion rate from *Argerich et al.* [manuscript in preparation, 2014] reveals a strongly coupled relationship between processes, with an interplay that drives stream pCO_2 (Figure 2.2). Stream pCO_2 tends to increase when hyporheic export rate is greater than the rate of CO_2 evasion while stream pCO_2 tends to decrease when the hyporheic export rate is less than the rate of CO_2 evasion. It appears that hyporheic exchange and CO_2 evasion alternate periods of control and, with changes in stream hydraulics, collectively drive stream pCO_2 in this system. Hyporheic exchange flow is proportionally less influential during high flows because the ratio of Q_{HEF} to Q_S decreases [*Findlay*, 1995] and rates of CO_2 efflux from the stream surface increase. Our model suggests that hyporeic exchange flow is most important in

driving stream pCO_2 during baseflow while CO_2 efflux is most important in driving stream pCO_2 during storm events.

Monte Carlo simulation results indicate considerable uncertainty in our estimates of hyporheic DIC export and the percent of total stream DIC export originating in the hyporheic zone. In the Monte Carlo simulations, we accounted for uncertainty in the derived model parameters and the modeled relationship between Q_{hef} and Q_s (Appendix A). Although we limited our error simulation to these terms, additional error may also be introduced by other components of the model analysis. We expect that temporal variations in hyporheic travel times within the watershed are not a large source of error to the model, as riparian hydraulic gradients are stable through the year and during storm events [*Kasahara and Wondzell*, 2003; Ward *et al.*, 2013; *Voltz et al.*, 2013]. Spatial variation in hyporheic travel times may be a larger source of error. For this analysis, we assume that the residence time distribution observed in the well network at the base of the watershed is representative of riparian exchange along the full length of the Watershed 1 channel. However, the residence time distribution may vary longitudinally, due to changes in the morphology of the stream channel. We currently have no way to estimate this variation. Further work is needed to better constrain our assumptions and the values of model parameters.

Ultimately, although error bounds on our estimates are large, we are confident that the mean values generated by the Monte Carlo simulations provide a reasonable estimate of hyporheic DIC export in the Watershed 1 system. Our result of 37.5 kg-C ha^{-1} yr^{-1} agrees well with an estimate of lateral DIC export of 32 (±1) kg-C ha^{-1} yr^{-1} in a boreal headwater stream in Sweden [*Öquist et al.*, 2009].

Storm discharge events strongly influenced pCO_2 and rates of inorganic carbon export within this system. During storm discharge events, stream and hyporheic pCO_2 were dynamic and exhibited very different responses to changes in flow. We hypothesize that the sharp drop in stream pCO_2 following the onset of storm events is due to either increased evasion under turbulent flow conditions or a dilution of stream CO_2 concentrations by storm runoff [Crawford et al., 2013]. The multistage hyporheic response, however, is more difficult to interpret. It has been shown in this and other streams that the rising limb of discharge events can have highly elevated DOC concentrations that recede through the peak of the storm [*Hood et al.,* 2006; *Raymond and Saiers*, 2010; *Corson-Rikert*, unpublished data,2014]. However, it is unlikely that the spike increase in hyporheic pCO_2 following the initial drop is the result of lagged respiration from a pulse of DOC-rich streamwater to the hyporheic, as the response peak for storm A and B, of 36 and 30 hours, is faster than the 62-hour hyporheic travel time to this well.

We suggest that the pCO_2 response in the hyporeic zone during storm events is triggered by dissolved organic carbon (DOC) transported to the hyporheic zone by vertical infiltration of storm precipitation. The initial drop in hyporheic pCO_2 following the onset the storm event is likely due to dilution from vertically infiltrating water that is low in CO_2. Although it is low in CO_2, we suggest that the infiltrating water transports DOC leached from terrestrial organic material to the hyporeic zone. The subsequent respiration of this DOC may account for the production of and observed increase in hyporeic zone pCO_2 following the peak of the storm hydrograph and during the first portion of the receding limb. As stream discharge continued to fall, observed hyporeic

pCO_2 concentrations peaked and then decreased and eventually fell below pre-storm concentrations. It is possible that the CO_2 production fueled by the terrestrial DOC is short-lived, and that hyporeic pCO_2 begins to decrease as the majority of this DOC is consumed and precipitation ceases. However, during this period stream pCO_2 was also below pre-storm concentrations. We expect that laterally infiltrating stream water also contributes to the decline in hyporheic pCO_2.

2.6 Conclusions

The processes that drive the temporal dynamics of pCO_2 and support sustained supersaturation are important for scaling CO_2 fluxes at local and larger scales. Our results suggest that hyporheic exchange flow may be an important control on stream pCO_2, and on watershed inorganic carbon export. The hyporheic zone contributes 37.5 kg-C ha^{-1} yr^{-1} (confidence interval 4.0–122.3 kg-C ha^{-1} yr^{-1}) to the stream, which is equal to approximately one third of the inorganic carbon evaded or exported downstream by WS01 each year. Hyporheic exchange flow serves to actively replenish stream pCO_2 and is most influential during low and high baseflow conditions.

2.7 Acknowledgements

We conducted this research at HJ Andrews Experimental Forest, which is funded by the US Forest Service, Pacific Northwest Research Station. This work was funded by the National Science Foundation's Long-Term Ecological Research Program (DEB 08–23380), National Science Foundation grant (EAR 09-43570, U.S.), and the Hollis M. Dole fund in Environmental Geology at Oregon State University. Data will be made

publically available through the HJ Andrews data catalog

http://andrewsforest.oregonstate.edu/lter/data.cfm?frameURL=173

2.8 References

Bard, Y. (1974), *Nonlinear parameter estimation*, Academic, San Diego, Calif.

Battin, T. J., L.A. Kaplan, S. Findlay, C.S. Hopkinson, E. Marti, A. I. Packman, D.J. Newbold, and F. Sabater (2008), Biophysical controls on organic carbon fluxes in fluvial networks. *Nature Geoscience, 1*, 95–100.

Bencala, K. E. (2011), *Stream–Groundwater Interactions, in Treatise on Water Science*, edited by P. Wilderer, pp. 537-546, Academic Press, Oxford.

Boano, F., J. W. Harvey, A. Marion, A. I. Packman, R. Revelli, L. Ridolfi, and A. Wörman (2014), Hyporheic flow and transport processes: Mechanisms, models, and biogeochemical implications, *Reviews of Geophysics*, 2012RG000417, doi:10.1002/2012RG000417.

Butman, D., and P. Raymond (2011), Significant efflux of carbon dioxide from streams and rivers in the United States, *Nat. Geosci.*, *4*, 839–842, doi:10.1038/NGEO1294.

Cole, J., and N. Caraco (2001), Carbon in catchments: connecting terrestrial carbon losses with aquatic metabolism. *Marine and Freshwater Research, 52*, 101–110.

Crawford, J. T., N. R. Lottig, E. H. Stanley, J. F. Walker, P. C. Hanson, J. C. Finlay, and R. G. Striegl (2014), CO_2 and CH_4 emissions from streams in a lake-rich landscape: Patterns, controls and regional significance, *Global Biogeochem. Cycles*, 197–210, doi:10.1002/2013GB004661.

Davidson, E. A., R. O. Figueiredo, D. Markewitz, and A.K. Aufdenkampe (2010), Dissolved CO_2 in small catchment streams of eastern Amazonia: A minor pathway of terrestrial carbon loss. *Journal of Geophysical Research, 115*, G04005. doi:10.1029/2009JG001202.

Dawson, J. J., C. Bakewell, and M.F. Billett (2001), Is in-stream processing an important control on spatial changes in carbon fluxes in headwater catchments? *The Science of the Total Environment, 265*, 153–67.

Dinsmore, K. J., M.B. Wallin, M.S. Johnson, M.F. Billett, K. Bishop, J. Pumpanen, and A. Ojala (2013), Contrasting CO_2 concentration discharge dynamics in headwater streams: A multi-catchment comparison. *Journal of Geophysical Research: Biogeosciences, 118*, 445–461.

Downing, J. A., J. J. Cole, C. M. Duarte, J. J. Middelburg, J. M. Melack, Y. T. Prairie, P. Kortelainen, R. G. Striegl, W. H. McDowell, and L. J. Tranvik (2012), Global abundance and size distribution of streams and rivers, *Inland Waters*, 2, 229-236, doi: 10.5268/IW-2.4.502.

Draper, N.R., and H. Smith (1981), *Applied regression analysis*, 2nd ed, John Wiley, New York.

Fiedler, S., S. B. Höll, and H. F. Jungkunst (2006), Discovering the importance of lateral CO_2 transport from a temperate spruce forest. *The Science of the Total Environment*, *368*, 909–15. doi:10.1016/j.scitotenv.2006.03.038.

Findlay, S., D. Strayer, C. Goumbala, and K. Gould (1993), Metabolism of streamwater dissolved organic carbon in the shallow hyporheic zone. *Limnology and Oceanography*, *38*, 1493–1499.

Grimm, N., and S. Fisher (1984), Exchange between interstitial and surface water: implications for stream metabolism and nutrient cycling. *Hydrobiologia*, 111, 219-228.

Haggerty, R., S.W. Flemming, L.C. Meigs, and S.A. McKenna (2001), Tracer tests in a fractured dolomite 2. Analysis of mass transfer in single-well injection-withdrawal tests. *Water Resources Research*, 37(5), 1129-1142.

Hood, E., M.N. Gooseff, and S.L. Johnson (2006), Changes in the character of stream water dissolved organic carbon during flushing in three small watersheds, Oregon. *Journal of Geophysical Research*, *111*, G01007, doi:10.1029/2005JG000082.

Humborg, C., C. Mörth, M. Sundbom, H. Borg, T. Blenckner, R. Giesler, and V. Ittekkot (2010), CO_2 supersaturation along the aquatic conduit in Swedish watersheds as constrained by terrestrial respiration, aquatic respiration and weathering. *Global Change Biology*, *16*, 1966–1978. doi:10.1111/j.1365-2486.2009.02092.x.

Johnson, M., M. Billett, and K. Dinsmore (2010), Direct and continuous measurement of dissolved carbon dioxide in freshwater aquatic systems—method and applications, *Ecohydrology*, *3*, 68–78, doi:10.1002/eco.95.

Jones, J. B., and P.J. Mulholland (1998), Carbon dioxide variation in a hardwood forest stream: an integrative measure of whole catchment soil respiration. *Ecosystems*, 1, 183–196.

Kasahara, T., and S.M. Wondzell (2003), Geomorphic controls on hyporheic exchange flow in mountain streams. *Water Resources Research*, *39*, SBH 3–1–SBH 3–14, doi:10.1029/2002WR001386.

Leopold, L.B., M.G. Wolman, and J.P. Miller (1964), *Fluvial Processes in Geomorphology*. San Francisco: WH Freeman, 522 pages.

Öquist, M. G., M.B. Wallin, J. Seibert, K. Bishop and H. Laudon (2009), Dissolved inorganic carbon export across the soil/stream interface and its fate in a boreal headwater stream. *Environmental Science & Technology*, *43*, 7364–7369.

Peter, H., G.A Singer, C. Preiler, P. Chiffard, G. Steniczka, and T.J. Battin (2014), Scales and drivers of temporal pCO2 dynamics in an Alpine stream. *Journal of Geophysical Research: Biogeosciences*, doi:10.1002/2013JG002552.

Raymond, P. A., and J.E. Saiers (2010), Event controlled DOC export from forested watersheds. *Biogeochemistry*, *100*, 197–209. doi:10.1007/s10533-010-9416-7.

Raymond, P. A., C.J. Zappa, D. Butman, T.L. Bott, J. Potter, P. Mulholland, A.E. Laursen, W.H. McDowell, and D. Newbold (2012), Scaling the gas transfer velocity and hydraulic geometry in streams and small rivers. *Limnology & Oceanography: Fluids & Environments*, *2*, 41–53. doi:10.1215/21573689-1597669.

Richey, J. E., J.M. Melack, A.K. Aufdenkampe, V.M. Ballester, and L.L. Hess (2002), Outgassing from Amazonian rivers and wetlands as a large tropical source of atmospheric CO2. *Nature*, *416*, 617–20, doi:10.1038/416617a.

Sobczak, W. V., and S. Findlay (2002), Variation in bioavailability of dissolved organic carbon among stream hyporheic flowpaths, *Ecology*, 83, 3194–3209.

Swanson, F. J and M.E. James (1975), Geology and geomorphology of the H.J. Andrews Experimental Forest, western Cascades, Oregon. Res. Pap. PNW-188. Portland, OR: U.S. Department of Agriculture, Forest Service, Pacific Northwest Forest and Range Experiment Station.

Valett, H. M., C. C. Hakenkamp, and A. J. Boulton (1993), Perspectives on the hyporheic zone: Integrating hydrology and biology. *Introduction, The North American Benthological Society*, 12(1), 40-43.

Vannote, R., G.W. Minshall, K.W. Cummins, J.R. Sedell, and C.E. Cushing (1980), The river continuum concept. *Canadian Journal of Fisheries and Aquatic Sciences*, *37*, 130–137.

Voltz, T., M. Gooseff, A.S. Ward, K. Singha, M. Fitzgerald, and T. Wagener (2013). Riparian hydraulic gradient and stream-groundwater exchange dynamics in steep headwater valleys. *Journal of Geophysical Research: Earth Surface*, *118*, 953–969, doi:10.1002/jgrf.20074

Wallin, M. B., I. Buffam, M. Öquist, H. Laudon, and K. Bishop (2010). Temporal and spatial variability of dissolved inorganic carbon in a boreal stream network: Concentrations and downstream fluxes. *Journal of Geophysical Research*, *115*, G02014. doi:10.1029/2009JG001100.

Wallin, M. B., T. Grabs, I. Buffam, H. Laudon, Å. Agren, M. G. Öquist, and K. Bishop (2013), Evasion of CO2 from streams - the dominant component of the carbon export through the aquatic conduit in a boreal landscape. *Global Change Biology*, *19*(3), 785–797, doi:10.1111/gcb.12083.

Ward, A. S., M. N. Gooseff, T. J. Voltz, M. Fitzgerald, K. Singha, and J. P. Zarnetske (2013), How does rapidly changing discharge during storm events affect transient storage and channel water balance in a headwater mountain stream? *Water Resources Research*, *49*, 5473–5486, doi:10.1002/wrcr.20434.

Wondzell, S. M. (2006), Effect of morphology and discharge on hyporheic exchange flows in two small streams in the Cascade Mountains of Oregon, USA. *Hydrological Processes, 20*, 267–287, doi:10.1002/hyp.5902.

Wondzell, S. M. (2011), The role of the hyporheic zone across stream networks. *Hydrological Processes, 25*, 3525–3532, doi:10.1002/hyp.8119.

Wondzell, S. M. (2012), Hyporheic zones in mountain streams: physical processes and ecosystem functions. *Stream Notes*, January-April 2012, Stream System Technology Center, Rocky Mountain Research Station, Ft. Collins, CO.

Yvon-Durocher, G. et al. (2012), Reconciling the temperature dependence of respiration across timescales and ecosystem types, *Nature*, *487*, 472–6, doi:10.1038/nature11205.

3 Drainage network variations in stream pCO_2 within the Lookout Creek watershed

3.1 Abstract

We measured stream carbon dioxide (CO_2) at monthly intervals from July 2013 through July 2014 across a forested headwater drainage network in the Western Cascades of Oregon. At a large majority of observations, stream CO_2 partial pressure (pCO_2) was supersaturated with respect to atmospheric concentrations. Stream pCO_2 ranged from atmospheric (~400 µatm) to 20 times atmospheric concentrations (8150 µatm) and exhibited strong spatial and temporal variability. At the watershed scale, pCO_2 decreased with distance downstream. At the reach scale, we did not detect clear patterns in the downstream direction. However, individual transects displayed persistent profile shape, with consistent high and low pCO_2 locations. We found negative relationships between stream pCO_2 and stream discharge, mean velocity and the carbon dioxide gas transfer velocity (k_{CO2}). Stream pCO_2 exhibited changes over short distances, with large changes in pCO_2 over 50 m. Longitudinal variability indicates spatial nonuniformity of in-stream controls on pCO_2 at this scale. Stream pCO_2 shows generally higher concentrations during the summer and lower concentrations in the winter, with considerable intrannual variability. The distribution of pCO_2 over the study period was significantly different in small and large streams within the drainage network.

3.2 Introduction

Recent work has established that streams and rivers play a disproportionately large role in the global carbon cycle relative to their size on the on the landscape [e.g., *Cole et al., 1994; Richey et al*., 2002; *Raymond et al.,* 2008; *Tranvik et al.,* 2009].

Despite making up only ~1% of terrestrial surface area, carbon fluxes per unit area in streams and rivers often surpass that of the landscape that makes up their watershed [*Cole et al.,* 2007]. Streams receive, transport, process, and emit large quantities of terrestrially derived carbon [*Aufdenkampe et al*., 2011; *Bianchi et al.,* 2013]. Annually, ~0.9 Pg of carbon are exported by rivers downstream and delivered to the ocean [*Cole et al.,* 2007; *Battin et al.,* 2009; *Stets and Striegl*, 2012]. However, a large fraction of the carbon that enters streams and rivers does not reside in streams long enough to be transported to the ocean and is emitted in the form of carbon dioxide (CO_2) from the stream surface. A recent global estimate reported as much as ~2.1 Pg C evades from stream surfaces annually [*Raymond et al.,* 2013].

Streams are typically supersaturated with CO_2, with partial pressures of carbon dioxide (pCO_2) that can far surpass atmospheric concentrations [e.g., *Jones et al.,* 2003; *Butman and Raymond*, 2011]. The pCO_2 concentration gradient across the stream-atmosphere interface can lead to CO_2 outgassing. Factors that influence the gaseous flux of CO_2 can vary between geographic regions and within watersheds [*Raymond et al.,* 2012]. Small headwater streams have been shown to have particularly high concentrations of pCO_2, and lose CO_2 to the atmosphere at higher rates than larger systems – a result that makes headwater streams quantitatively important in the global carbon cycle [*Jones and Mulholland*, 1989a; *Johnson et al.,* 2008; *Butman and Raymond*, 2011].

Studies have characterized spatial variability in stream pCO_2 at various scales. Many studies have sampled within regions, along transects or at points in a stream [e.g., *Jones and Mulholland*, 1998b; *Hope et al.,* 2001; *Striegl et al.,* 2012]. Studies at regional

or larger spatial scales tend to observe general decreasing trends in stream pCO_2 with distance downstream [e.g., *Humborg et al.*, 2010; *Butman and Raymond*, 2011]. However, studies of stream pCO_2 at smaller scales with higher spatial resolution, report strong spatial stream pCO_2 variability, with no consistent downstream trend [e.g., *Dawson et al.*, 2001; *Crawford et al.*, 2014]. The spatial resolution of stream pCO_2 measurements appears to be important, with fine scale measurements revealing patterns in stream CO_2 not discernable from coarse sampling [*Crawford et al.*, 2013]. The degree of of spatial variability across a watershed and the factors that influence this variability remain uncertain.

In this study, we assessed the magnitude and spatial scale of stream pCO_2 variability in a headwater catchment in order to identify features and processes that drive changes in stream CO_2 concentrations. To do so, we calculated pCO_2 at 38 sites at monthly intervals over one year. We selected the sites to capture a range of spatial resolutions and to represent the physical variability of the catchment.

3.3 Site Description

This study was conducted within HJ Andrews Experimental Forest (HJA) (44°14'N, 122°11'W), in the Western Cascades of Central Oregon, USA. The boundary of HJA is delineated by the Lookout Creek watershed, a 64 km^2 drainage basin ranging in elevation from 410 m to 1630 m. Lookout Creek drains a network of forested headwater streams and is a tributary of Blue River and the McKenzie River. The HJA is underlain by bedrock of volcanic origin, Oligocene to Lower Miocene in age, and is free of carbonates. Low elevation areas are largely composed of tuffs, breccias and stream

deposited alluvium while higher areas are composed basalt and andesite flows of Miocene age and of younger, High Cascade rock [*Swanson and James,* 1975]. Weathering and glaciation within the Lookout Creek drainage basin has led to locally steep topography and well-defined subbasins within the Lookout Creek drainage network [*Swanson and James,* 1975]. Soils across HJA are mainly sandy or gravelly loam inceptisols, developed from parent bedrock. The climate of the Western Cascades consists of warm, dry summers and cool, wet winters. Snow and rainfall typically begin in November and continue through June, with a transient snowline mid-elevation of HJA. Mean annual precipitation is 2200-2600 mm.

Forests of the HJA are dominated by Douglas-fir (*Pseudotsuga menziesiiare*), western hemlock (*Tsuga heterophylla*), and red cedar (*Thuja plicata*) with pacific yew (*Taxus brevifolia*) common in the understory [*Rothacher et al.,* 1967]. When the HJA was established, much of the area was covered by old-growth (> 400 years), and mature (100-150 years) forest. Beginning in the early 1950s portions of HJA forest were manipulated (clear cutting, burning, replanting treatments, and thinning) to establish a series of experimental watersheds within the HJA. These experimental watersheds have been subject to long-term studies of basin hydrology, ecology and biogeochemistry, an initiative to better understand and quantify the influence of forest management history on ecosystem and hydrologic processes [*Dyrness,* 1969].

38 sample sites at were established across the Lookout Creek drainage network were at a variety of sites that captured the diverse natural and managed landscape of the HJA. Sample sites were chosen to ensure they included streams from a range of basin sizes, elevations, discharge regimes, subclimates and forest management histories.

Multiple sample sites were placed along Lookout Creek and its major tributaries and were sampled as longitudinal transects from the highest upstream point to the lowest downstream point accessible by truck. Samples were collected at all gauge stations and from all experimental watersheds. Major confluences were included in sampling design, with sample sites placed above and below these locations.

These 38 sampling locations were located along 13 streams, including Lookout Creek (LO) and twelve of its major tributaries within HJA. Information regarding stream and associated watershed properties is detailed in Table 3.1. The major tributaries include: Watershed 1 (W1), Watershed 2 (W2), Watershed 3 (W3), Watershed 6 (W6), Watershed 7 (W7), Watershed 8 (W8), Watershed 9 (W9), Watershed 10 (W10), MacRae Creek (MR), Mack Creek (MK), Cold Creek (CC) and an unnamed stream referred to here as No Name Creek (NN). Each sample site was assigned a four or five character title for identification. Each title is composed of two stream identification characters (with the exception of Watershed 10, which was assigned 3 characters), in parentheses above, followed by two transect order identification numbers. Sites that were the highest elevation sites on a given transect, i.e., the closest point to the stream origin, were given the transect order identification numbers of "01". The next downstream sampled site, i.e., the site second closest to the stream origin, was given the numbers "02", and so on to the lowest sample site along a given stream transect. For example, the highest elevation sample site in Watershed 1 was titled W101 and the third downstream site along the Lookout Creek transect was titled LO03. Several streams were only accessible in one location and were not sampled as transects. These sites were simply assigned the number "01". For example, Watershed 6 is not part of a sampling transect, thus, the only site was

titled W601. A list of sample collection sites and site specific physical properties are outlined in (Table 3.2). The location of HJA and the sample sites within the LO drainage network are illustrated in (Figure 3.1).

The longitudinal distance between sample sites was also considered in sample design. To address this variable, a dense sampling array was set up along the W1 transect, with samples collected every 50m downstream along the entirety of the second order portion of W1 to its confluence with LO. In contrast, average longitudinal spacing between sampling sites along the LO transect was 2.9 km. The density of longitudinal sampling is of primary interest in this study, as the scales at which pCO_2 variability occurs within streams remains poorly quantified [*Hope et al.,* 2004; *Wallin et al.,* 2010; *Striegl et al.,* 2012]. The magnitude of pCO_2 variability at the 50m scale implemented in W1 may be instructive in interpreting larger scale variability observed across the HJA.

Table 3.1 – Study watersheds within HJA with physical information and management history

Stream	Basin Area (km^2)	Elevation (m)	Basin Slope %	Aspect (Degrees)	Soil	Forest Management History
Watershed 1	0.96	450-1027	59.35	286	Gravel Clay Loam	100% clearcut, 1962-66; prescribed burned in 1967
Watershed 2	0.20	476-1079	53.19	318	Gravel Loam	Control; Old-Growth and Mature
Watershed 3	0.97	475-1080	52.39	313	Gravel Loam	1.5 km (6%) roads, 1959; 25% clearcut in 3 patches, 1963
Watershed 6	0.12	893-1029	25.19	165	Gravel Clay Loam	100% clearcut in 1974
Watershed 7	0.17	931-1102	33.68	158	Gravelly Loam	50% selective canopy removal, 1974; remaining canopy removed 1984; 12% thin 2001
Watershed 8	0.20	968-1182	25.78	165	Gravel Sandy Loam	control; old-growth and mature
Watershed 9	0.09	438-731	58.36	247	Gravel Clay Loam	control; old-growth and mature
Watershed 10	0.10	679-471	58.12	250	Gravel Loam	100% clearcut, 1975
Lookout Creek	63.35	434-1627	40.28	267	Gravel Sandy Loam	mature and old-growth, 25% plantations <50 yrs
Mack Creek	8.64	671-1626	48.41	306	Gravel Sandy Loam	control; old-growth and mature
McRae Creek	15.46	555-1570	42.55	242	Gravel Sandy Loam	patch cut
Cold Creek	0.64	980-1495	46.21	208	Gravel Sandy Loam	patch cut
No Name	1.23	809-1182	25.20	120	Gravel Sandy Loam	patch cut

*Basin size and basin slope reported here may be different than reported by H.J. Andrews. These values are based off this study's analysis of geospatial data

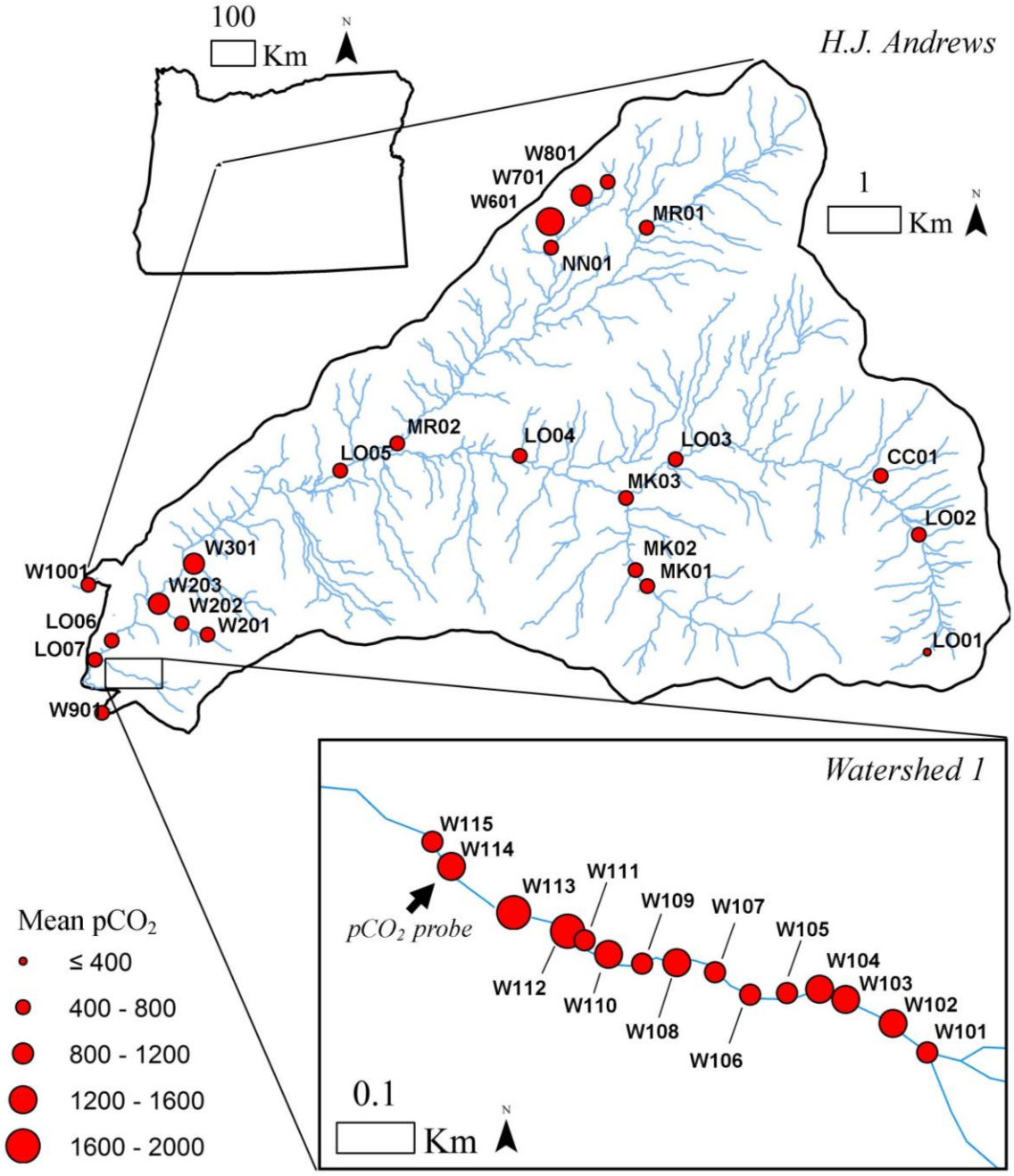

Figure 3.1 - (Top) Location of H.J. Andrews Experimental Forest within Oregon. (Middle) H.J. Andrews and (Bottom) Watershed 1 with sample site locations detailed (*n* = 38). Size of location dots proportional to mean pCO_2 (given in Table 3.3). The pCO_2 probes from Chapter 2 are located at W114 near the base of the W1 transect (labeled).

Table 3.2 – Sample site locations within HJA, and associated physical properties

Site ID	Watershed	Latitude N (decimal)	Longitude W (decimal)	Elevation m	Drainage Area km^2	Distance Downstream m	Slope %
W101	Watershed 1	44.20451	122.24989	563	0.62	555	24.4
W102	Watershed 1	44.20504	122.25018	554	0.63	605	19.9
W103	Watershed 1	44.2052	122.25105	544	0.68	655	11.7
W104	Watershed 1	44.20507	122.25131	537	0.72	705	13.1
W105	Watershed 1	44.2053	122.25191	528	0.74	755	20.6
W106	Watershed 1	44.20534	122.25253	519	0.74	805	19.5
W107	Watershed 1	44.20565	122.25302	510	0.78	855	20.6
W108	Watershed 1	44.20575	122.25368	503	0.83	905	11.8
W109	Watershed 1	44.20574	122.25423	496	0.85	955	14.6
W110	Watershed 1	44.20581	122.25482	486	0.86	1005	18.0
W111	Watershed 1	44.20609	122.25514	481	0.88	1055	10.6
W112	Watershed 1	44.20612	122.25539	477	0.89	1105	18.8
W113	Watershed 1	44.20636	122.25632	466	0.91	1155	17.0
W114	Watershed 1	44.20704	122.25713	452	0.94	1245	9.2
W115	Watershed 1	44.20704	122.25768	444	0.95	1295	24.9
W201	Watershed 2	44.20164	122.24097	664	0.20	455	37.4
W202	Watershed 2	44.21201	122.24522	543	0.61	903	25.6
W203	Watershed 2	44.21427	122.2493	476	0.74	1488	17.9
W301	Watershed 3	44.21953	122.24294	475	0.97	1552	19.5
W601	Watershed 6	44.26149	122.18079	878	0.12	211	26.2
W701	Watershed 7	44.26469	122.17537	919	0.17	184	26.3
W801	Watershed 8	44.26632	122.17097	962	0.20	412	20.1
W901	Watershed 9	44.20147	122.25894	423	0.09	201	31.5
W1001	Watershed 10	44.21702	122.26109	459	0.10	255	19.7
LO01	Lookout Creek	44.20756	122.11718	1224	0.05	692	29.4
LO02	Lookout Creek	44.2222	122.11781	1012	3.03	2877	11.1
LO03	Lookout Creek	44.23187	122.15955	723	15.58	7422	8.4
LO04	Lookout Creek	44.23258	122.18631	607	30.89	9626	4.4
LO05	Lookout Creek	44.23089	122.21742	532	51.54	12523	11.8
LO06	Lookout Creek	44.21002	122.25725	422	62.10	17695	6.6
LO07	Lookout Creek	44.20785	122.25995	414	63.35	18022	4.2
MK01	Mack Creek	44.21619	122.16468	798	5.12	3653	13.5
MK02	Mack Creek	44.21768	122.16771	770	5.34	4078	14.4
MK03	Mack Creek	44.22713	122.16817	677	8.64	5167	9.8
MR01	McRae Creek	44.26073	122.1644	883	3.86	3261	13.8
MR02	McRae Creek	44.23409	122.20743	554	15.46	8676	5.5
CC01	Cold Creek	44.2947	122.12386	980	0.64	1313	20.8
NN01	No Name	44.25823	122.18061	810	1.23	1770	13.0

3.4 Methods

3.4.1 Field Methods

Synoptic field measurements and water samples were collected 12 times over a 13-month study period from July 2013 to July 2014. Sampling occurred at approximately monthly intervals; no samples were collected during April 2014. Low elevation sites were sampled during all 12 sample periods. High elevation sites were sometimes inaccessible due to snowfall and were therefore not sampled during some winter months. Streams that were designed as longitudinal transects were sampled from high elevation to low. Sites were sampled at approximately the same time of day over the study period.

Water samples for the analysis of stream alkalinity were collected in 250 mL HDPE (high-density polyethylene) bottles (Nalgene, Inc., United States). Bottles were acid washed according to the Oregon State University and U.S. Forest Service Cooperative Chemical Analytical Laboratory (CCAL) quality assurance plan [*CCAL*, 2013]. Prior to collection, bottles were rinsed three times with stream water by filling the sample container 1/4 full, then shaking vigorously with the lid loosely tightened to the bottle, making sure to rinse the inside walls, threads, and cap of the bottle. Samples were collected from the thalweg in locations deep enough to fully submerge the bottle while the sample collector stood downstream of the sampling location. In larger streams, samples were taken as close to the thalweg as possible and always collected from locations with strong downstream transport, thereby avoiding stagnant pools or lateral cavities. Sample bottle caps were secured underwater to minimize air collected with the sample and to minimize the amount of sediment or other particulates collected with the

water sample. Nitrile gloves were worn during sampling to minimize sample contamination. After collection, samples were placed on ice in a dark container until laboratory processing.

Stream pH and temperature were measured at sample sites using a YSI Model 63 handheld pH, conductivity, salinity and temperature system (YSI, Inc., United States). The meter was calibrated for pH at the beginning of each field day with a two point calibration at pH 7.0 and 10.0, bracketing the range of expected field pH values. When making field measurements, the probe was placed in the thalweg of the stream, slightly downstream from the location of water sampling. The meter was given a minimum of 10 minutes to stabilize prior to reading. The probe was positioned so that the pH electrode was suspended in the water column and not resting in mud or sediment.

Direct stream pCO_2 measurements were collected in July 2014 in W1 using a handheld Vaisala Carbocap CO_2 meter (Vaisala, Inc., Finland), calibrated within ±1.5% of the reading. The probe was modified following the methods in *Johnson et al.* [2010] and was implemented in the field following *Crawford et al.* [2013]. The probe was positioned horizontally just below the water surface and was allowed to equilibrate for a minimum of 10 minutes. Depth from the water surface to the center of the probe was recorded with a measuring tape for water pressure correction. The probe was placed in a protective PVC sleeve during measurements, and while in transport, to protect the PTFE (polytetrafluoroethylene) fabric from scratches or scuffs.

3.4.2 Laboratory Methods

Analytical lab work was conducted at the Institute for Water and Watersheds Collaboratory at Oregon State University. Carbonate alkalinity was determined using a Radiometer TIM840 AutoTitrator (Radiometer Analytical, SAS, France) according to CCAL procedure 10C.0 by titrating 100 mL of unfiltered sample to a pH of 4.5 with 0.02 N H_2SO_4 [*CCAL*, 2013]. Detection limits associated with this method are 0.2 mg CaCO3 L^{-1}. Samples were processed within 7 days of field collection.

3.4.3 pCO_2 Calculation and Data Processing

Stream pCO_2 was calculated with the CO2SYS program [e.g., *Barnes and Raymond*, 2009; *Butman and Raymond,* 2011; *van Heuven et al.,* 2011] using field measurements of temperature and pH, and lab measurements of alkalinity. This calculation is based on equilibrium concentrations of the carbonate species in water at a given pressure, temperature, and pH. The dissociation constants of the carbonate species used for this calculation were those from *Millero* [1979] for freshwater systems.

This calculation of pCO_2 is sensitive to uncertainties in field and lab data, with particular sensitivity to pH [*Lauerwald et al.,* 2013]. To minimize the effect of individual values overall outcomes while still recognizing the importance of all measurements, we chose to compute study site mean annual pCO_2 for spatial analyses. Measurement averages over the study period provide greater confidence in spatial patterns, minimizing the effect of sample errors that potentially hinder spot measurements [*Roberts et al.*, 2007]. Although individual high and low values of pCO_2 are quantitatively important to

overall basin fluxes, mean pCO_2 has been found to be the best estimator for spatial coverage and is used for our analysis of spatial patterns [*Striegl et al.*, 2012].

For inter-site comparison, sites that were missed more than twice have been excluded from the study due to the potential for seasonal bias in mean pCO_2. The highest elevation sampling location in the lookout transect (LO01) was unreachable between November 2013 and May 2014 due to snow. This site has been excluded from the spatial analysis.

3.4.4 Calculation of Catchment Properties

We determined catchment properties and spatial variables within the HJA using a 1 m LIDAR-based digital elevation model, a soils map, a geology map, and a stream network model. This and other spatial data were made available through the H.J. Andrews Long Term Ecological Research Station data catalog (http://andrewsforest.oregonstate.edu/lter/data.cfm?frameURL=269). Spatial data analyses were performed in ArcGIS (ESRI, United States). Sample sites were located in the field using a handheld GPS (Garmin, United States). Downstream distance was estimated by summing the length of all stream segments between the sampling location and stream origin point. Drainage area was computed for individual sites using the DEM and a flow accumulation model. Stream slope for each sample site was computed by taking the average slope over the local stream segment, where average stream segment length was 192 m (n = 1079).

3.4.5 Calculation of Physical Variables

Gauge stations within the HJA were co-located at sample sites W115, W202, W301, W601, W701, W801, W1001, LO06 and MK02. Discharge data were available for all samples collected at gauge stations. Discharge was calculated for sites that were not positioned at gauge stations but were located along streams that contained gauge stations. Measured discharge was scaled linearly with contributing drainage area [*Dunne and Leopold*, 1979] using the following equation:

$$Q_2 = Q_{GS}(DA_2/DA_{GS}) \quad (1)$$

Where Q_{GS} is discharge recorded at the gauge station at the time of measurement (L s^{-1}), Q_2 is the scaled discharge (L s^{-1}), DA_{GS} is the contributing drainage area above the gauge station (m^2) and DA_2 is the drainage area above the sample point (m^2). Specific discharge (Q_S) was calculated by normalizing each discharge measurement by the contributing drainage area of that location.

The gas transfer velocity, a term that describes gas exchange across the air-water interface of stream, is a function of stream turbulence and can be successfully modeled based on physical characteristics of a site. The gas transfer velocity for carbon dioxide (k_{CO2}) was estimated at each value of discharge. First, stream velocity was calculated for all values of discharge using hydraulic geometry relationships for small streams (median depth 0.28 m) [*Leopold and Maddock*, 1953; *Raymond et al.*, 2012]. Gas transfer velocity normalized to a fixed temperature with a Schmidt number of 600 ($k_{600,}$ m day^{-1}) can be calculated following *Raymond et al.* [2012] with the following equation:

$$k_{600} = 1162 \pm 192 \times S^{0.77\pm0.028} V^{0.85\pm0.045} \quad (2)$$

where S is reach slope and V is stream velocity ($m^3\ s^{-1}$). Values of k_{600} can be converted to discrete values of the CO_2 gas transfer velocity (k_{CO2}) by applying the following equation:

$$k_{CO2} = (Sc_{CO2}/600)^{-n} * k_{600} \quad (3)$$

where Sc_{CO2} is the Schmidt number for carbon dioxide at a given temperature following *Wanninkhof* [1992], and n is the Schmidt number exponent which characterizes the stream water and surface conditions. Here, we assigned it a value of 0.5 to represent uncontaminated water with a moderately turbulent surface [*Raymond et al.*, 2012; *Crawford et al.*, 2014].

3.4.6 Statistical Analyses

Linear regressions and one-way analysis of variance (ANOVA) tests were performed to examine the ability of catchment properties and physical variables to explain spatial variability in stream pCO_2. These analyses were completed in Matlab (Mathworks, USA). The purpose of these analyses is to identify properties associated with controls of stream pCO_2. In identification of these variables we aim to define the processes that drive stream pCO_2 concentrations. We also calculated the variogram of mean monthly pCO_2 in the W1 transect to gauge the spatial correlation of this measurement in a longitudinal profile of stream at 50 m intervals. The variogram is defined as the variance between field values at two locations across the field of measurements [*Isaaks and Srivastava*, 1989].

We performed a comparison of mean site pCO_2 with downstream distance, contributing drainage area, elevation and slope – all physical parameters relating to

drainage network location and relative to stream origin – to interpret the spatial variations of stream pCO_2 within the Lookout creek drainage network [*Leopold and Maddock*, 1953]. We log transformed response and explanatory variables prior to fitting a linear regression.

3.5 Results

Stream pCO_2 within the Lookout Creek drainage network was highly variable both spatially and over the study period. Calculated pCO_2 ranged from atmospheric concentrations (~400 μatm) to approximately 20 times atmospheric concentrations (8150 μatm) (Table 3.3). Individual sites exhibited a range in pCO_2 over the study period. Mean stream pCO_2 for all sites was 945 μatm. The average site pCO_2 range was 1674 μatm, and the average site pCO_2 standard deviation was 464 μatm. We applied several interpretative approaches to identify patterns within the dataset. First, we examined spatial patterns of stream pCO_2 variability within the Lookout Creek drainage network. We compared site average concentrations with local and catchment properties from spatial data, and contrasted patterns between and within longitudinal transects. Second, we examined temporal variations in pCO_2 across the watershed and compared monthly watershed pCO_2 to measured variables. Third, we examined additional measured physical properties and analyze them as physical controls of observed variation in stream pCO_2.

Table 3.3 – Summary of average pH, temperature, alkalinity, and pCO_2 for each sample site

Site ID	Mean pH	Mean Alkalinity $CaCO_3$ (mg/L)	Mean Temp °C	Mean pCO_2 µatm	pCO_2 Std Dev. µatm
W101	7.5	23.51	9.71	950	655
W102	7.3	23.39	9.67	1359	705
W103	7.4	23.44	9.77	1254	553
W104	7.3	23.32	9.79	1411	784
W105	7.5	23.25	9.76	874	362
W106	7.5	23.01	9.82	910	385
W107	7.4	22.90	9.83	1106	446
W108	7.3	22.85	9.93	1326	604
W109	7.4	22.76	9.93	1122	426
W110	7.4	22.52	9.91	1204	601
W111	7.4	22.52	10.09	971	472
W112	7.3	22.88	9.94	1887	2179
W113	7.2	22.93	9.92	2091	1448
W114	7.3	22.71	10.01	1354	669
W115	7.4	22.25	10.18	1038	450
W201	7.4	16.17	9.19	728	382
W202	7.5	19.71	10.51	717	390
W203	7.4	20.18	9.14	1057	527
W301	7.4	20.62	10.10	868	294
W601	7.4	20.16	9.50	1212	1022
W701	7.4	24.95	9.34	1080	324
W801	7.5	21.86	9.62	735	269
W901	7.6	24.84	10.58	665	272
W1001	7.6	23.93	11.15	713	324
LO02	7.2	9.15	8.01	578	204
LO03	7.6	20.33	7.10	571	168
LO04	7.4	18.03	8.80	799	210
LO05	7.4	17.14	9.62	747	158
LO06	7.6	17.55	10.87	549	167
LO07	7.5	17.68	10.93	613	193
MK01	7.5	16.37	8.90	610	173
MK02	7.5	15.90	9.23	761	757
MK03	7.5	14.94	8.56	590	169
MR01	7.4	11.62	8.01	545	185
MR02	7.5	15.94	10.00	625	175
CC01	7.7	25.67	6.76	553	215
NN01	7.5	21.19	9.79	800	105

3.5.1 Spatial Patterns

3.5.1.1 Catchment Patterns

Linear regressions between site mean pCO_2 and downstream distance (p = 0.0036), contributing drainage area (p = 0.009), and elevation (p = 0.024) all exhibit a significant ($p < 0.05$) negative relationship (Figure 3.2 a, b, c). Stream pCO_2 concentration change across the watershed appears to be best characterized by logarithmic transforms. The regression of site mean pCO_2 and slope did not exhibit a significant relationship (Figure 3.2 d). This result contrasts with the other statistical relationships between stream pCO_2 and watershed location. Site slope - like the downstream distance, contributing drainage area and elevation - changes predictably with increasing distance from the stream origin [*Leopold and Maddock*, 1953]. Highest (>25%) and lowest (<15%) site slope exhibited relatively lower associated pCO_2 while moderate slopes (15-25%) showed higher pCO_2.

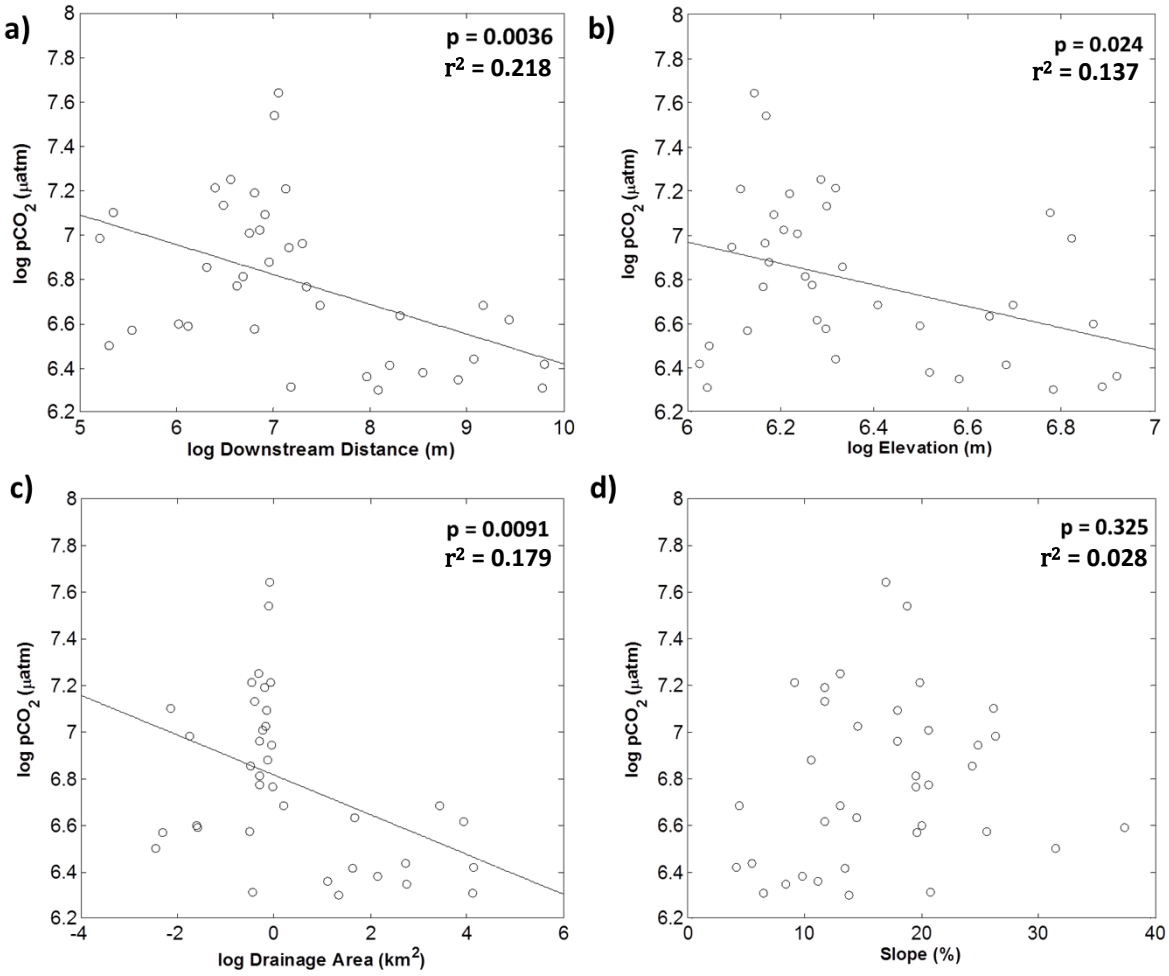

Figure 3.2 – Log (base *e*) and semi-log transform linear regressions of site average pCO_2 and (a) site downstream distance (b) site elevation (c) site contributing drainage area (d) reach slope. *p*-values from these linear regressions are displayed in the upper right corner of each plot, with significant values < 0.05.

3.5.1.2 Transect Patterns

There was considerable variability in observed pCO_2 between and within longitudinal transects studied. There was no consistent downstream trend among the five transects (W1, W2, LO, MK, MR), with W2, and MR displaying increasing trends, while MK, LO and W1 exhibited no directional trend with similar concentrations at upstream and downstream sites. Variation within transects yielded persistent spatial patterns, with transects exhibiting profiles of similar shape over the study period. All profiles contained sites with relatively higher and lower pCO_2 when compared with adjacent transect sampling sites.

Transect profiles W1 and LO are of particular interest (Figure 3.3), as W1 was the most densely sampled transect (15 sites, sample interval = 50m) and LO was the longest transect sampled (transect length = 17.33 km). The W1 profile displays considerable variation in site pCO_2 and no consistent downstream trends. Two sites near the base of the W1 transect (W112 and W113) that became spatially intermittent during summer low flow had comparatively high mean pCO_2. Sites W112 and W113 had significantly different pCO_2 concentrations from the other sites along W1 transect (one-way ANOVA test, $p = 0.040$). Similarly, the LO transect does not exhibit a consistent increasing or decreasing trend in the downstream direction. The mean pCO2 differs among sites along the LO transect (one-way ANOVA test, $p = 0.0078$). The greatest observed pCO_2 in this transect occurred in the middle sites of the LO transect, with lower concentrations at the top and bottom sites.

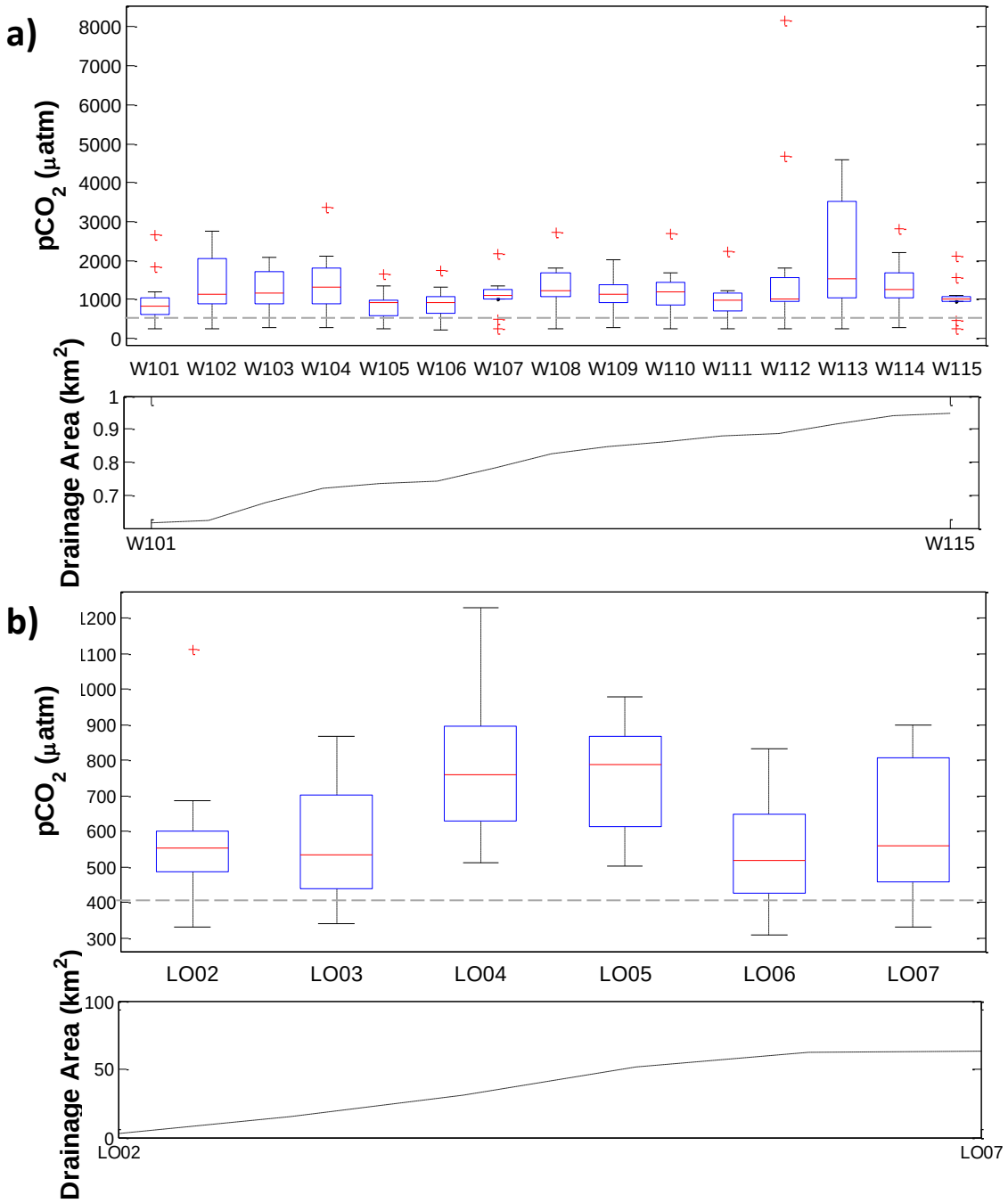

Figure 3.3 – Longitudinal pCO_2 profile variability and contributing transect drainage area. Box plots show medians (red lines), quartiles (boxes), 90 percent confidence intervals (whiskers) and range (red plus symbols) of measured pCO_2 in (a) Watershed 1 transect (b) Lookout Creek transect. The grey dotted line represents atmospheric concentrations of CO_2.

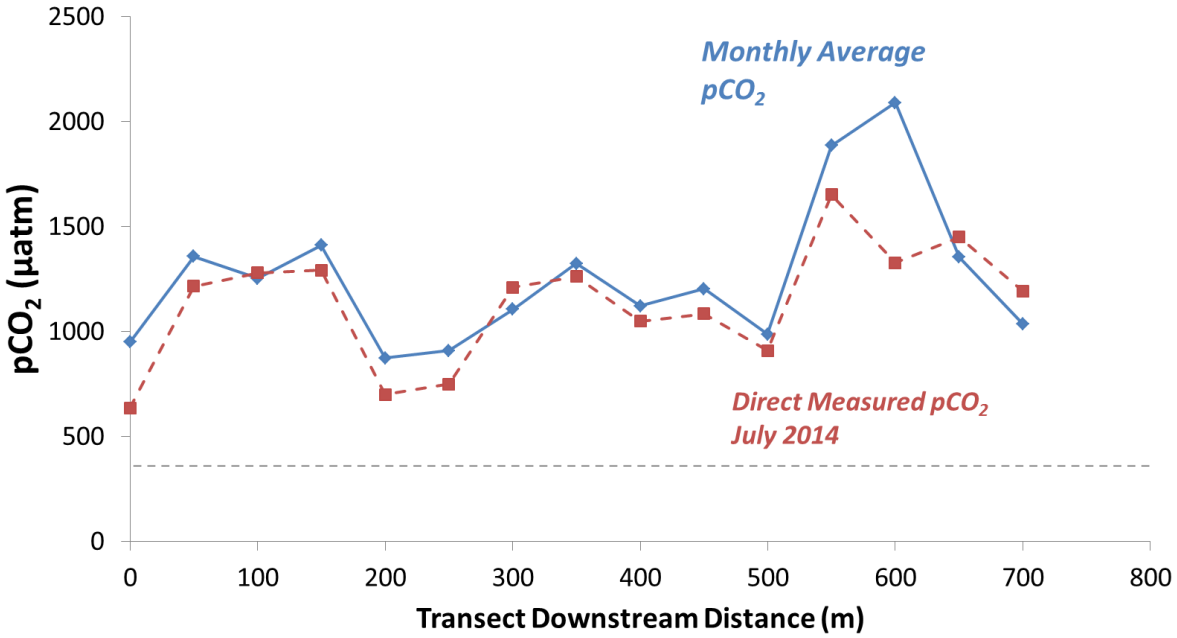

Figure 3.4 – Persistent spatial trends in longitudinal pCO_2 in W1. Direct measurements of pCO_2 from July 2014 produced a similar longitudinal concentration profile to that from site average pCO_2. Dotted line represents atmospheric pCO_2.

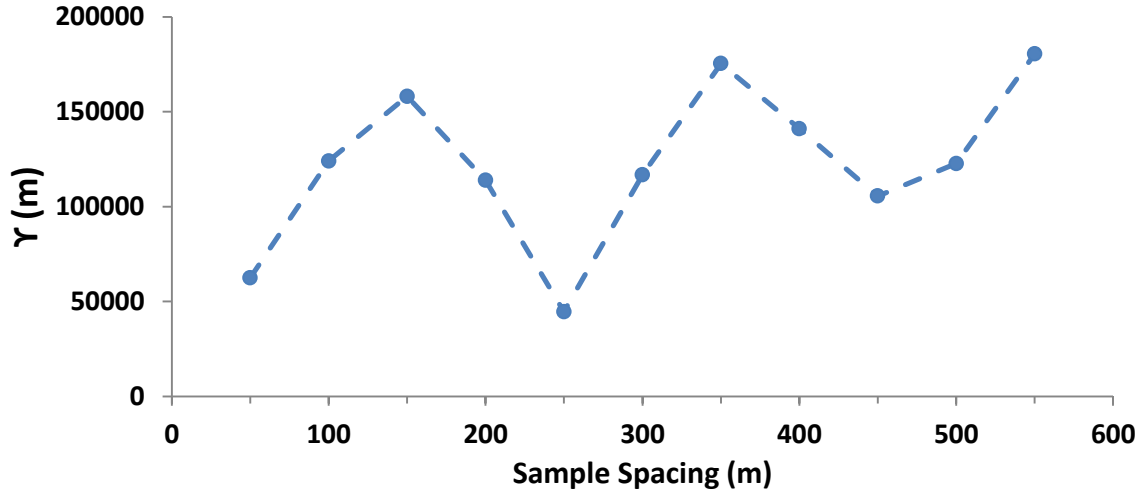

Figure 3.5 – Variogram of mean pCO_2 measurements in Watershed 1, where ϒ is the variogram strength, a measure of covariance as a function of sample spacing.

There was also variation between transects. W1 and W2 had different pCO_2 than LO, MK and MR (one-way ANOVA, $p < 0.001$). W1 and W2 are considerably smaller streams in the drainage network, MK, and MR are major tributaries, and LO is the largest stream in the catchment.

Direct pCO_2 measurements collected along the W1 transect in July of 2014 were in close agreement to site annual averages. The concentration profile along the longitudinal transect was similar to the profile produced by site average pCO_2, with strong spatial consistency with relative low and high concentration sites along the profile (Figure 3.4). The variogram for W1 pCO_2 suggests that the correlation scale for pCO_2 is less than 50m (Figure 3.5).

3.5.2 Temporal patterns

At individual sites, stream pCO_2 was highly variable over the study period (Figure 3.6), with changes in mean concentration and concentration variance on monthly and seasonal time scales (Figure 3.7; Table 3.4). Mean stream pCO_2 concentrations were supersaturated with respect to the atmosphere during all sampling periods. Concentrations showed generally greater mean pCO_2 during warm summer months and lower mean pCO_2 during cool winter months. This is also true of observed pCO_2 variance, with a greater range of observed concentrations in summer months and a smaller range of values observed during the winter. The highest average stream pCO_2 was observed in October, with an average stream concentration of 1356 μatm. The lowest average stream pCO_2 was observed in May, with an average stream concentration of 434 μatm. Stream temperature and alkalinity exhibited much stronger seasonal variation

(Figure D.6). A linear regression of stream temperature and alkalinity produced a positive relationship ($p < 0.001$), with higher stream alkalinity occurring at higher temperatures.

A linear regression of the log transformed excess stream pCO_2 (concentrations in excess of atmospheric concentrations, i.e., $pCO_{2\ S} - pCO_{2\ atm}$) and temperature normalized to an arbitrary reference temperature (15 °C) according to the Arrhenius relationship following *Yvon-Droucher et al.*, [2012], produced a weakly significant ($p = 0.049$) negative relationship, indicating some evidence for lower excess stream pCO_2 with increasing water temperature (Figure 3.8). We applied the Arrhenius relationship to isolate the effect of temperature change and to remove the influence of ecosystem respiration, which does not scale linearly with temperature. This regression using mean site pCO_2 produces a relationship with greater negative significance ($p = 0.020$), suggesting stronger predictive value at the annual scale (Figure D.5).

Table 3.4 – Watershed Average pCO_2 for each sample run and percent change from the previous month

Month	**July**	**Aug**	**Sep**	**Oct**	**Nov**	**Dec**	**Jan**	**Feb**	**Mar**	**May**	**June**	**July**
Run	1	2	3	4	5	6	7	8	9	10	11	12
Average pCO_2 (µatm)	1233	915	1172	1356	844	905	906	1133	614	434	1185	823
Change From Previous Month (+/- %)		- 26%	+ 28%	+ 16%	- 38%	+ 7%	0%	+ 25%	- 46%	- 29%	+ 173%	- 31%

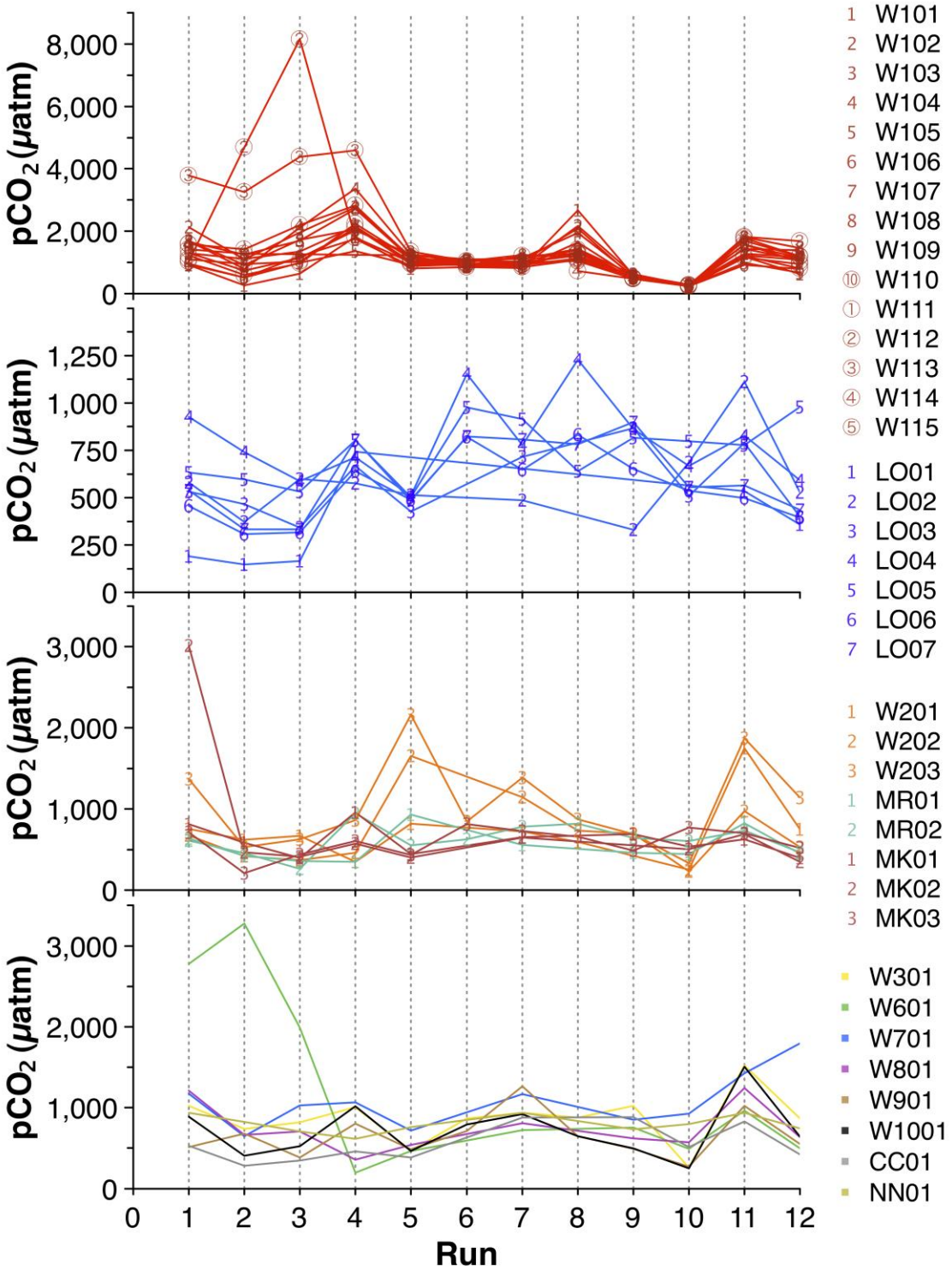

Figure 3.6 - Temporal variations in site pCO_2 over the study period, separated by sample collection run. Each line represents a single sample location. Lines of the same color are sites along a longitudinal transect. Numbers on longitudinal transect lines indicate location along transect.

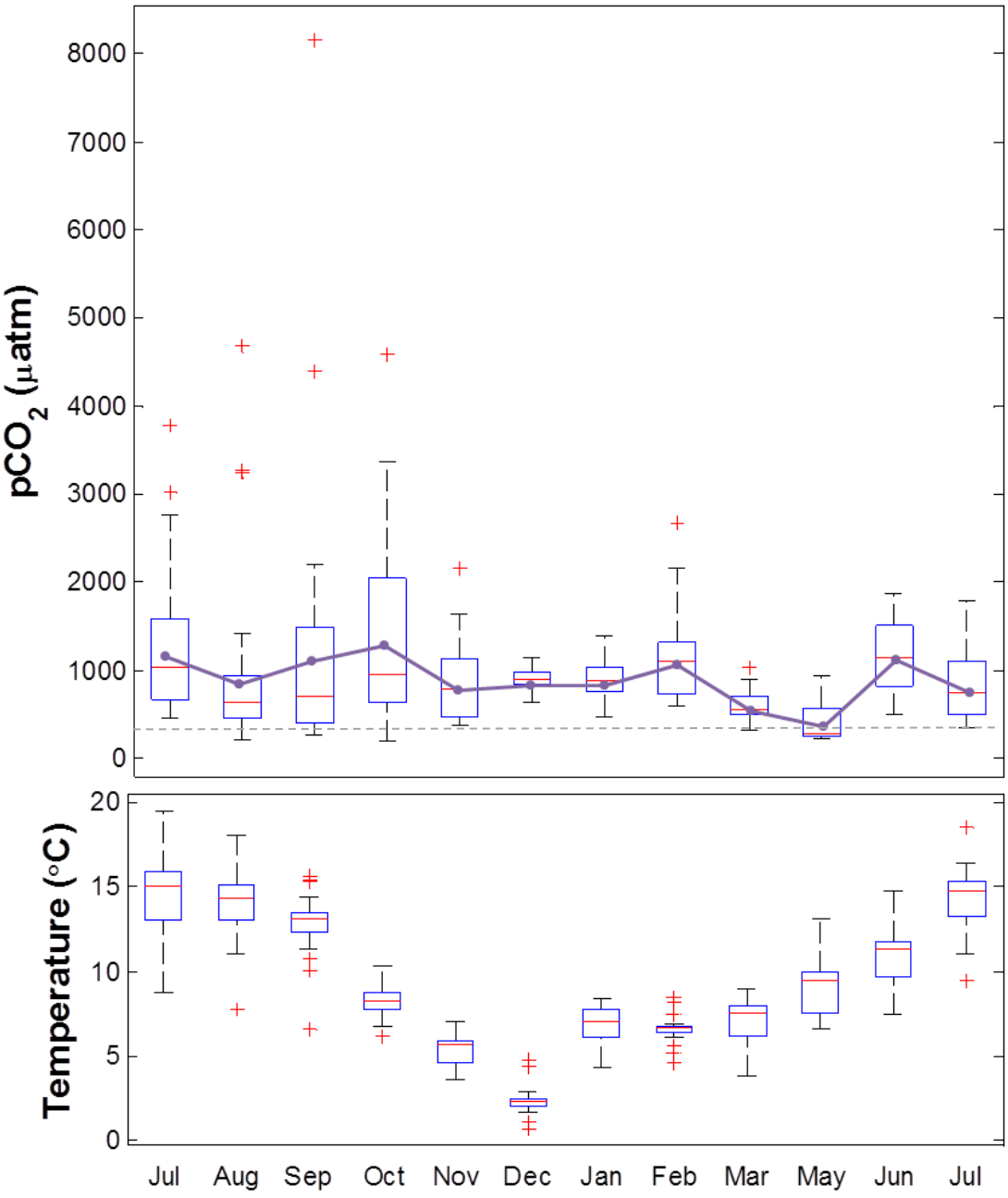

Figure 3.7 – Annual variation in calculated stream pCO_2 and stream temperature from the Lookout Creek drainage network from July 2013 to July 2014. Box plots show medians (red lines), quartiles (boxes), 90 percent confidence intervals (whiskers) and range (red plus symbols) of measured pCO_2. Purple dots within box plots represent mean monthly pCO_2. The dashed line in the top plot represents approximate atmospheric concentration (~400 µatm).

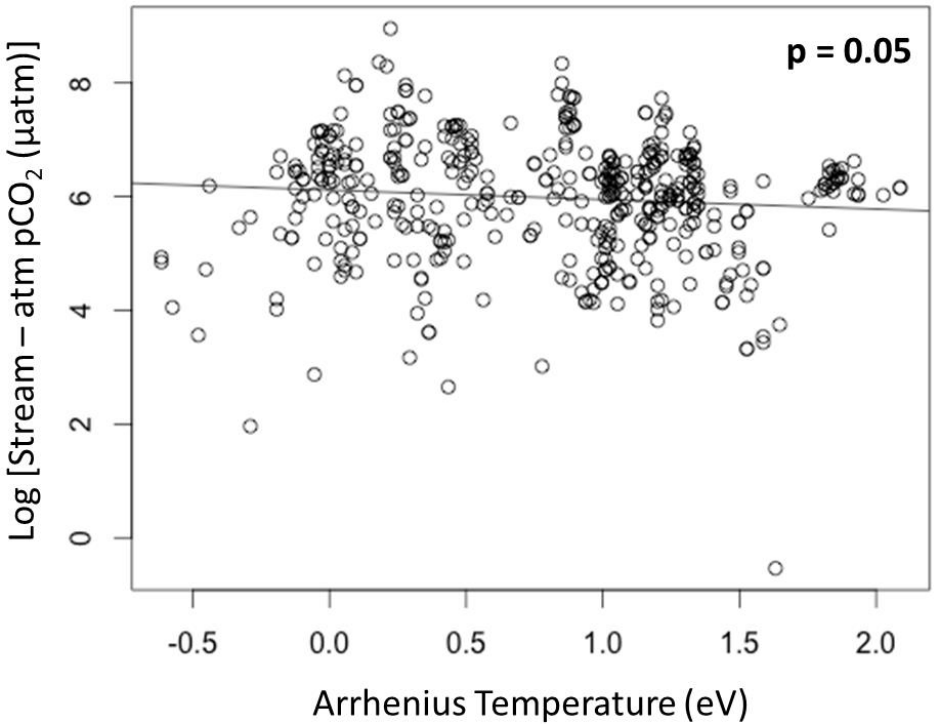

Figure 3.8 – Linear regression of Arrhenius temperature normalized to a reference temperature (15 ºC) and the logarithm of stream minus atmospheric pCO_2.

3.5.3 Hydraulic Patterns

We found negative relationships ($p < 0.001$) between excess stream pCO_2 and stream discharge, stream velocity, and gas transfer velocity (Figure 3.9). Greater discharge, stream velocity and gas exchange led to decreased observed CO_2 supersaturation. We also found a negative relationship between stream excess stream pCO_2 and specific discharge (Figure D.7), though this relationship did not explain any additional variance in that the regression between excess pCO2 and standard discharge. Log transforms were applied to the explanatory variables discharge and gas transfer velocity to produce a linear relationship. Only measurements of pCO_2 that were

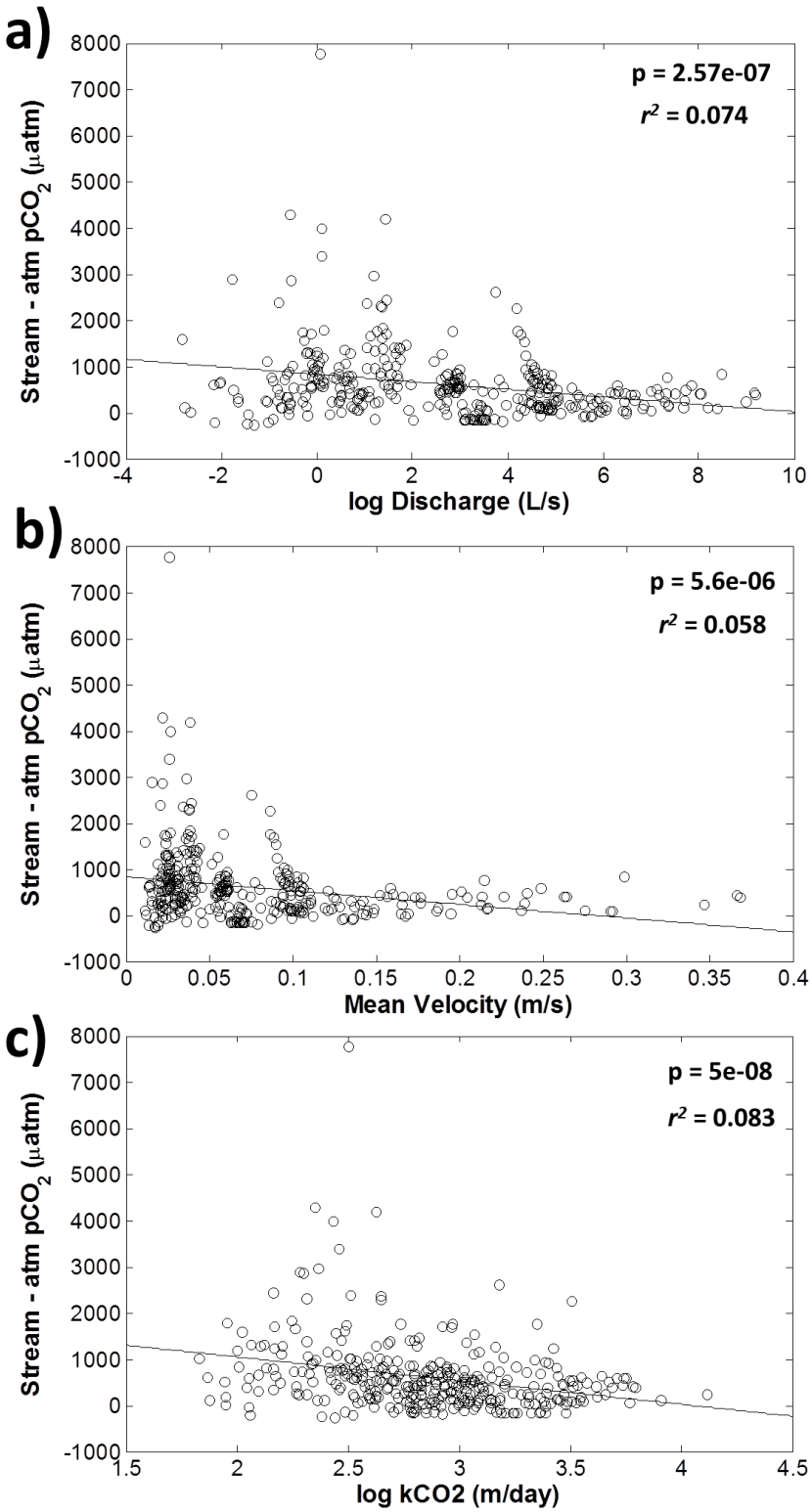

Figure 3.9 – Linear regressions of excess stream pCO_2 and (a) log discharge (b) mean velocity (c) log carbon dioxide transfer velocity(k_{CO2}).

collected with concurrent values of discharge (calculated or measured) were included in this analysis.

3.6 Discussion

3.6.1 Spatial Controls on Stream pCO_2

The spatial relationships examined in our analysis suggest decreasing stream pCO_2 with increasing distance from stream origin. This relationship was established with linear regressions between stream pCO_2 and several physical variables associated with relative position in a watershed. Downstream distance, contributing drainage area and elevation all exhibited significant negative relationships. This finding is consistent with other work regarding watershed or regional scale variations of stream pCO_2. A study of broad-scale stream pCO_2 across the contiguous United States by *Butman and Raymond* [2011] found widespread decrease in stream pCO_2 as a function of Strahler stream order. This pattern has also been observed in studies conducted at the watershed scale. A study conducted by *Jones and Mulholland* [1998a] found a decrease in stream pCO_2 of approximately 50% within two watersheds in the Smoky Mountains, along 46- and 65-km transects. *Crawford et al.* [2013] found a strong decreasing trend in stream pCO_2 with increasing tributary Strahler stream order in the headwater tributaries of the Yukon River in Alaska. Additionally, *Hope et al*. [2001] observed this pattern at the reach scale, reporting high rates of CO_2 removal along a 2.7-km reach of a first-order peatland stream in NE Scotland, with pCO_2 decreasing six-fold from upper to lower study sites.

The finding of decreasing pCO_2 with increasing distance from headwaters is consistent with geomorphic and fluvial changes in a watershed. Headwater streams are

consistently supersaturated with pCO_2 [e.g., *Jones and Mulholland*, 1998b; *Cole and Caraco,* 2001; *Humborg et al.,* 2010]. These streams receive high inputs organic matter, are heterotrophic, and receive proportionally large inflows of groundwater considered to be CO_2-rich [*Cole and Caraco,* 2001; *Battin et al*, 2008]. As distance from headwater increases, stream discharge increases, streams become increasingly autotrophic, and terrestrial and groundwater inputs become proportionally less important to overall stream chemistry [*Vanote et al.,* 1980]. In this study, decreasing stream pCO_2 scales with distance from headwater, contributing drainage area, and elevation. These properties applied as explanatory variables of stream pCO_2 yield significant predictive values in this study. These relationships may be valuable at the watershed scale, but do not fully explain variance observed in pCO_2. Stream slope has been shown to scale linearly with watershed position [*Leopold and Maddock,* 1953]. However, slope measurements on the reach scale obtained from spatial data do not appear to scale with pCO_2, indicating that these slopes may not accurately represent stream characteristics at the scale of sample collection, or stream pCO_2 influence.

It is possible that the magnitude of apparent CO_2 loss could be augmented by a shift in carbonate speciation. A study conducted by *Wallin et al.* [2010] found that, in addition to decreases in stream dissolved inorganic carbon (a summation of dissolved carbon dioxide $\{CO_2\}$, bicarbonate $\{HCO_3^-\}$, and carbonate $\{CO_3^{-2}\}$) in the downstream direction within a Swedish headwater drainage network, there was a marked increase in the proportion of DIC in the form of bicarbonate due to carbonate weathering. This effect, however, is an unlikely spatial control of pCO_2 in the Lookout Creek catchment. This watershed has no carbonate bedrock [*Swanson and James*, 1975], thus conversion of

free CO_2 to DIC via carbonate weathering is not likely an important pathway for CO_2 loss in this catchment. We also observe a decrease in alkalinity as a function of downstream distance ($p < 0.001$). Additionally, pH did not show any significant trends with downstream distance, making it difficult to identify consistent patterns of DIC partitioning as a function of position in the Lookout creek drainage network.

Local geomorphic features not characterized by variables associated with watershed position may also be important in controlling gas transfer velocity. Increased stream turbulence, caused by riffle sequences, waterfalls, in-stream woody debris, or boulders can enhance gas exchange between steam and atmosphere, thereby influencing stream pCO_2. We found a significant negative relationship between k_{CO2} and stream excess pCO_2. We also found a significant relationship between discharge and velocity with stream excess pCO_2 - factors important in scaling site k_{CO2} [*Billet and Harvey,* 2012; *Raymod et al.,* 2012]. These results agree with reported findings that increased gas exchange leads to lower site pCO_2 concentration [*Wallin et al.,* 2011].

The factors that influence gas exchange, however, are difficult to characterize on large scales. A study of watershed-scale patterns in the gas transfer velocity (k_{CO2}) by *Wallin et al.* [2011] found that this value is highly spatially variable but could be adequately characterized in space by site-specific measurements of slope and hydraulic geometry. A meta-analysis of gas transfer velocity measurements by *Raymond et al.* [2012] successfully modeled k_{CO2} with site characteristics and indicated the importance of local slope, and in small streams, bed roughness. Another study by *Hall et al.* [2012] investigated variations in pCO_2 along a transect of the Colorado River, and reported variations in the gas transfer velocity spanning two orders of magnitude across rough and

smooth reaches of river. It appears that site gas transfer velocity, though spatially variable, is an important influence on local stream pCO_2.

The spatial distribution of groundwater and hyporheic inputs may also be important to longitudinal variation in stream pCO_2. Groundwater and hyporheic water can be CO_2-rich [e.g., *Schindler and Krabbenhoft*, 1998; *Duarte and Prairie*, 2005; *Öquist et al*., 2009]. Inputs tend to be focused along preferential flow paths and enter the stream at points of subsurface upwelling [*Findlay et al.*, 1993; *Boulton et al.*, 1998]. Zones of upwelling are associated with marked changes in stream chemistry [e.g., *Boulton et al.*, 1998; *Franken et al*., 2001]. The distribution of hyporheic and groundwater inputs along a stream may explain variations in longitudinal stream pCO_2.

Longitudinal transect concentration profiles from this study appear to support the hypothesis of site-scale controls of stream pCO_2. We observed persistent transect pCO_2 variability inconsistent with watershed scale patterns of pCO_2 in the downstream direction. Headwater streams in the HJA are characterized by longitudinal changes in stream morphology with alternating sequences of pools, bedrock, steps and riffles [*Kasahara and Wondzell*, 2003]. These changes influence local k_{CO2} and may contribute to persistent site variance in average pCO_2 along longitudinal transects in this study (Figure 3.3, Figure 3.4). However, we also observe local increases in stream pCO_2 along transects in addition to observed decreases. This indicates that there must also be continual sources of CO_2 to the stream along these transects. Sections of stream that have relatively low turbulence, and therefore low k_{CO2}, may allow for local recovery of pCO_2 and account for local increases in pCO_2 along a transect. Diffuse inputs of CO_2-rich

groundwater or hyporheic exchange flows may control stream pCO_2 in these locations [*Dawson et al.*, 2001; *Crawford et al.*, 2014; *Peter et al.*, 2014].

Studies that have observed longitudinal pCO_2 changes at the reach-scale have found similar results. *Crawford et al.* [2014] measured stream pCO_2 along six, 2000-m transects and found spatially variable pCO_2 with persistent profile shape. *Dawson et al.* [2001] observed persistent peaks and troughs in a pCO_2 profile over a year along a headwater reach of stream. Longitudinal transect pCO_2 profiles at the reach-scale suggest that in-stream processes, groundwater inputs, and local morphology control stream pCO_2 at this scale, and longitudinal changes in stream pCO_2 cannot be accurately characterized by unidirectional downstream trends [*Lauerwald et al*., 2013; *Crawford et al.*, 2014].

3.6.2 Spatial Considerations

The scale of stream pCO_2 variability is important for scaling point measurements of pCO_2 to the reach or watershed scale. Results from the variogram analysis in W1 (Figure 3.5) illustrate the importance of site-scale controls on pCO_2, with no identifiable covariance at sample intervals of 50 m. Stream pCO_2 increment tolerance in W1 appears to be smaller than this interval, indicating that finer resolution sampling may be required to capture longitudinal stream pCO_2 gradients. Field duplicates collected in this study showed very good agreement (±0.03%) with original aliquots, indicating negligible kernel effect (variance with a sample spacing of 0 m) [*Isaaks and Srivastava*, 1989]. These findings suggest that the appropriate scale for identifying pCO_2 gradients in W1 is at some interval between 0 and 50 m. It is difficult to predict how fine of sample spacing is required as it will likely depend on site specific geomorphic or environmental factors.

Extreme examples of spatial pCO_2 variation were reported by *Fiedler et al.* [2006] and *Johnson et al.* [2008]. *Fiedler et al.* sampled spring water at its source and then again 17 m downstream and found a 93% decrease in dissolved CO_2 on average over this distance. *Johnson et al.* also monitored a site of groundwater emergence in an Amazonian headwater stream and found changes in pCO_2 greater than 500% within 50 m downstream of the spring due to rapid outgassing. It appears that stream pCO_2 can vary greatly over short distances. We observed similar phenomena at sites W112 and W113 during August and September sample runs. The W1 stream became spatially intermittent at these locations as a result of low discharge, with the stream entering subsurface flowpath and reemerging downstream. At W112 and W113 in August and September, water samples were collected where stream water emerged from the subsurface. Measured pCO_2 at these instances were between ~4500-8000 μatm, considerably higher than all other measurements collected across the Lookout Creek drainage network during the entire study period (Figure 3.6; Figure 3.7). Concentrations at the W114 and W115 – sites 50 m and 100 m below the stream discontinuity – had much lower pCO_2. The magnitude and spatial controls of stream pCO_2 variability may have important implications for representative scaling across drainage networks and estimations of carbon fluxes.

3.6.3 Temporal Controls on pCO_2

We observed monthly variability in the mean and variance of measured stream pCO_2 and found weak evidence of seasonal patterns. The magnitude of seasonal variation was smaller than we expected. A different study that performed high resolution

monitoring of pCO_2 over 11 months in W1 found strong seasonal variations, with concentrations on average 2.5 times larger during summer months than winter months [*Dosch*, 2014]. Other studies have also observed strong annual variability with a seasonal pattern in stream pCO_2 [e.g., *Raymond et al.,* 1997; *Jones and Mulholland,* 1998b; *Parasad et al.,* 2013]. In this study, temporal variations across the entire Lookout Creek drainage network were variable from month to month (Table 3.4) and lacked a coherent seasonal pattern (Figure 3.7). However, most studies that report seasonal variations in pCO_2 do so from a single location. It is possible that aggregating watershed data to produce basin-wide monthly averages masks seasonal trends. However, we found that individual sites did not exhibit discernable seasonal patterns (Figure 3.6). We did not find spatially uniform seasonal variation in stream pCO_2 at the basin-scale. It is likely that temporal changes in small streams are different from those large streams within this network. This hypothesis is supported by results from the ANOVA test that indicate annual distributions of pCO_2 in the small tributaries W1 and W2 are significantly different than those in larger streams LO, MR, MK.

Stream temperature had strong monthly variability with a distinct seasonal trend, but was a weak predictive variable of stream pCO_2 in this study. Stream temperature did not scale with stream pCO_2 as well as we expected. A study that collected stream pCO_2 measurements at 30-minute intervals in W1 found that stream temperature explained 53 percent of the variance in observed pCO_2 [*Dosch*, 2014]. In this study, however, stream temperature was only able to explain 5 percent of the variance. We did find a significant negative relationship between standardized temperature (Arrhenius temperature) and stream pCO_2 excess. It is possible that this inverse relationship is due to changing

solubility of CO_2 in water as a function of temperature, with CO_2 being more soluble at cool temperatures [*Stumm and Morgan*, 1996]. However, it is difficult to isolate the effect of a single process in the Lookout Creek drainage network. Temperature has been shown to influence the gas transfer velocity, enhancing gas fluxes at warmer temperatures [*Demars and Manson*, 2013]. Stream temperature also has a strong positive influence on ecosystem metabolism, with warmer temperatures leading to increased respiration and thereby local CO_2 production [*Bott et al.*, 1984; *Roberts et al.*, 2007; *Yvon-Durocher*, 2012]. Stream temperature was also indirectly associated with seasonal and hydrologic changes, with the warmest waters observed in late summer when discharge is also lowest. When discharge is low, surface turbulence and k_{CO2} are decreased [*Billet and Harvey,* 2012; *Raymond et al.*, 2012] and stream travel time is increased. These conditions increase the probability that an individual parcel of water will enter the subsurface via hyporheic exchange, encounter subsurface microbial communities, and become enriched in CO_2 while also decreasing the probability of CO_2 loss through evasion [*Crawford et al.*, 2014].

The scale of temporal sampling may also have an influence on the temporal results in this study. Synoptic sampling offers only a snapshot of stream chemistry and does not yield insight toward event- or finer-scale dynamics. Several studies that have applied continuous or high resolution sampling reveal diurnal and event-scale patterns of variability that were indiscernible by discrete sampling alone [*Dinnsmore et al.,* 2013; *Crawford et al.,* 2013; *Peter et al.,* 2014; *Dosch,* 2014]. It is possible that the measurements presented in this study are representative of basin temporal variations in pCO_2 at a fixed time. However, it appears that the discrete nature of point sampling

misses the context of these changes. We conclude that the samples collected at monthly intervals can provide coarse temporal patterns, but do not offer sufficient resolution to identify processes that drive stream pCO_2 on a seasonal scale.

3.6.4 Assessment of Parameter Uncertainty

Calculations of pCO_2 are sensitive to error in field measurements of pH. Variations in the accuracy of measured pH are probable, but there is no evidence to indicate directionality of these errors [*Jones et al.*, 2003]. It is also possible that there were sources of noncarbonate alkalinity that could contribute to an over estimation of pCO_2, specifically organic acids or mineral rich groundwater. However, neither of these appear to be major sources of error, as a regression between direct pCO_2 measurements agreed well (Figure D.10) with a series of pCO_2 calculations made with the methods described in this study. Additionally, direct measurements are in close agreement with monthly averaged calculated pCO_2 along the W1 transect (Figure 3.4). This result gives us confidence in our calculated values and the use of mean site averages as predictors of transect profile variability. Other work that has calculated values of pCO_2 report method accuracy of 10% of the true value [*Raymond et al.,* 1997], which is a safe confidence interval for the values reported here.

We also sought to test the temporal stability of the alkalinity in HJA water samples over time, to assess directional error introduced by variable sample-processing intervals, eight random samples were processed within the initial 7 day window, then again 31 days later (Figure D.9). Results show no evident change in alkalinity (r^2 =0.997; slope = 1.0098), with differences within the detection limit of the autotitrator. This result

suggests that alkalinity in surface water samples collected from the HJA are stable over this time period.

3.7 Conclusions

Stream pCO_2 across the HJA was consistently supersaturated with respect to atmospheric concentrations and exhibited strong spatial and temporal variability. Declines in pCO_2 were observed at the watershed scale with increasing distance from headwaters, but results at the reach-scale did not exhibit clear patterns in the downstream direction. We find strong negative relationships between stream pCO_2 and stream discharge, calculated mean velocity and calculated carbon dioxide gas transfer velocity. The correlation scale for pCO_2 appears to be less than 50 m in second-order Watershed 1, indicating that some of the processes that control CO_2 are highly variable at scales less than 50 m. This longitudinal variability underscores the importance of in-stream drivers of pCO_2 at reach and subreach scales. Stream pCO_2 shows generally higher concentrations during the summer and lower concentrations in the winter, with considerable intrannual variability. The distribution of CO_2 concentrations was larger in small streams than in large streams within the drainage network. Monthly sampling may provide approximate annual patterns in watershed pCO_2, but higher resolution sampling is needed to capture event-scale dynamics and to give context to discrete measurements. This work indicates the importance of measurement scale, and we find that use of coarse resolution pCO_2 data for flux estimates or spatial coverage may bias results to reflect local or transient conditions.

3.8 Acknowledgements

We conducted this research at HJ Andrews Experimental Forest, which is funded by the US Forest Service, Pacific Northwest Research Station. This work was funded by the National Science Foundation's Long-Term Ecological Research Program (DEB 08–23380), National Science Foundation grant (EAR 09-43570, U.S.), and the Hollis M. Dole fund in Environmental Geology at Oregon State University. Data will be made publically available through the HJ Andrews data catalog http://andrewsforest.oregonstate.edu/lter/data.cfm?frameURL=173

3.9 References

Aufdenkampe, A. K., E. Mayorga, P. A. Raymond, J. M. Melack, S. C. Doney, S. R. Alin, R. E. Aalto, and K. Yoo (2011), Riverine coupling of biogeochemical cycles between land, oceans, and atmosphere, *Front. Ecol. Environ.*, *9*, 53–60, doi:10.1890/100014.

Barnes, R. T., and P.A. Raymond (2009), The contribution of agricultural and urban activities to inorganic carbon fluxes within temperate watersheds. *Chemical Geology*, *266*, 318–327, doi:10.1016/j.chemgeo.2009.06.018.

Battin, T. J., L. A. Kaplan, S. Findlay, C. S. Hopkinson, E. Marti, A. I. Packman, J. D. Newbold, and F. Sabater (2008), Biophysical controls on organic carbon fluxes in fluvial networks, *Nat. Geosci.*, *1*, 95–100, doi:10.1038/ngeo101.

Battin, T. J., S. Luyssaert, L. A. Kaplan, A. K. Aufdenkampe, A. Richter, and L. J. Tranvik (2009), The boundless carbon cycle, *Nat. Geosci.*, *2*, 598–600, doi:10.1038/ngeo618.

Bianchi, T. S. et al. (2013), Enhanced transfer of terrestrially derived carbon to the atmosphere in a flooding event, *Geophys. Res. Lett.*, *40*, 116–122, doi:10.1029/2012GL054145.

Billett, M. F., and F. H. Harvey (2012), Measurements of CO_2 and CH_4 evasion from UK peatland headwater streams, *Biogeochemistry*, doi:10.1007/s10533-012-9798-9.

Bott, T. L., L. A. Kaplan, and F. T. Kuserk (1984), Benthic Bacterial Biomass Supported by Streamwater Dissolved Organic Matter, *Microb. Ecol.*, *10*, 335–344.

Boulton, A. J., S. Findlay, P. Marmonier, E. H. Stanley, A. J. Boulton, S. Findlay, P. Marmonier, E. H. Stanley, and H. M. Valett (1998), The functional significance of the hyporheic zone in streams and rivers, *Annu. Rev. Ecol. Syst.*, *29*, 59–81.

Butman, D., and P. A. Raymond (2011), Significant efflux of carbon dioxide from streams and rivers in the United States, *Nat. Geosci.*, *4*, 839-842, doi:10.1038/NGEO1294.

CCAL (2013), CCAL water analysis quality assurance plan. Oregon State University and United States Forest Service Cooperative Analytical Laboratory.

Cole, J., and N. Caraco (2001), Carbon in catchments: connecting terrestrial carbon losses with aquatic metabolism, *Mar. Freshw. Res.*, *52*, 101–110.

Cole, J. J., N. F. Caraco, G. W. Kling, and T. K. Kratz (1994), Carbon dioxide supersaturation in the surface waters of lakes, *Science*, *265*, 1568–1570.

Cole, J. J. et al. (2007), Plumbing the Global Carbon Cycle: Integrating Inland Waters into the Terrestrial Carbon Budget, *Ecosystems*, *10*, 172–185, doi:10.1007/s10021-006-9013-8.

Crawford, J. T., N. R. Lottig, E. H. Stanley, J. F. Walker, P. C. Hanson, J. C. Finlay, and R. G. Striegl (2014), CO2 and CH4 emissions from streams in a lake-rich landscape: Patterns, controls and regional significance, *Global Biogeochem. Cycles*, 197–210, doi:10.1002/2013GB004661.

Crawford, J. T., R. G. Striegl, K. P. Wickland, M. M. Dornblaser, and E. H. Stanley (2013), Emissions of carbon dioxide and methane from a headwater stream network of interior Alaska, *J. Geophys. Res. Biogeosciences*, *118*, 482–494, doi:10.1002/jgrg.20034.

Dawson, J. J., C. Bakewell, and M. F. Billett (2001), Is in-stream processing an important control on spatial changes in carbon fluxes in headwater catchments? *Sci. Total Environ.*, *265*, 153–67.

Demars, B. O. L., and J. R. Manson (2013), Temperature dependence of stream aeration coefficients and the effect of water turbulence: A critical review, Water Res., 47(1), 1–15, doi:10.1016/j.watres.2012.09.054.

Dinsmore, K. J., M. B. Wallin, M. S. Johnson, M. F. Billett, K. Bishop, J. Pumpanen, and A. Ojala (2013), Contrasting CO_2 concentration discharge dynamics in headwater streams: A multi-catchment comparison, *J. Geophys. Res. Biogeosciences*, *118*, 445–461, doi:10.1002/jgrg.20047.

Dosch, N. T. (2014), Spatiotemporal dynamics and drivers of stream pCO_2 in a headwater mountain catchment in the Cascade Mountains, Oregon. M.S. Thesis. Oregon State University.

Duarte, C. M., and Y. T. Prairie (2005), Prevalence of Heterotrophy and Atmospheric CO_2 Emissions from Aquatic Ecosystems, *Ecosystems*, *8*, 862–870, doi:10.1007/s10021-005-0177-4.

Dunne, T., and L. B. Leopold (1979), *Water in environmental planning*, New York, W.H. Freeman and Company, 818 p.

Dyrness, C. T. (1969), Hydrologic properties of soils on three small watersheds in the western cascades of Oregon. In *Res. Note PNW-111. Portland, OR: U.S. Department of Agriculture, Forest Service, Pacific Northwest Forest and Range Experiment Station,*17 p.

Fiedler, S., B. S. Höll, and H. F. Jungkunst (2006), Discovering the importance of lateral CO_2 transport from a temperate spruce forest., *Sci. Total Environ.*, *368*, 909–15, doi:10.1016/j.scitotenv.2006.03.038.

Findlay, S., D. Strayer, C. Goumbala, and K. Gould (1993), Metabolism of streamwater dissolved organic carbon in the shallow hyporheic zone, *Limnol. Oceanogr.*, *38*, 1493–1499, doi:10.4319/lo.1993.38.7.1493.

Franken, R. M. J., R. G. Storey, and D. D. Williams (2001), Biological, chemical and physical characteristics of downwelling and upwelling zones in the hyporheic zone of a north-temperate stream. Hydrobiologia, 444, 183-195.

Hall, R. O., T. a. Kennedy, and E. J. Rosi-Marshall (2012), Air-water oxygen exchange in a large whitewater river, *Limnol. Oceanogr. Fluids Environ.*, *2*, 1–11, doi:10.1215/21573689-1572535.

Hope, D., S. M. Palmer, M. F. Billett, and J. J. C. Dawson (2001), Carbon dioxide and methane evasion from a temperate peatland stream, *Limnol. Oceanogr.*, *46*, 847–857, doi:10.4319/lo.2001.46.4.0847.

Hope, D., S. M. Palmer, M. F. Billett, and J. J. C. Dawson (2004), Variations in dissolved CO_2 and CH_4 in a first-order stream and catchment: an investigation of soil-stream linkages, *Hydrol. Process.*, *18*, 3255–3275, doi:10.1002/hyp.5657.

Humborg, C., C. M. Mörth, M. Sundbom, H. Borg, T. Blenckner, R. Giesler, and V. Ittekkot (2010), CO_2 supersaturation along the aquatic conduit in Swedish watersheds as constrained by terrestrial respiration, aquatic respiration and weathering, *Glob. Chang. Biol.*, *16*, 1966–1978, doi:10.1111/j.1365-2486.2009.02092.x.

Isaaks, E.H., and R. M. Srivastava (1989), An introduction to applied geostatistics, Oxford University Press, New York, 561 p.

Johnson, M., M. Billett, and K. Dinsmore (2010), Direct and continuous measurement of dissolved carbon dioxide in freshwater aquatic systems—method and applications, *Ecohydrology*, *3*, 68–78, doi:10.1002/eco.95.

Johnson, M. S., J. Lehmann, S. J. Riha, A. V. Krusche, J. E. Richey, J. P. H. B. Ometto, and E. G. Couto (2008), CO_2 efflux from Amazonian headwater streams represents a significant fate for deep soil respiration, *Geophys. Res. Lett.*, *35*, L17401, doi:10.1029/2008GL034619.

Jones, J. B., and P. J. Mulholland (1998a), Influence of drainage basin topography and elevation on carbon dioxide and methane supersaturation of stream water, *Biogeochemistry*, *40*, 57–72, doi:10.1023/A:1005914121280.

Jones, J. B., and P.J. Mulholland (1998b), Carbon dioxide variation in a Hardwood Forest Stream : An Integrative Measure of Whole Catchment Soil Respiration. *Ecosystems*, 1, 183–196.

Jones, J. B., E. H. Stanley, and P. J. Mulholland (2003), Long-term decline in carbon dioxide supersaturation in rivers across the contiguous United States, *Geophys. Res. Lett.*, *30*, 0–3, doi:10.1029/2003GL017056.

Kasahara, T., and S. M. Wondzell (2003), Geomorphic controls on hyporheic exchange flow in mountain streams, *Water Resour. Res.*, *39*, SBH 3–1–SBH 3–14, doi:10.1029/2002WR001386.

Lauerwald, R., J. Hartmann, N. Moosdorf, S. Kempe, and P. a. Raymond (2013), What controls the spatial patterns of the riverine carbonate system? — A case study for North America, *Chem. Geol.*, *337-338*, 114–127, doi:10.1016/j.chemgeo.2012.11.011.

Leopold, L.B, and T. Maddock (1953), Hydraulic Geometry of Stream Channels and Some Physiological Implications, U.S. Government Printing Office, 57.

Millero, F. (1979), The thermodynamics of the carbonate system in seawater, *Geochimica Et Cosmochimica Acta*, *43*, 1651–1661.

Öquist, M. G., M. Wallin, J. Seibert, K. Bishop, and H. Laudon (2009), Dissolved inorganic carbon export across the soil/stream interface and its fate in a boreal headwater stream, *Environ. Sci. Technol.*, *43*, 7364–9.

Prasad, M. B. K., S. S. Kaushal, and R. Murtugudde (2013), Long-term pCO_2 dynamics in rivers in the Chesapeake Bay watershed. *Applied Geochemistry*, *31*, 209–215, doi:10.1016/j.apgeochem.2013.01.006.

Peter, H., G. A. Singer, C. Preiler, P. Chiffard, G. Steniczka, and T. J. Battin (2014), Scales and drivers of temporal pCO_2 dynamics in an Alpine stream, *J. Geophys. Res. Biogeosciences*, doi:10.1002/2013JG002552.Received.

Raymond, P. A et al. (2013), Global carbon dioxide emissions from inland waters, *Nature*, *503*, 355–9, doi:10.1038/nature12760.

Raymond, P., N. Caraco, and J. Cole (1997), Carbon dioxide concentration and atmospheric flux in the Hudson River, *Estuaries*, *20*, 381–390.

Raymond, P., N. Oh, R. Turner, and W. Broussard (2008), Anthropogenically enhanced fluxes of water and carbon from the Mississippi River, *Nature*, *451*(January), 449–452, doi:10.1038/nature06505.

Raymond, P. a., C. J. Zappa, D. Butman, T. L. Bott, J. Potter, P. Mulholland, a. E. Laursen, W. H. McDowell, and D. Newbold (2012), Scaling the gas transfer velocity and hydraulic geometry in streams and small rivers, *Limnol. Oceanogr. Fluids Environ.*, *2*, 41–53, doi:10.1215/21573689-1597669.

Richey, J. E., J. M. Melack, A. K. Aufdenkampe, V. M. Ballester, and L. L. Hess (2002), Outgassing from Amazonian rivers and wetlands as a large tropical source of atmospheric CO_2, *Nature*, *416*, 617–20, doi:10.1038/416617a.

Roberts, B. J., P. J. Mulholland, and W. R. Hill (2007), Multiple Scales of Temporal Variability in Ecosystem Metabolism Rates: Results from 2 Years of Continuous Monitoring in a Forested Headwater Stream, *Ecosystems*, *10*, 588–606, doi:10.1007/s10021-007-9059-2.

Rothacher, J., C. T. Dyrness, and R. L. Fredriksen (1967), Hydrologic and related characteristics of three small watersheds in the Oregon Cascades. In *Portland, OR: U.S. Department of Agriculture, Forest Service, Pacific Northwest Forest and Range Experiment Station*, 54 p.

Schindler, J., and D. Krabbenhoft (1998), The hyporheic zone as a source of dissolved organic carbon and carbon gases to a temperate forested stream, *Biogeochemistry*, *43*, 157–174.

Stets, E., and R. Striegl (2012), Carbon export by rivers draining the conterminous United States, *Inl. Waters*, *2*, 177–184, doi:10.5268/IW-2.4.510.

Striegl, R. G., M. M. Dornblaser, C. P. McDonald, J. R. Rover, and E. G. Stets (2012), Carbon dioxide and methane emissions from the Yukon River system, *Global Biogeochem. Cycles*, *26*, GB0E05, doi:10.1029/2012GB004306.

Stumm, W., and J. J. Morgan (1996), Aquatic Chemistry, Chemical Equilibria and Rates in Natural Waters, 3rd ed., John Wiley, New York.

Swanson, F. J., and M.E. James (1975), Geology and geomorphology of the H.J. Andrews Experimental Forest, Western Cascades, Oregon. In *Res. Pap. PNW-188. Portland, OR: U.S. Department of Agriculture, Forest Service, Pacific Northwest Forest and Range Experiment Station,* 14 p.

Tranvik, L. J. et al. (2009), Lakes and reservoirs as regulators of carbon cycling and climate, *Limnol. Oceanogr.*, *54*, 2298–2314.

van Heuven, S., D. Pierrot, J. W. B. Rae, E. Lewis, and D. W. R. Wallace (2011), MATLAB Program Developed for CO_2 System Calculations. ORNL/CDIAC-105b. Carbon Dioxide Information Analysis Center, Oak Ridge National Laboratory, U.S. Department of Energy, Oak Ridge, Tennessee. http://dx.doi.org/10.3334/CDIAC/ otg.CO2SYS_MATLAB_v1.1.

Vannote, R., G.W. Minshall, K.W. Cummins, J.R. Sedell, and C.E. Cushing (1980), The river continuum concept, *Canadian Journal of Fisheries and Aquatic Sciences*, *37*, 130–137.

Wallin, M., I. Buffam, M. Öquist, H. Laudon, and K. Bishop (2010), Temporal and spatial variability of dissolved inorganic carbon in a boreal stream network: Concentrations and downstream fluxes, *J. Geophys. Res.*, *115*, G02014, doi:10.1029/2009JG001100.

Wallin, M. B., M. G. Öquist, I. Buffam, M. F. Billett, J. Nisell, and K. H. Bishop (2011), Spatiotemporal variability of the gas transfer coefficient (K_{CO2}) in boreal streams: Implications for large scale estimates of CO_2 evasion, *Global Biogeochem. Cycles*, *25*, GB3025, doi:10.1029/2010GB003975.

Wanninkhof, R. (1992), Relationship Between Wind Speed and Gas Exchange Over the Ocean. *Journal of Geophysical Research*, *97*, 7373–7382.

Yvon-Durocher, G. et al. (2012), Reconciling the temperature dependence of respiration across timescales and ecosystem types., *Nature*, *487*, 472–6, doi:10.1038/nature11205.

4 Conclusion

We examined the dynamics of stream and hyporheic pCO_2 in headwater stream ecosystems located in H.J. Andrews Experimental Forest in the Western Cascades of Oregon. We conducted our data collection and analysis in two parts. The first part focused on temporal variability in and drivers of stream and hyporheic pCO_2 in Watershed 1, a small 95.5-ha catchment. We utilized high resolution pCO_2 measurements to observe seasonal and storm-driven patterns in hyporheic and stream pCO_2 and to evaluate the potential for hyporheic exchange flow to influence stream water pCO_2. The second part focused on spatial variability in stream pCO_2 within the 6400-ha Lookout Creek drainage network. We investigated physical and hydraulic drivers of spatial variation at the watershed scale and along longitudinal transects.

In Watershed 1, stream and hyporheic pCO_2 showed strong seasonal and event-scale variability with distinct stream and hyporheic dynamics during storm discharge events. By measuring and modeling hyporheic DIC, we estimate 37.5 kg-C yr^{-1} per watershed hectare (confidence interval 4.0–122.3 kg-C ha^{-1} yr^{-1}) is exported to the stream via hyporheic exchange flow. This result indicates that approximately one third of stream inorganic carbon export from the sum of CO_2 evasion and downstream advection originated in the hyporheic zone. Hyporheic exchange flow had greatest influence over stream pCO_2 during low and high baseflow, while CO_2 evasion had greatest influence during storm discharge events. These findings suggest that the hyporheic zone actively participates in carbon cycling in this headwater stream and continuously replenishes stream CO_2.

In the Lookout Creek drainage network, we calculated pCO_2 at 38 sites at monthly intervals over one year. We selected the sites to capture a range of spatial resolutions and to represent the physical variability of the catchment. Stream pCO_2 was consistently supersaturated with respect to atmospheric concentrations at all 38 locations. Stream pCO_2 ranged from atmospheric (~400 µatm) to 20 times atmospheric concentrations (8150 µatm) and exhibited strong spatial and temporal variability. The distribution of pCO_2 over the study period was different in small and large streams within the drainage network. At the watershed scale, pCO_2 decreased with distance downstream. At the reach scale, we did not detect clear patterns in the downstream direction. However, individual transects displayed persistent profile shape, with consistent high and low pCO_2 locations. We found negative relationships between stream pCO_2 and stream discharge, mean velocity and the carbon dioxide gas transfer velocity. Stream pCO_2 exhibited changes over short distances, with large changes in pCO_2 over less than 50 m. Longitudinal variability indicates spatial non-uniformity of in-stream controls on pCO_2 at this scale.

Our analysis of temporal dynamics in stream and hyporheic pCO_2 in Watershed 1 illustrates that high resolution temporal sampling captures event-scale dynamics and could provide context to discrete measurements. Larger-scale efforts in the Lookout Creek drainage network in turn indicate that the spatial scale at which stream pCO_2 is measured is important. The use of coarse resolution pCO_2 data for flux estimates or spatial coverage may bias results to reflect local or transient conditions. Future work will focus on combining these techniques to scale high-temporal resolution pCO_2 data longitudinally and across drainage networks.

BIBLIOGRAPHY

Aufdenkampe, A. K., E. Mayorga, P.A. Raymond, J. M. Melack, S. C. Doney, S. R. Alin, R. E. Aalto, and K. Yoo (2011), Riverine coupling of biogeochemical cycles between land, oceans, and atmosphere, *Front. Ecol. Environ.*, *9*, 53–60, doi:10.1890/100014.

Bard, Y. (1974), Nonlinear parameter estimation, Academic, San Diego, Calif.

Barnes, R. T., and P.A. Raymond (2009), The contribution of agricultural and urban activities to inorganic carbon fluxes within temperate watersheds. *Chemical Geology*, *266*, 318–327, doi:10.1016/j.chemgeo.2009.06.018.

Battin, T. J., L.A. Kaplan, S. Findlay, C. S. Hopkinson, E. Marti, A. I. Packman, J. D. Newbold, and F. Sabater (2008), Biophysical controls on organic carbon fluxes in fluvial networks, *Nat. Geosci.*, *1*, 95–100, doi:10.1038/ngeo101.

Battin, T. J., S. Luyssaert, L. A. Kaplan, A. K. Aufdenkampe, A. Richter, and L. J. Tranvik (2009), The boundless carbon cycle, *Nat. Geosci.*, *2*, 598–600, doi:10.1038/ngeo618.

Bencala, K. E. (2011), Stream–Groundwater Interactions, in Treatise on Water Science, edited by P. Wilderer, pp. 537-546, Academic Press, Oxford.

Bianchi, T. S. et al. (2013), Enhanced transfer of terrestrially derived carbon to the atmosphere in a flooding event, *Geophys. Res. Lett.*, *40*, 116–122, doi:10.1029/2012GL054145.

Billett, M. F., and F. H. Harvey (2012), Measurements of CO_2 and CH_4 evasion from UK peatland headwater streams, *Biogeochemistry*, doi:10.1007/s10533-012-9798-9.

Boano, F., J. W. Harvey, A. Marion, A. I. Packman, R. Revelli, L. Ridolfi, and A. Wörman (2014), Hyporheic flow and transport processes: Mechanisms, models, and biogeochemical implications, *Reviews of Geophysics*, 2012RG000417, doi:10.1002/2012RG000417.

Bott, T. L., L. A. Kaplan, and F. T. Kuserk (1984), Benthic Bacterial Biomass Supported by Streamwater Dissolved Organic Matter, *Microb. Ecol.*, *10*, 335–344.

Boulton, A. J., S. Findlay, P. Marmonier, E. H. Stanley, A. J. Boulton, S. Findlay, P. Marmonier, E. H. Stanley, and H. M. Valett (1998), The functional significance of the hyporheic zone in streams and rivers, *Annu. Rev. Ecol. Syst.*, *29*, 59–81.

Butman, D., and P. A. Raymond (2011), Significant efflux of carbon dioxide from streams and rivers in the United States, *Nat. Geosci.*, *4*, 839-842, doi:10.1038/NGEO1294.

CCAL (2013), CCAL water analysis quality assurance plan. Oregon State University and United States Forest Service Cooperative Analytical Laboratory.

Cole, J., and N. Caraco (2001), Carbon in catchments: connecting terrestrial carbon losses with aquatic metabolism, *Mar. Freshw. Res.*, *52*, 101–110.

Cole, J. J., N. F. Caraco, G. W. Kling, and T. K. Kratz (1994), Carbon dioxide supersaturation in the surface waters of lakes, *Science*, *265*, 1568–1570.

Cole, J. J. et al. (2007), Plumbing the Global Carbon Cycle: Integrating Inland Waters into the Terrestrial Carbon Budget, *Ecosystems*, *10*, 172–185, doi:10.1007/s10021-006-9013-8.

Crawford, J. T., N. R. Lottig, E. H. Stanley, J. F. Walker, P. C. Hanson, J. C. Finlay, and R. G. Striegl (2014), CO2 and CH4 emissions from streams in a lake-rich landscape: Patterns, controls and regional significance, *Global Biogeochem. Cycles*, 197–210, doi:10.1002/2013GB004661.

Crawford, J. T., R. G. Striegl, K. P. Wickland, M. M. Dornblaser, and E. H. Stanley (2013), Emissions of carbon dioxide and methane from a headwater stream network of interior Alaska, *J. Geophys. Res. Biogeosciences*, *118*, 482–494, doi:10.1002/jgrg.20034.

Davidson, E. A., R. O. Figueiredo, D. Markewitz, and A.K. Aufdenkampe (2010), Dissolved CO_2 in small catchment streams of eastern Amazonia: A minor pathway of terrestrial carbon loss. *Journal of Geophysical Research*, *115*, G04005. doi:10.1029/2009JG001202.

Dawson, J. J., C. Bakewell, and M. F. Billett (2001), Is in-stream processing an important control on spatial changes in carbon fluxes in headwater catchments? *Sci. Total Environ.*, *265*, 153–67.

Demars, B. O. L., and J. R. Manson (2013), Temperature dependence of stream aeration coefficients and the effect of water turbulence: A critical review, Water Res., 47(1), 1–15, doi:10.1016/j.watres.2012.09.054.

Dinsmore, K. J., M. B. Wallin, M. S. Johnson, M. F. Billett, K. Bishop, J. Pumpanen, and A. Ojala (2013), Contrasting CO_2 concentration discharge dynamics in headwater streams: A multi-catchment comparison, *J. Geophys. Res. Biogeosciences*, *118*, 445–461, doi:10.1002/jgrg.20047.

Dosch, N. T. (2014), Spatiotemporal dynamics and drivers of stream pCO_2 in a headwater catchment in the Western Cascade Mountains, Oregon. M.S. Thesis. Oregon State University.

Downing, J. A., J. J. Cole, C. M. Duarte, J. J. Middelburg, J. M. Melack, Y. T. Prairie, P. Kortelainen, R. G. Striegl, W. H. McDowell, and L. J. Tranvik (2012), Global abundance and size distribution of streams and rivers, *Inland Waters*, 2, 229-236, doi: 10.5268/IW-2.4.502.

Draper, N.R., and H. Smith (1981), *Applied regression analysis*, 2nd ed, John Wiley, New York.

Duarte, C. M., and Y. T. Prairie (2005), Prevalence of Heterotrophy and Atmospheric CO_2 Emissions from Aquatic Ecosystems, *Ecosystems*, *8*, 862–870, doi:10.1007/s10021-005-0177-4.

Dunne, T., and L. B. Leopold (1979), *Water in environmental planning*, New York, W.H. Freeman and Company, 818 p.

Dyrness, C. T. (1969), Hydrologic properties of soils on three small watersheds in the western cascades of Oregon. In *Res. Note PNW-111. Portland, OR: U.S. Department of Agriculture, Forest Service, Pacific Northwest Forest and Range Experiment Station,*17 p.

Fiedler, S., B. S. Höll, and H. F. Jungkunst (2006), Discovering the importance of lateral CO_2 transport from a temperate spruce forest., *Sci. Total Environ., 368*, 909–15, doi:10.1016/j.scitotenv.2006.03.038.

Findlay, S., D. Strayer, C. Goumbala, and K. Gould (1993), Metabolism of streamwater dissolved organic carbon in the shallow hyporheic zone. *Limnology and Oceanography, 38*, 1493–1499.

Franken, R. M. J., R. G. Storey, and D. D. Williams (2001), Biological, chemical and physical characteristics of downwelling and upwelling zones in the hyporheic zone of a north-temperate stream. Hydrobiologia, 444, 183-195.

Grimm, N., and S. Fisher (1984), Exchange between interstitial and surface water: implications for stream metabolism and nutrient cycling. *Hydrobiologia*, 111, 219-228.

Haggerty, R., S.W. Flemming, L.C. Meigs, and S.A. McKenna (2001), Tracer tests in a fractured dolomite 2. Analysis of mass transfer in single-well injection-withdrawal tests. *Water Resources Research*, 37, 1129-1142.

Hall, R. O., T. a. Kennedy, and E. J. Rosi-Marshall (2012), Air-water oxygen exchange in a large whitewater river, *Limnol. Oceanogr. Fluids Environ.*, *2*, 1–11, doi:10.1215/21573689-1572535.

Hood, E., M.N. Gooseff, and S.L. Johnson (2006), Changes in the character of stream water dissolved organic carbon during flushing in three small watersheds, Oregon. *Journal of Geophysical Research*, *111*, G01007, doi:10.1029/2005JG000082.

Hope, D., S. M. Palmer, M. F. Billett, and J. J. C. Dawson (2001), Carbon dioxide and methane evasion from a temperate peatland stream, *Limnol. Oceanogr.*, *46*, 847–857, doi:10.4319/lo.2001.46.4.0847.

Hope, D., S. M. Palmer, M. F. Billett, and J. J. C. Dawson (2004), Variations in dissolved CO_2 and CH_4 in a first-order stream and catchment: an investigation of soil-stream linkages, *Hydrol. Process.*, *18*, 3255–3275, doi:10.1002/hyp.5657.

Humborg, C., C. M. Mörth, M. Sundbom, H. Borg, T. Blenckner, R. Giesler, and V. Ittekkot (2010), CO_2 supersaturation along the aquatic conduit in Swedish watersheds as constrained by terrestrial respiration, aquatic respiration and weathering, *Glob. Chang. Biol.*, *16*, 1966–1978, doi:10.1111/j.1365-2486.2009.02092.x.

Isaaks, E.H., and R. M. Srivastava (1989), *An introduction to applied geostatistics*, Oxford University Press, New York, 561 p.

Johnson, M., M. Billett, and K. Dinsmore (2010), Direct and continuous measurement of dissolved carbon dioxide in freshwater aquatic systems—method and applications, *Ecohydrology*, *3*, 68–78, doi:10.1002/eco.95.

Johnson, M. S., J. Lehmann, S. J. Riha, A. V. Krusche, J. E. Richey, J. P. H. B. Ometto, and E. G. Couto (2008), CO_2 efflux from Amazonian headwater streams represents a significant fate for deep soil respiration, *Geophys. Res. Lett.*, *35*, L17401, doi:10.1029/2008GL034619.

Jones, J. B., and P. J. Mulholland (1998a), Influence of drainage basin topography and elevation on carbon dioxide and methane supersaturation of stream water, *Biogeochemistry*, *40*, 57–72, doi:10.1023/A:1005914121280.

Jones, J. B., and P.J. Mulholland (1998b), Carbon dioxide variation in a Hardwood Forest Stream : An Integrative Measure of Whole Catchment Soil Respiration. *Ecosystems*, 1, 183–196.

Jones, J. B., E. H. Stanley, and P. J. Mulholland (2003), Long-term decline in carbon dioxide supersaturation in rivers across the contiguous United States, *Geophys. Res. Lett.*, *30*, 0–3, doi:10.1029/2003GL017056.

Kasahara, T., and S. M. Wondzell (2003), Geomorphic controls on hyporheic exchange flow in mountain streams, *Water Resour. Res.*, *39*, SBH 3–1–SBH 3–14, doi:10.1029/2002WR001386.

Lauerwald, R., J. Hartmann, N. Moosdorf, S. Kempe, and P. a. Raymond (2013), What controls the spatial patterns of the riverine carbonate system? — A case study for North America, *Chem. Geol.*, *337-338*, 114–127, doi:10.1016/j.chemgeo.2012.11.011.

Leopold, L.B, and T. Maddock (1953), *Hydraulic Geometry of Stream Channels and Some Physiological Implications*, U.S. Government Printing Office, 57.

Millero, F. (1979), The thermodynamics of the carbonate system in seawater, *Geochimica Et Cosmochimica Acta*, *43*, 1651–1661.

Öquist, M. G., M. Wallin, J. Seibert, K. Bishop, and H. Laudon (2009), Dissolved inorganic carbon export across the soil/stream interface and its fate in a boreal headwater stream, *Environ. Sci. Technol.*, *43*, 7364–9.

Prasad, M. B. K., S. S. Kaushal, and R. Murtugudde (2013), Long-term pCO_2 dynamics in rivers in the Chesapeake Bay watershed. *Applied Geochemistry*, *31*, 209–215, doi:10.1016/j.apgeochem.2013.01.006.

Peter, H., G. A. Singer, C. Preiler, P. Chiffard, G. Steniczka, and T. J. Battin (2014), Scales and drivers of temporal pCO_2 dynamics in an Alpine stream, *J. Geophys. Res. Biogeosciences*, doi:10.1002/2013JG002552.Received.

Raymond, P. A et al. (2013), Global carbon dioxide emissions from inland waters, *Nature*, *503*, 355–9, doi:10.1038/nature12760.

Raymond, P., N. Caraco, and J. Cole (1997), Carbon dioxide concentration and atmospheric flux in the Hudson River, *Estuaries*, *20*, 381–390.

Raymond, P., N. Oh, R. Turner, and W. Broussard (2008), Anthropogenically enhanced fluxes of water and carbon from the Mississippi River, *Nature*, *451*(January), 449–452, doi:10.1038/nature06505.

Raymond, P. A., and J.E. Saiers (2010), Event controlled DOC export from forested watersheds. *Biogeochemistry*, *100*, 197–209. doi:10.1007/s10533-010-9416-7.

Raymond, P. a., C. J. Zappa, D. Butman, T. L. Bott, J. Potter, P. Mulholland, a. E. Laursen, W. H. McDowell, and D. Newbold (2012), Scaling the gas transfer velocity and hydraulic geometry in streams and small rivers, *Limnol. Oceanogr. Fluids Environ.*, *2*, 41–53, doi:10.1215/21573689-1597669.

Richey, J. E., J. M. Melack, A. K. Aufdenkampe, V. M. Ballester, and L. L. Hess (2002), Outgassing from Amazonian rivers and wetlands as a large tropical source of atmospheric CO_2, *Nature*, *416*, 617–20, doi:10.1038/416617a.

Roberts, B. J., P. J. Mulholland, and W. R. Hill (2007), Multiple Scales of Temporal Variability in Ecosystem Metabolism Rates: Results from 2 Years of Continuous Monitoring in a Forested Headwater Stream, *Ecosystems*, *10*, 588–606, doi:10.1007/s10021-007-9059-2.

Rothacher, J., C. T. Dyrness, and R. L. Fredriksen (1967), Hydrologic and related characteristics of three small watersheds in the Oregon Cascades. In *Portland, OR: U.S. Department of Agriculture, Forest Service, Pacific Northwest Forest and Range Experiment Station,* 54 p.

Schindler, J., and D. Krabbenhoft (1998), The hyporheic zone as a source of dissolved organic carbon and carbon gases to a temperate forested stream, *Biogeochemistry*, *43*, 157–174.

Sobczak, W. V., and S. Findlay (2002), Variation in bioavailability of dissolved organic carbon among stream hyporheic flowpaths, *Ecology*, 83, 3194–3209.

Stets, E., and R. Striegl (2012), Carbon export by rivers draining the conterminous United States, *Inl. Waters*, *2*, 177–184, doi:10.5268/IW-2.4.510.

Striegl, R. G., M. M. Dornblaser, C. P. McDonald, J. R. Rover, and E. G. Stets (2012), Carbon dioxide and methane emissions from the Yukon River system, *Global Biogeochem. Cycles*, *26*, GB0E05, doi:10.1029/2012GB004306.

Stumm, W., and J. J. Morgan (1996), *Aquatic Chemistry, Chemical Equilibria and Rates in Natural Waters*, 3rd ed., John Wiley, New York.

Swanson, F. J., and M.E. James (1975), Geology and geomorphology of the H.J. Andrews Experimental Forest, Western Cascades, Oregon. In *Res. Pap. PNW-188. Portland, OR: U.S. Department of Agriculture, Forest Service, Pacific Northwest Forest and Range Experiment Station,* 14 p.

Tranvik, L. J. et al. (2009), Lakes and reservoirs as regulators of carbon cycling and climate, *Limnol. Oceanogr.*, *54*, 2298–2314.

Valett, H. M., C. C. Hakenkamp, and A. J. Boulton (1993), Perspectives on the hyporheic zone: Integrating hydrology and biology. *Introduction, The North American Benthological Society*, 12, 40-43.

van Heuven, S., D. Pierrot, J. W. B. Rae, E. Lewis, and D. W. R. Wallace (2011), MATLAB Program Developed for CO_2 System Calculations. ORNL/CDIAC-105b.

Carbon Dioxide Information Analysis Center, Oak Ridge National Laboratory, U.S. Department of Energy, Oak Ridge, Tennessee. http://dx.doi.org/10.3334/CDIAC/otg.CO2SYS_MATLAB_v1.1.

Vannote, R., G.W. Minshall, K.W. Cummins, J.R. Sedell, and C.E. Cushing (1980), The river continuum concept, *Canadian Journal of Fisheries and Aquatic Sciences*, *37*, 130–137.

Voltz, T., M. Gooseff, A.S. Ward, K. Singha, M. Fitzgerald, and T. Wagener (2013). Riparian hydraulic gradient and stream-groundwater exchange dynamics in steep headwater valleys. *Journal of Geophysical Research: Earth Surface*, *118*, 953–969, doi:10.1002/jgrf.20074

Wallin, M., I. Buffam, M. Öquist, H. Laudon, and K. Bishop (2010), Temporal and spatial variability of dissolved inorganic carbon in a boreal stream network: Concentrations and downstream fluxes, *J. Geophys. Res.*, *115*, G02014, doi:10.1029/2009JG001100.

Wallin, M. B., M. G. Öquist, I. Buffam, M. F. Billett, J. Nisell, and K. H. Bishop (2011), Spatiotemporal variability of the gas transfer coefficient (K_{CO2}) in boreal streams: Implications for large scale estimates of CO_2 evasion, *Global Biogeochem. Cycles*, *25*, GB3025, doi:10.1029/2010GB003975.

Wallin, M. B., T. Grabs, I. Buffam, H. Laudon, Å. Agren, M. G. Öquist, and K. Bishop (2013), Evasion of CO_2 from streams - the dominant component of the carbon export through the aquatic conduit in a boreal landscape. *Global Change Biology*, *19*(3), 785–797, doi:10.1111/gcb.12083.

Wanninkhof, R. (1992), Relationship Between Wind Speed and Gas Exchange Over the Ocean. *Journal of Geophysical Research*, *97*, 7373–7382.

Ward, A. S., M. N. Gooseff, T. J. Voltz, M. Fitzgerald, K. Singha, and J. P. Zarnetske (2013), How does rapidly changing discharge during storm events affect transient storage and channel water balance in a headwater mountain stream? *Water Resources Research*, *49*, 5473–5486, doi:10.1002/wrcr.20434.

Wondzell, S. M. (2006), Effect of morphology and discharge on hyporheic exchange flows in two small streams in the Cascade Mountains of Oregon, USA. *Hydrological Processes*, *20*, 267–287, doi:10.1002/hyp.5902.

Wondzell, S. M. (2011), The role of the hyporheic zone across stream networks. *Hydrological Processes*, *25*, 3525–3532, doi:10.1002/hyp.8119.

Wondzell, S. M. (2012), Hyporheic zones in mountain streams: physical processes and ecosystem functions. *Stream Notes*, January-April 2012, Stream System Technology Center, Rocky Mountain Research Station, Ft. Collins, CO.

Yvon-Durocher, G. et al. (2012), Reconciling the temperature dependence of respiration across timescales and ecosystem types., *Nature*, *487*, 472–6, doi:10.1038/nature11205.

APPENDICES

Appendix A Monte Carlo Simulation Supporting Information

We performed a Monte Carlo simulation to constrain the total uncertainty of modeled hyporheic DIC export. We randomly selected values within the confidence bounds of parameters listed in Table A.1 and completed 10000 iterative calculations of DIC export according to (1), (2) and (3) from the text. Confidence intervals (CI) for model inputs that were time varying (i.e. stream discharge $\{Q_s\}$, and stream temperature $\{T_s\}$) were obtained from H.J. Andrews experimental Forest gauge station metadata. The confidence interval for apparent ecosystem activation energy (E_o) was obtained form *Yvon-Durocher et al.* [2012]. CIs for nonlinear parameters DIC_{max} and λ_o were calculated according to (A.1) [*e.g., Bard,* 1974; *Draper and Smith,* 1981; *Haggerty et al.,* 2001]. J is the Jacobian, which is the matrix of sensitivities to model output to the parameter estimates DIC_{max} and λ_o. σ is the common variance of the terms (assumed here to be RMSE according to *Haggerty et al.,* [2001]) and V_p is the first-order approximation to the parameter covariance matrix. Confidence intervals for Q_{hef} were calculated form the standard errors of the coefficients (Table A.1; *a* and *b*) of the regression model between Q_s and Q_{hef} according to (A.2). The mean of these 10000 models was used as a statistically representative value of hyporheic DIC export. We calculate 95 percent confidence intervals for total estimate uncertainty (Figure A.1, Table A.2). The percentage of stream inorganic carbon export originating in the hyporheic was calculated according to (A.3). To constrain the total error of this estimate, we performed a Monte Carlo simulation to calculate 1000 values of hyporheic DIC export (from this study) and

1000 values of total DIC export (the sum of stream DIC export and CO_2 evasion) with data from *Argerich et al.* [manuscript in preparation, 2014]. The percentage of hyporheic contribution to total inorganic carbon export was calculated 1000 times for each iterative calculation. The mean value was used as a representative percentage of hyporheic contribution, and the 95 percent confidence intervals were calculated for total uncertainty.

Table A.1 – Hyporheic DIC model parameter confidence intervals (CI)

Entity	Variable	Value	CI (±)	Units
Inputs - Time Varying				
	Q_s	-	0.10%	L s^{-1}
	T_s	-	1.0	°C
Derived Constants				
	E_o	0.58	0.14	eV
	λ_o	1.01E-02	3.96E-03	hr^{-1}
	DIC_{max}	5.04E-04	1.37E-04	mol L^{-1}
	a	-0.3279	0.63796	-
	b	-0.83	0.35304	-

$$V_p = \sigma^2 (J^T J)^{-1} \quad \text{(A.1)}$$

$$\%HZ = 0.47 {Q_s}^{-0.83} = 10^a {Q_s}^b \quad \text{(A.2)}$$

$$\%\, Export\ Hyporheic\ = \frac{Hyporheic\ DIC\ Export}{Stream\ DIC\ Export + CO_2\ Evasion} x\ 100 \quad \text{(A.3)}$$

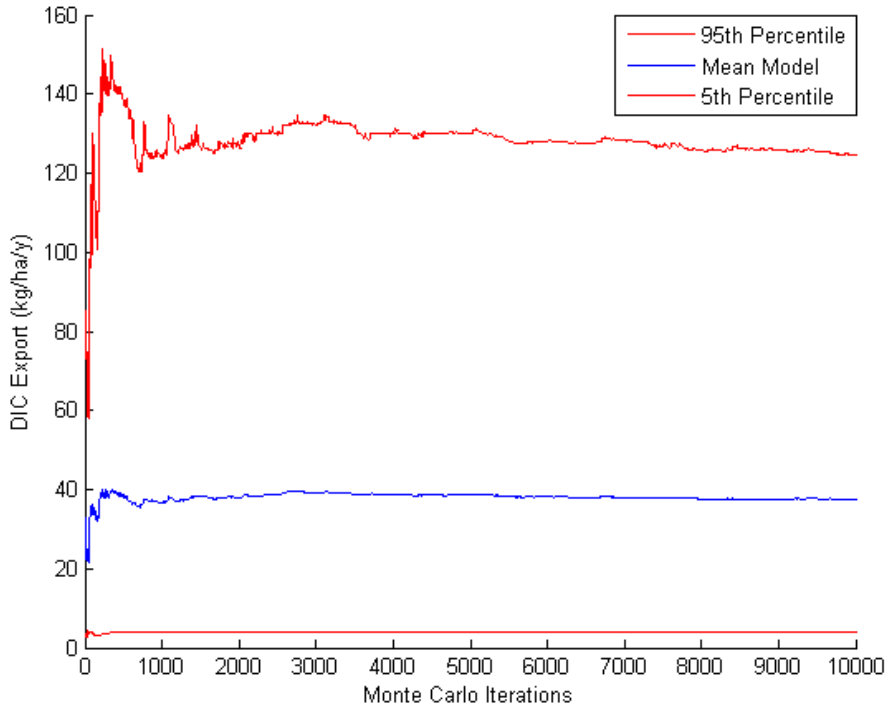

Figure A.1 - Monte Carlo simulation results for 10,000 iterations. Upper red line is the 95 percent confidence interval, the blue line is the mean model, and the lower red line is the 5 percent confidence interval. This figure shows these values as a function of iterations. Mean and 5% confidence interval show convergence after 1,000 -2,000 iterations, while 95% confidence interval reaches convergence near 10,000 iterations.

Table A.2 - Monte Carlo simulation results of hyporheic DIC export, 10,000 iterations

Mean Hyporheic Export (kg-C ha^{-1} yr^{-1})	37.5383
95 Percent Confidence interval (kg-C ha^{-1} yr^{-1})	122.3278
5 Percent confidence interval (kg-C ha^{-1} yr^{-1})	4.0314

Table A.3 - Monte Carlo simulation results of the percentage of total Watershed 1 DIC export originating from the hyporheic zone, 1000 iterations

Mean Hyporheic Contribution (%)	34.6
95 Percent Confidence Interval (%)	3.6
5 Percent Confidence Interval (%)	100.0

Appendix B Additional Figures and Tables Chapter 1

Table B.1 - Recovery in stream pCO_2 following fall/winter storms

Storm Event	Recovery Period		Stream pCO_2	Recovery		
				magnitude	% Increase	Rate of Recovery
	Date	time	µatm	µatm	%	µatm /day
1	1-Oct	13:30	607	333	55	41.8
	8-Oct	12:30	940			
2	9-Oct	13:30	853	512	60	33.6
	24-Oct	19:00	1365			
3	20-Nov	8:30	574	244	43	22.6
	1-Dec	3:00	818			
4	2-Dec	17:30	540	152	22	9.4
	18-Dec	23:00	692			
5	25-Dec	0:30	573	178	31	13.3
	7-Jan	9:00	751			
6	14-Jan	22:30	519	253	49	18.8
	28-Jan	9:00	772			
7	16-Mar	16:30	517	39	7.5	4.8
	24-Mar	20:00	556			

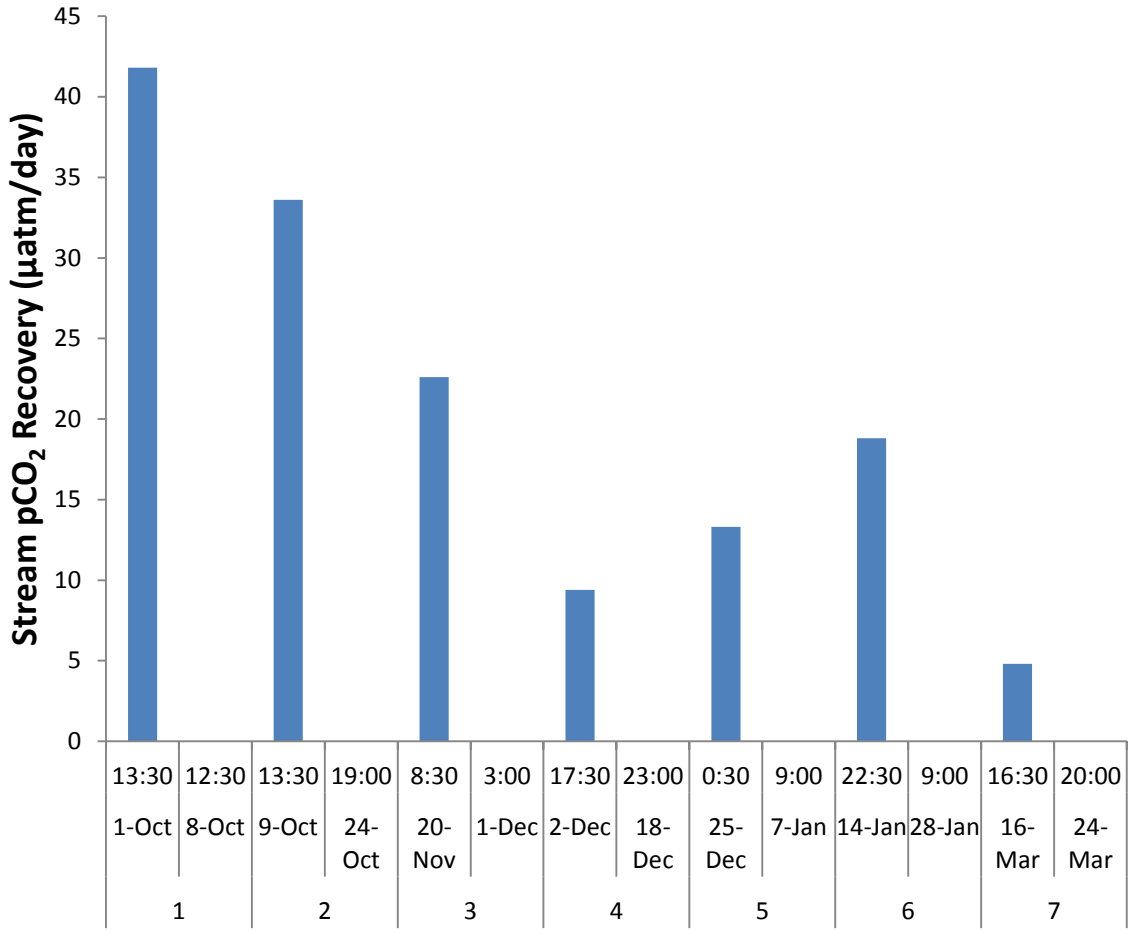

Figure B.1 – Rate of recovery in stream pCO_2 following fall/winter storms

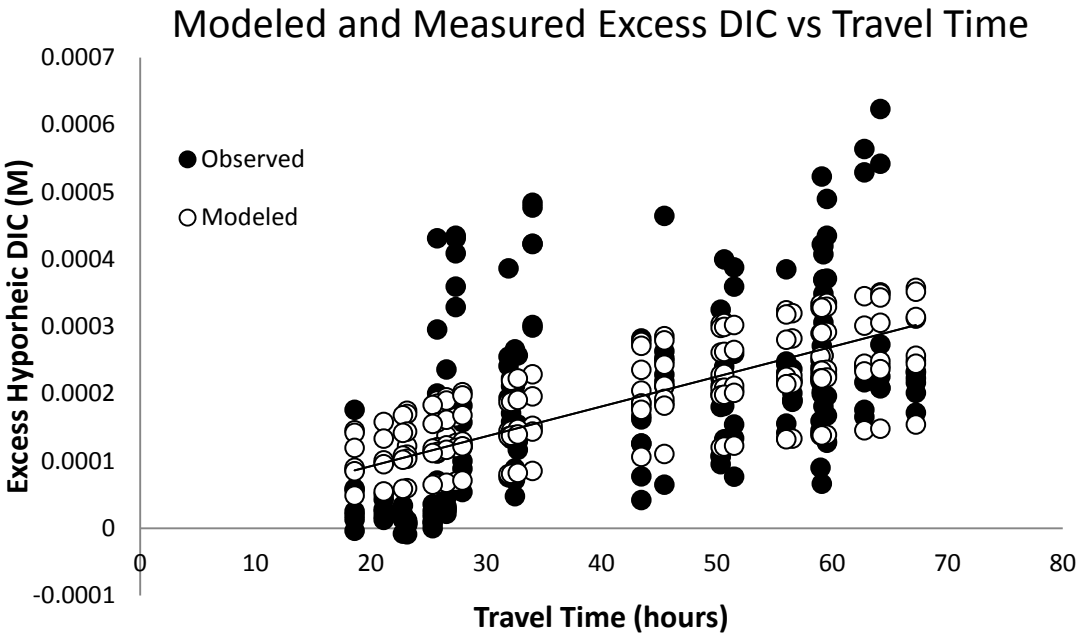

Figure B.2 - Modeled and Measured Excess hyporheic DIC with respect to travel time. Results of model calibration to lowest RMSE.

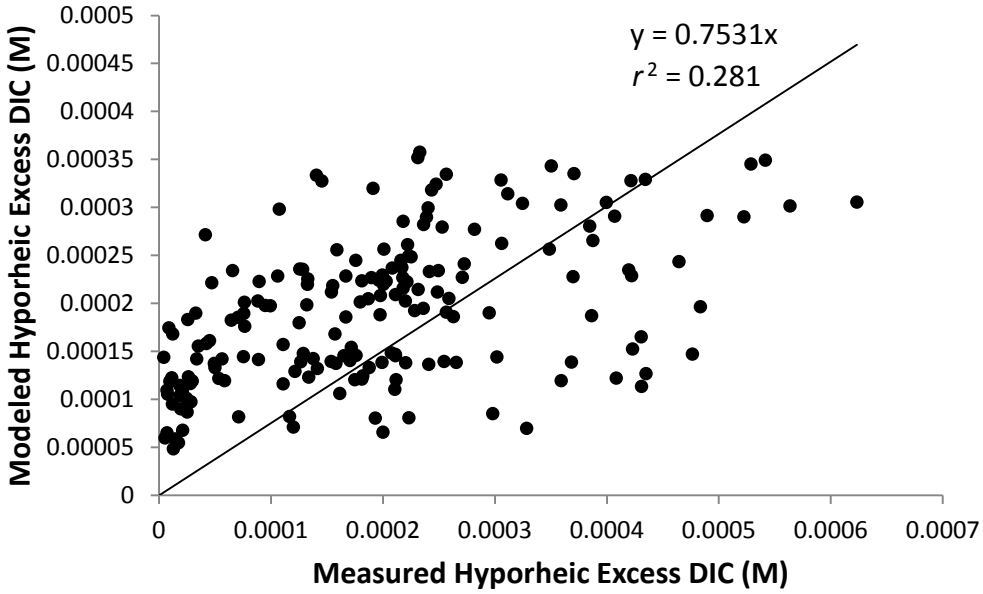

Figure B.3 – Model calibration results, modeled as a function of measured excess hyporheic DIC.

Appendix C Vaisala GMM220 CO_2 Module Modification/Implementation Instructions

The purpose of this appendix is to provide instructions for the modification of Vaisala CARBOCAP GMM220 CO_2 modules for aquatic deployment for continuous aquatic measurements of pCO_2. This method was adapted following :

Johnson, M., M. Billett, and K. Dinsmore (2010), Direct and continuous measurement of dissolved carbon dioxide in freshwater aquatic systems—method and applications, *Ecohydrology*, *3*, 68–78, doi:10.1002/eco.95.

Please refer to this publication for additional details on deployment and correction of sensor output.

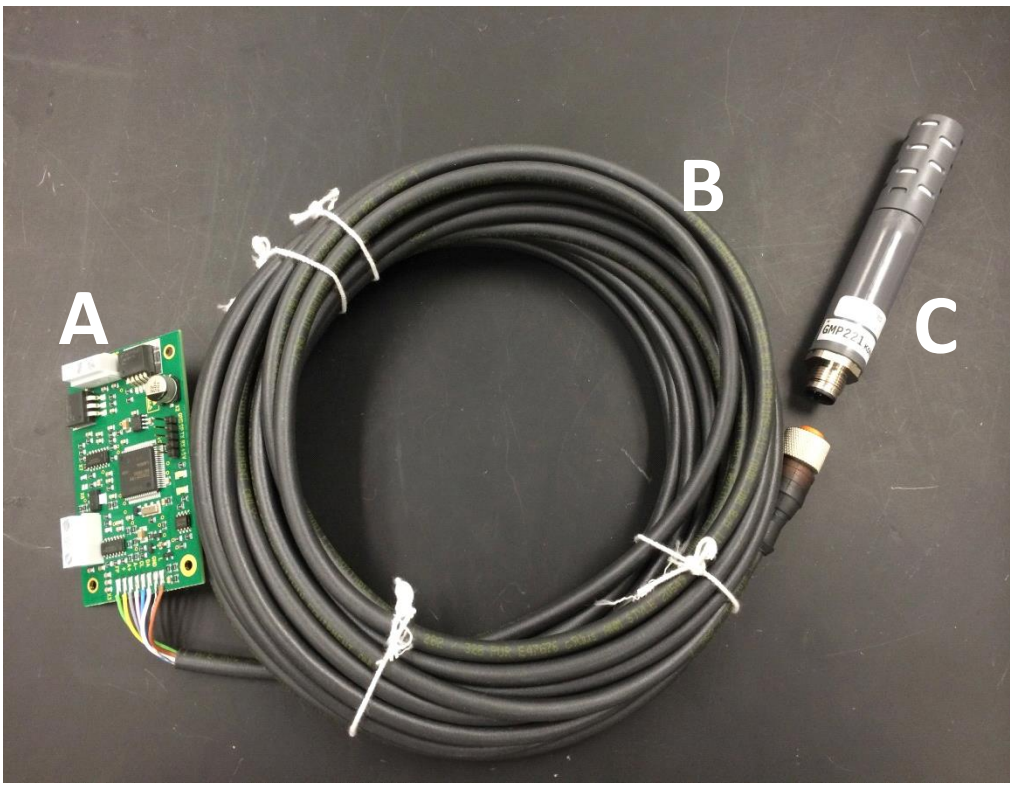

Figure C.1 - Overview of the Vaisala GMM 220 CO_2 probe pre-modification. Three main components (A) Component board (B) cable (C) CO_2 probe

Figure C.2 - Close-up view of the CO_2 probe. The infrared sensor is housed within the vented section. This will be sealed by the PTFE fabric.

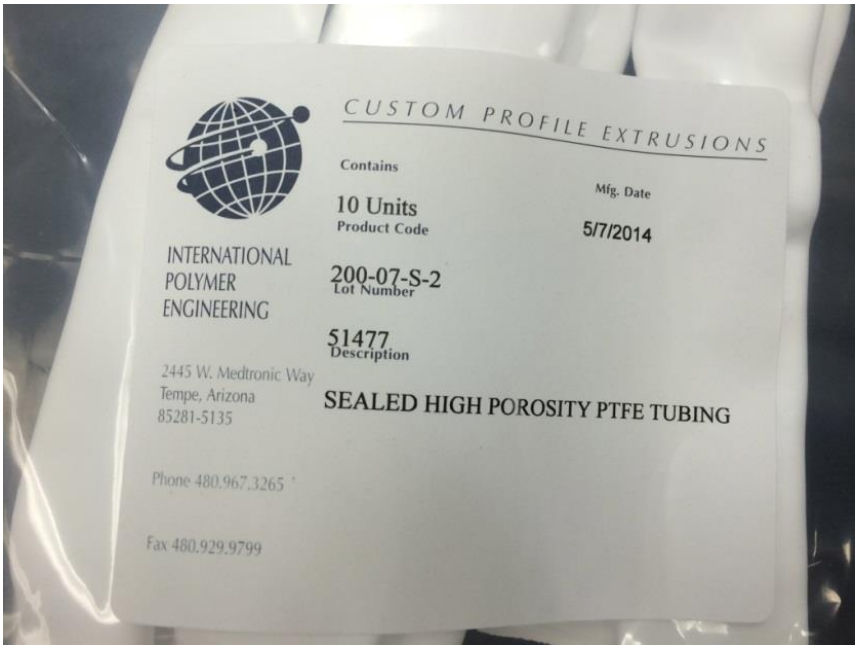

Figure C.3 - PTFE fabric used for the modification from International Polymer Engineering, Inc. This model is 200-07-S-2 and was sealed at one end like a sock.

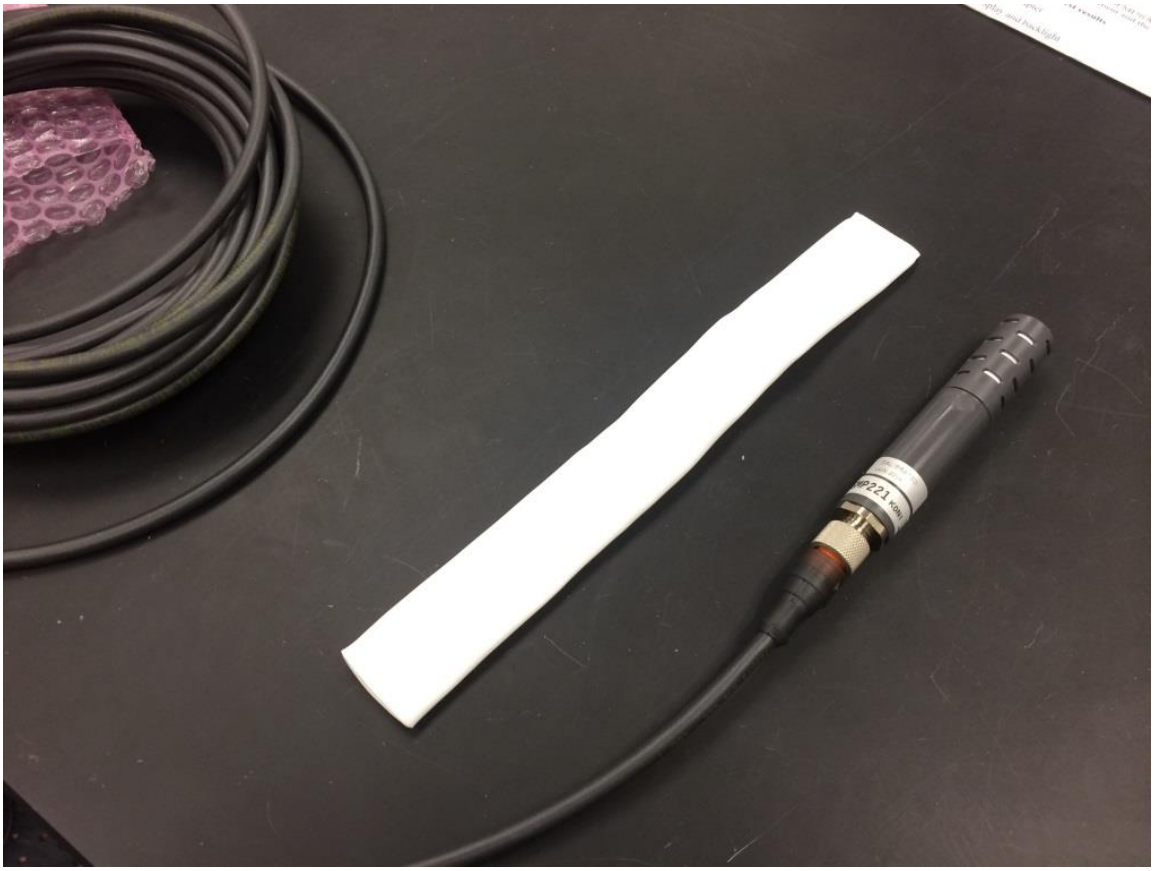

Figure C.4 - PTFE sleeve adjacent to Vaisala pCO_2 probe, here attached to the cable. The First step of modification is to place the probe inside the PTFE sleeve

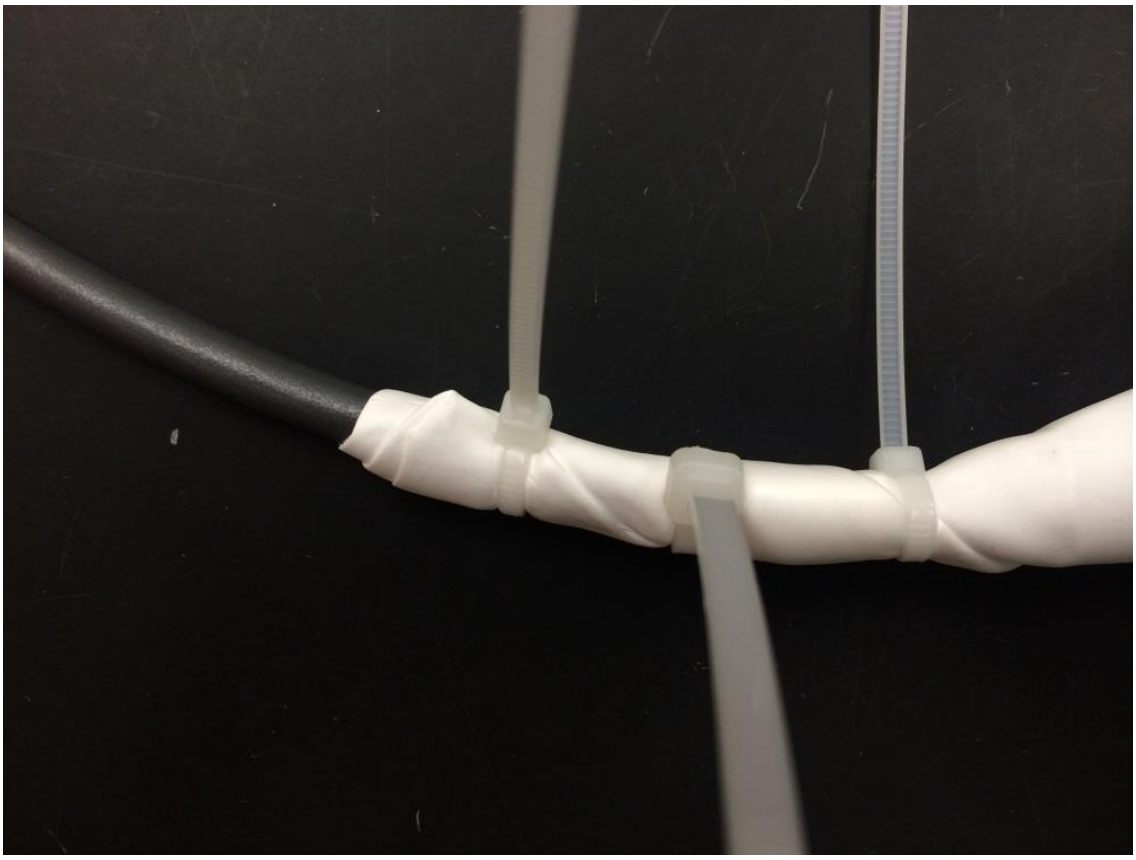

Figure C.5 - Once the probe is inside the PTFE sleeve, secure the open end around the cable by wrapping the loose sleeve tightly and securing with zip ties. We have used 3 zip ties in alternating orientations.

Figure C.6 - Trim the excess plastic from the zip ties. Make sure to be gentle with the PTFE tubing during this step – any abrasions or holes created may allow water to penetrate the sleeve and damage the sensor. If any holes in the PTFE fabric are identified, they must be patched during the next step of the modification process

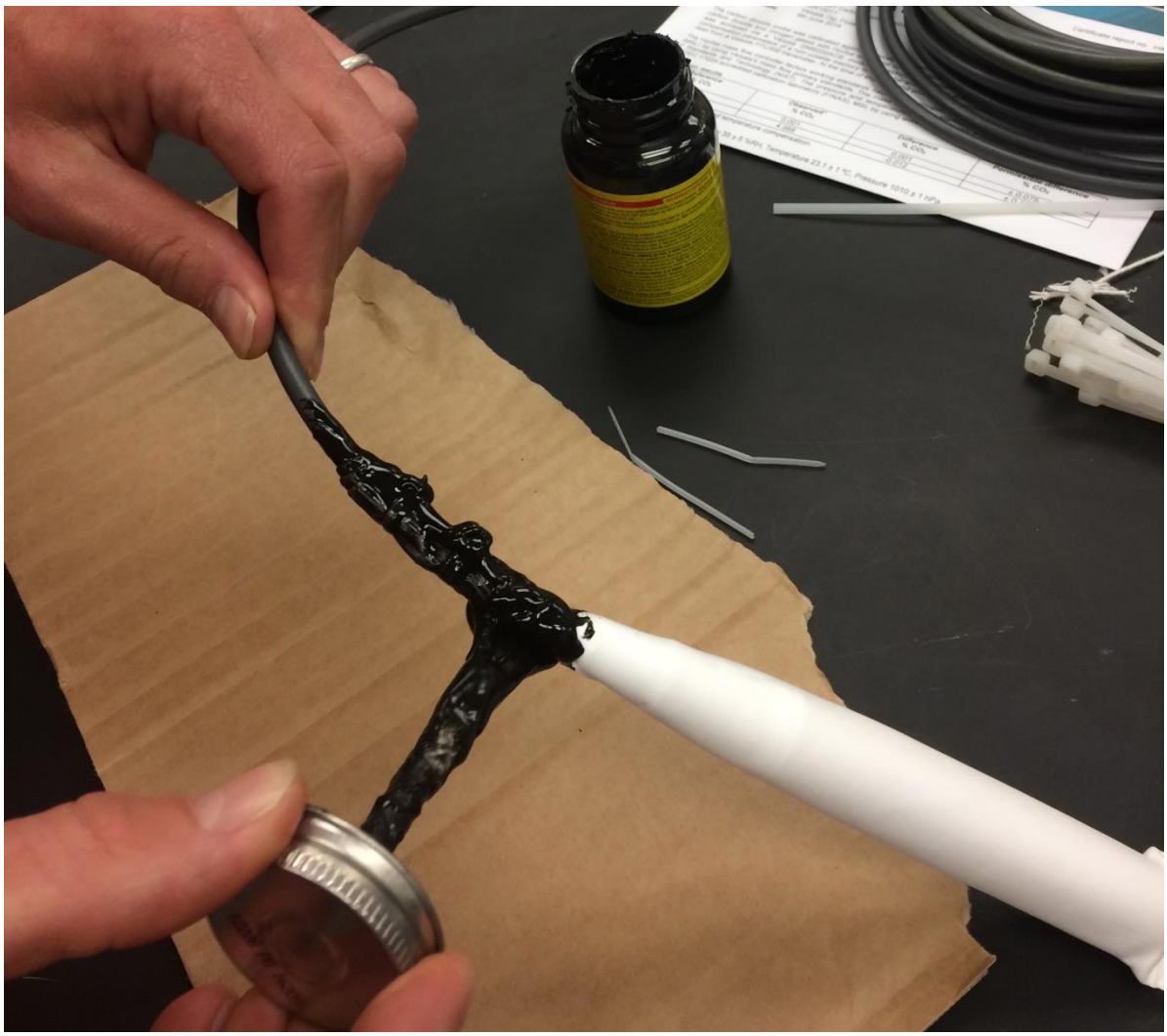

Figure C.7 - Apply a thick but even layer of Liquid Tape (Plasti Dip International, USA) with the brush applicator around the edge of the PTFE fabric and cable and the zip ties. Make sure to cover all places where water could enter the sleeve.

Figure C.8 - Apply the liquid tape above the zip ties and below the bottom of the PTFE. Look for any abrasions or rips in the fabric that require spot applications of liquid tape for waterproofing.

Figure C.9 - After the first layer is applied, allow the probe to dry in a well-ventilated area (i.e., fume hood) for 4-5 hours. Reapply an additional 3 to 4 layers of liquid tape in the same location. Make sure to look for bubbles or holes in the dry liquid tape. It is critical that there is a complete seal over the end of the probe. Once the 4^{th} or 5^{th} layer of liquid tape has been applied and given sufficient time to dry, the probe is ready for field deployment.

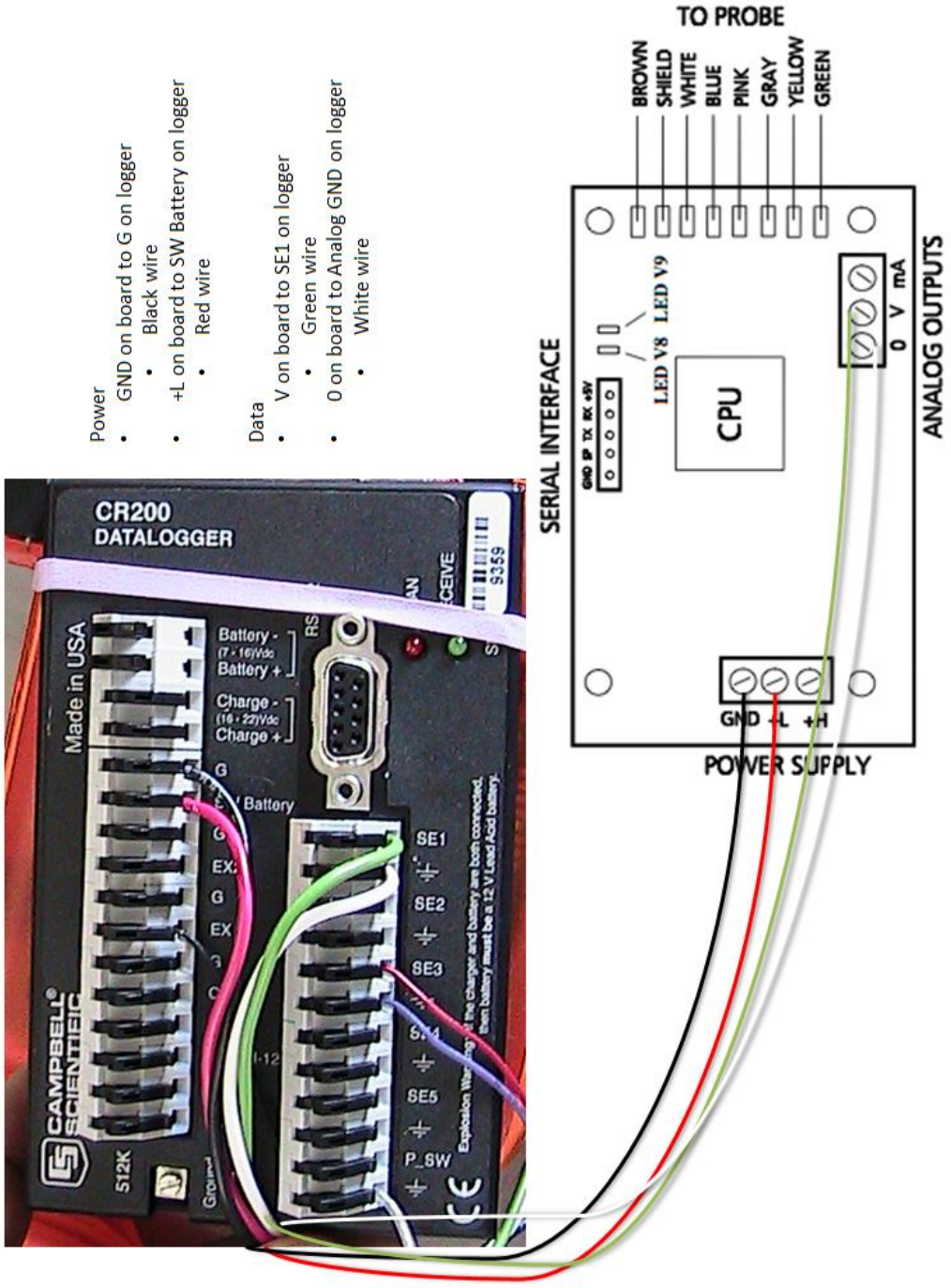

Figure C.10 - Schematic wiring diagram to connect a Vaisala GMM 220 pCO_2 probe to a Campbell C200 series data logger. The diagram on the upper right is the GMM 200 component board. Red and black wires are power supply and green and white are sensor output. The data logger needs to be attached to an external power source. We used a 12-V deep cycle car battery. Image courtesy of Dr. Mark Johnson.

Figure C.11 - Data logger and GMM 220 deployed in the field. This box contains the data logger. Cables leaving the box lead to the probe and external power supply.

Figure C.12 - GMM deployed in the field. Probe is attached to Styrofoam float below the surface of the stream. The cable leads to the data logger in the logger box in Figure C.11

Table C.1 - Material list for modified stream pCO_2 probe

Stream/hyporheic pCO2 measurement shopping list - Materials for one modified probe

Roy Haggerty and Nick Dosch, May 2014

	Item	Code	link to item	Company	Description	Number	Aproximate unit cost
1	NDIR Probe	GMM 220	http://www.vaisala.com/en/products/carbondioxide/Pages/GMM220.aspx	Vaisalla	This is the nondispersive infrared CO2 sensor	1	$870
2	PTFE sleve	200-07-S-2 F1	http://www.ipeweb.com/joomla/index.php/products/ptfe-tubes	International Polymer Engineering	This is the gas permeable but water impermeable sleeve to be fit to the outside of the probe before it can be submerged in water.	1	$39
3	Campbell datalogger	CR200X	http://www.campbellsci.com/cr200x	Campbell Scientific	CO2 and Temperature datalogger	1	$223
4	Temperature sensor	109-L	https://www.campbellsci.com/109-temperature	Campbell Scientific	Temperature probe	1	$108
5	Campbell Datalogger case	ENC 10/12R	https://www.campbellsci.com/enc10-12r-ordering	Campbell Scientific	Weatherproof Datalogger encolsure	1	$120
6	plasti dip liquid tape	Liquid Tape 4 oz	http://www.plastidip.com/home_solutions/Liquid_Tape	Plasti Dip International, Inc	Waterproof sealant to prevent water from entering the PTFE sleeve.	1	$10

Table C.2 - Additional items for probe modification

Additional items for construction/operation		
	Item	**Purpose**
7	zip ties	To secure the the PTFE sleeve to the cable and get a partial seal between the two. Plasti-dip liquid tape is required to achieve a full seal
8	electrical wire	Connect the logger to the power supply and the logger to the component board of the GMM 220
9	2" pvc	To be zip-tied around the modified probe with holes drilled for probe protection if deployed in stream
10	Deep cycle 12 volt battery	To power the system
11	Battery maintainer	If there is AC power nearby, this has been a useful item for us to keep a constant charge in the batteries

Appendix D Additional Figures and Tables Chapter 2

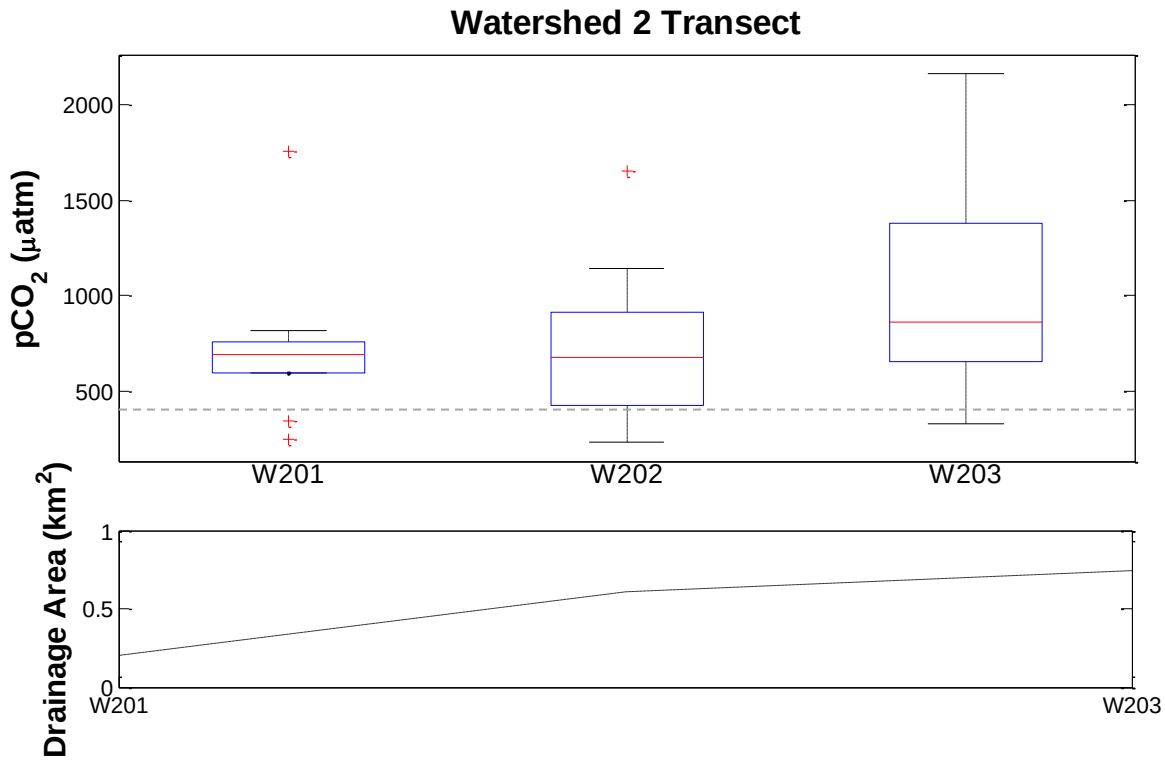

Figure D.1 - Longitudinal pCO_2 profile variability and contributing transect drainage area. Box plots show medians (red lines), quartiles (boxes), 90 percent confidence intervals (whiskers) and range (red plus symbols) of measured pCO_2 in Watershed 2 transect. The grey dotted line represents atmospheric concentrations of CO_2.

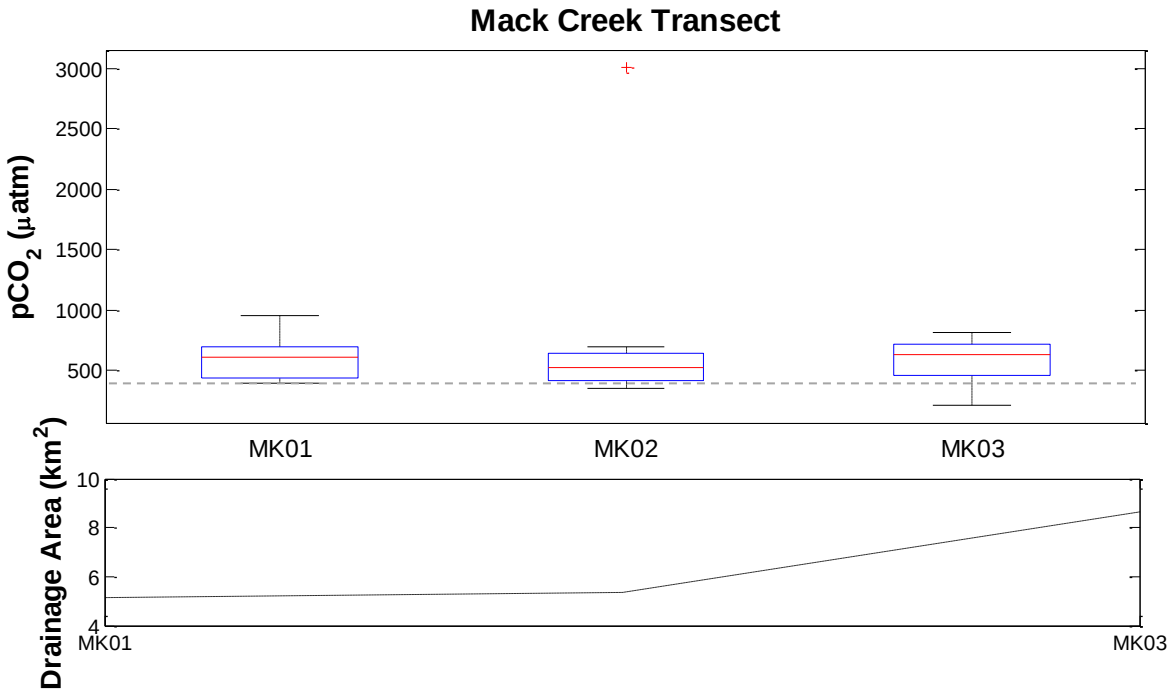

Figure D.2 - Longitudinal pCO_2 profile variability and contributing transect drainage area. Box plots show medians (red lines), quartiles (boxes), 90 percent confidence intervals (whiskers) and range (red plus symbols) of measured pCO_2 in Mack Creek transect. The grey dotted line represents atmospheric concentrations of CO_2.

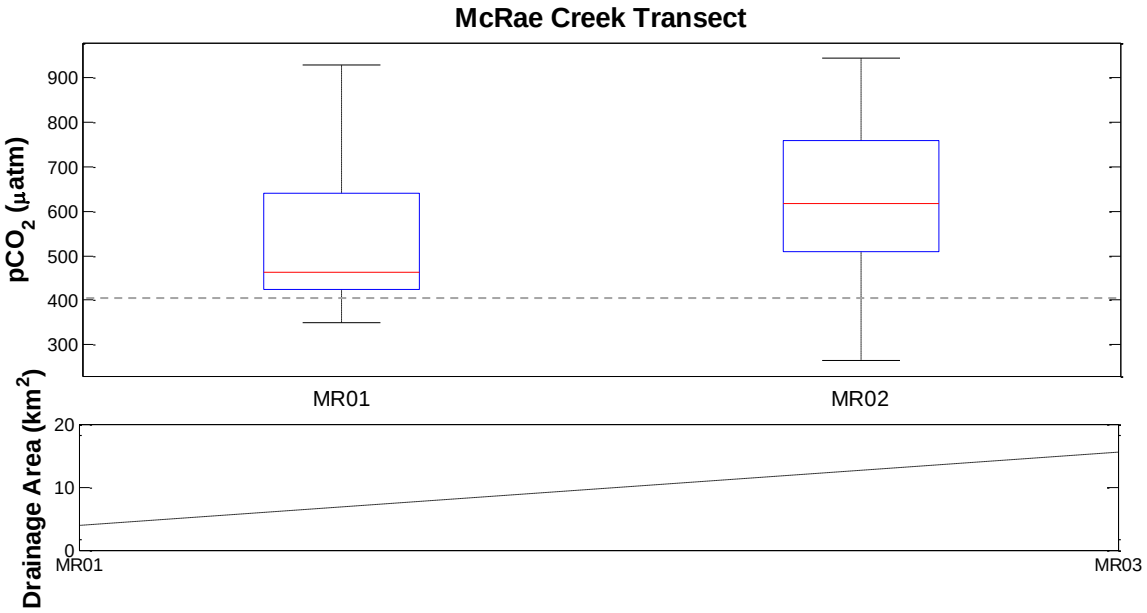

Figure D.3 - Longitudinal pCO_2 profile variability and contributing transect drainage area. Box plots show medians (red lines), quartiles (boxes), 90 percent confidence intervals (whiskers) and range (red plus symbols) of measured pCO_2 in McRae Creek transect. The grey dotted line represents atmospheric concentrations of CO_2.

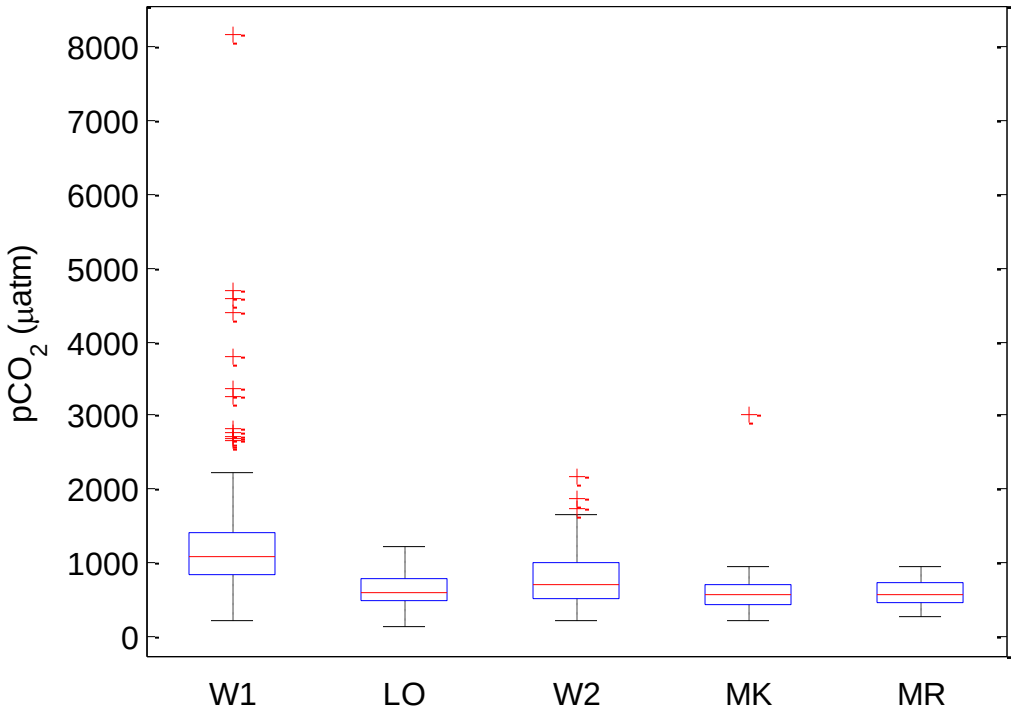

Figure D.4 - Box plots show medians (red lines), quartiles (boxes), 90 percent confidence intervals (whiskers) and range (red plus symbols) of measured pCO_2 in the 5 longitudinal transects. W1 and W2 are significantly different than the other transects (One-way ANOVA test, $p < 0.001$)

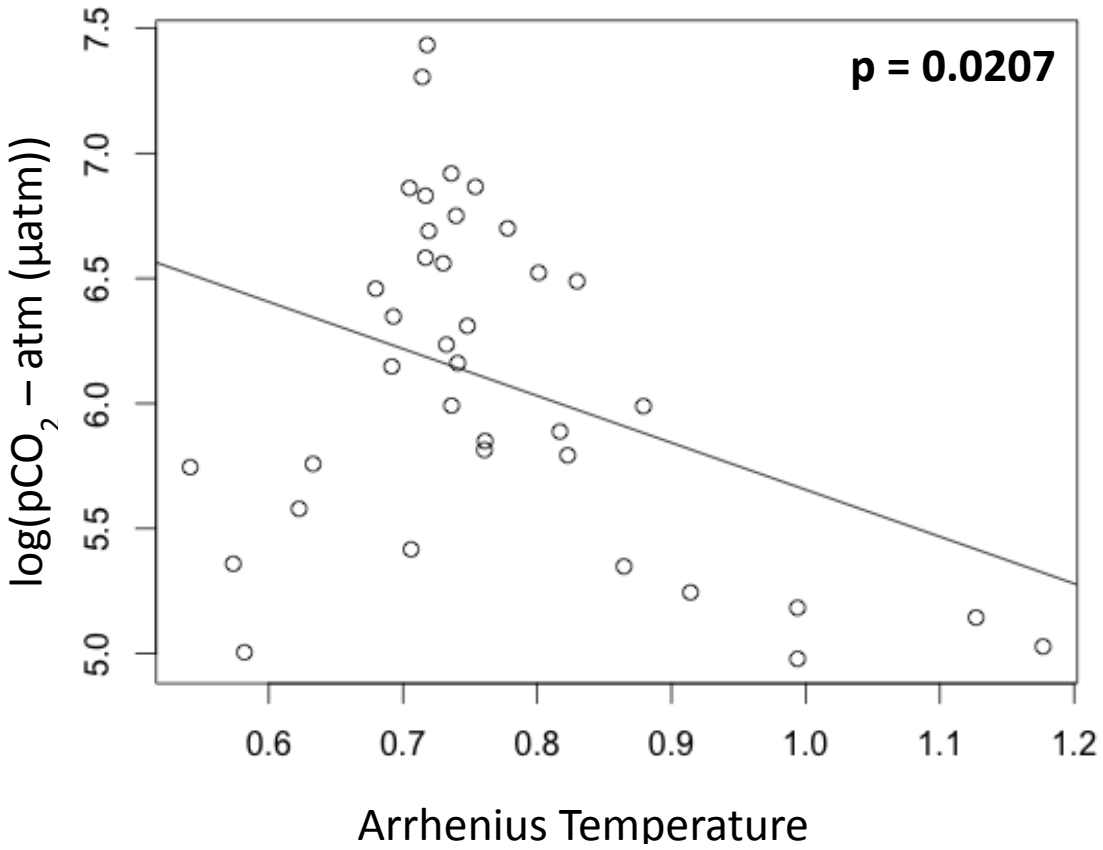

Figure D.5 - Linear regression of Arrhenius temperature normalized to a reference temperature (15 ºC) and the logarithm of mean site stream pCO_2 minus atmospheric pCO_2.

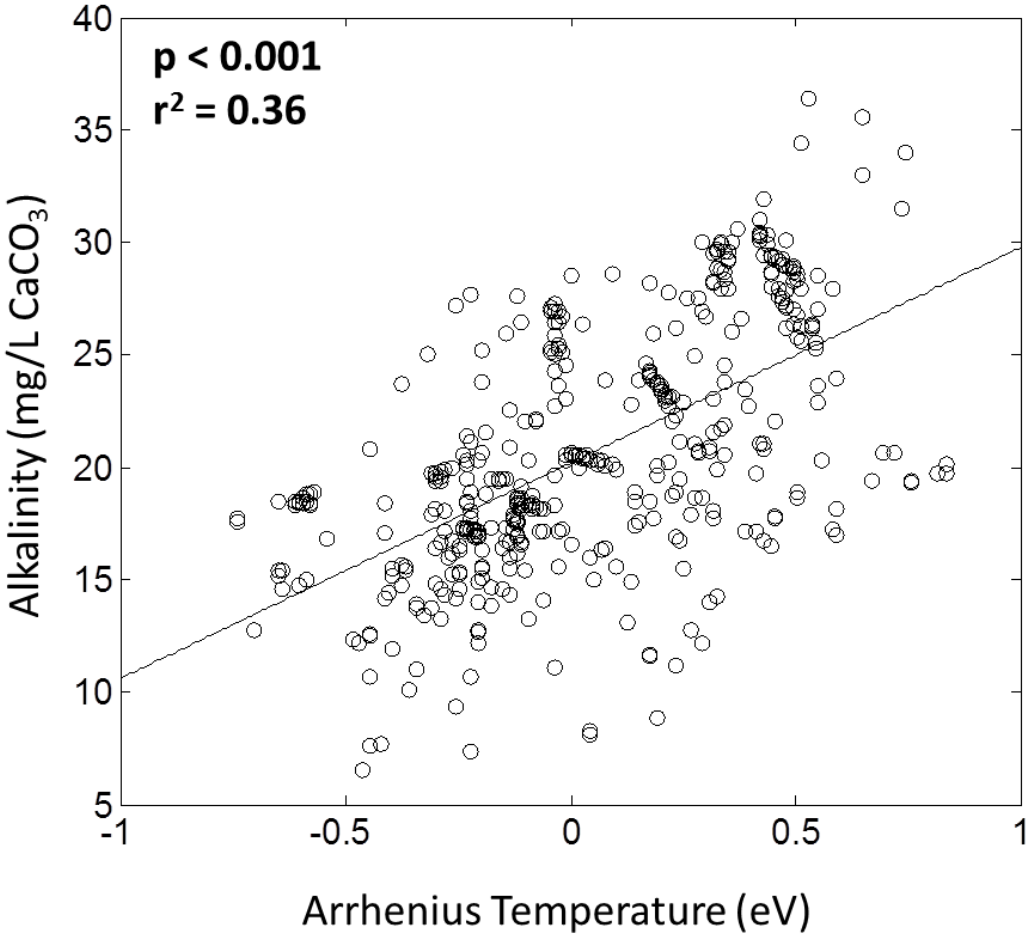

Figure D.6 - Linear regression of Arrhenius temperature normalized to a reference temperature (15 ºC) and carbonate alkalinity.

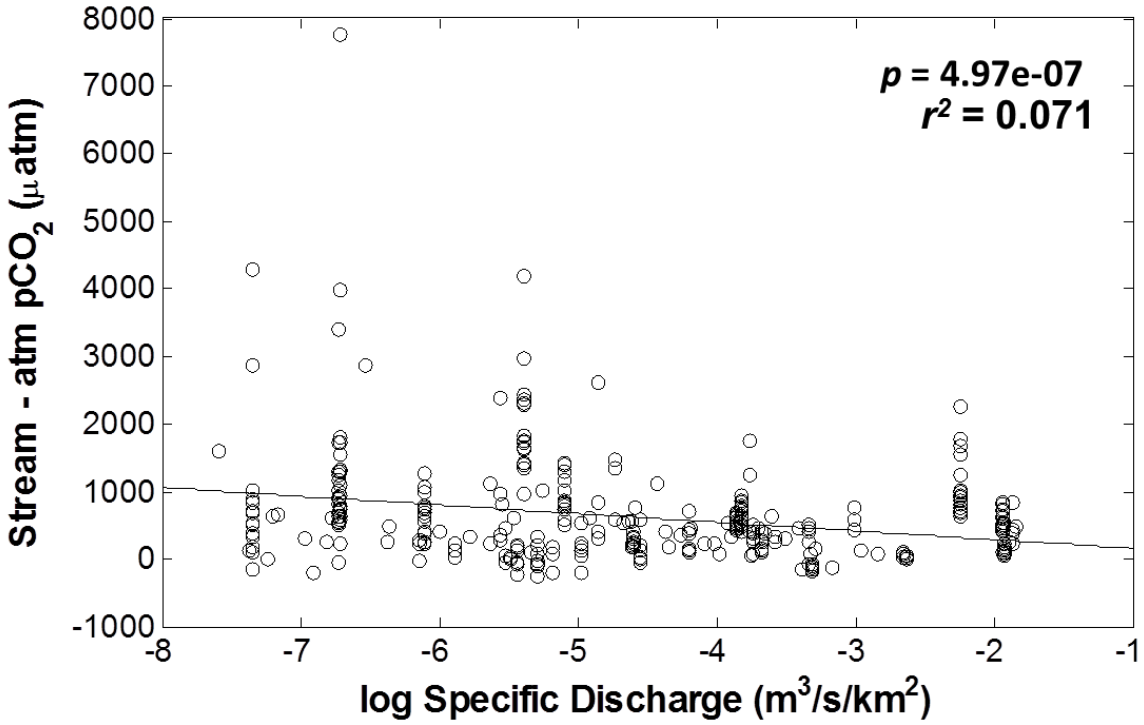

Figure D.7 – Regression between the log of specific discharge and excess stream pCO_2

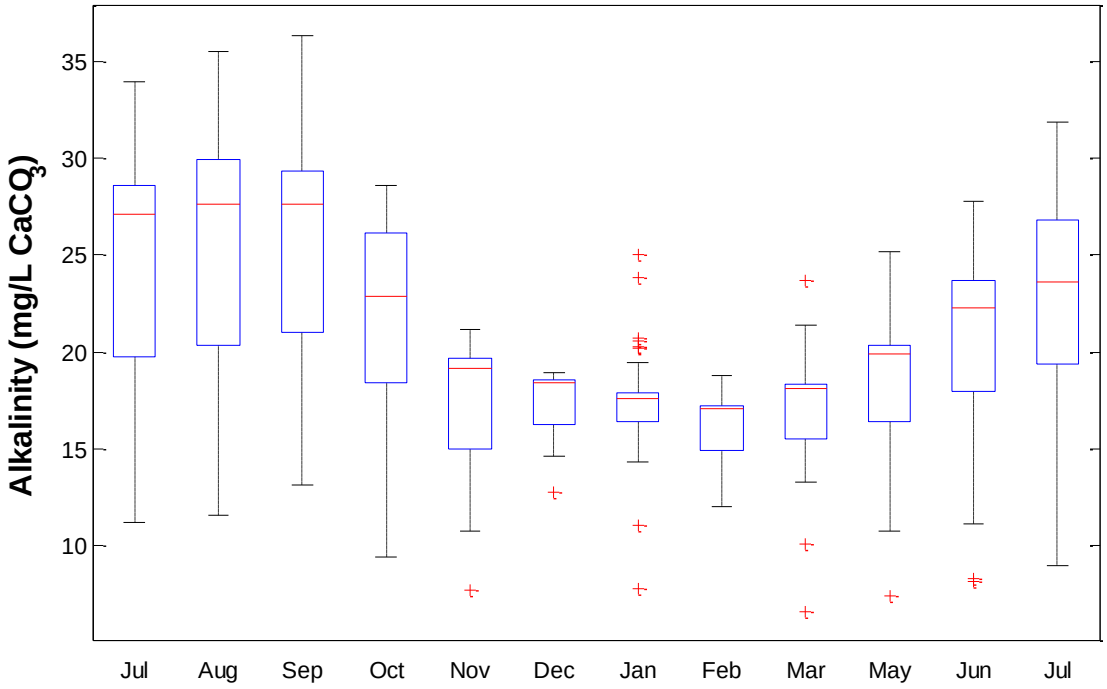

Figure D.8 - Annual variation in stream carbonate alkalinity from the Lookout Creek drainage network from July 2013 to July 2014. Box plots show medians (red lines), quartiles (boxes), 90 percent confidence intervals (whiskers) and range (red plus symbols) of measured alkalinity.

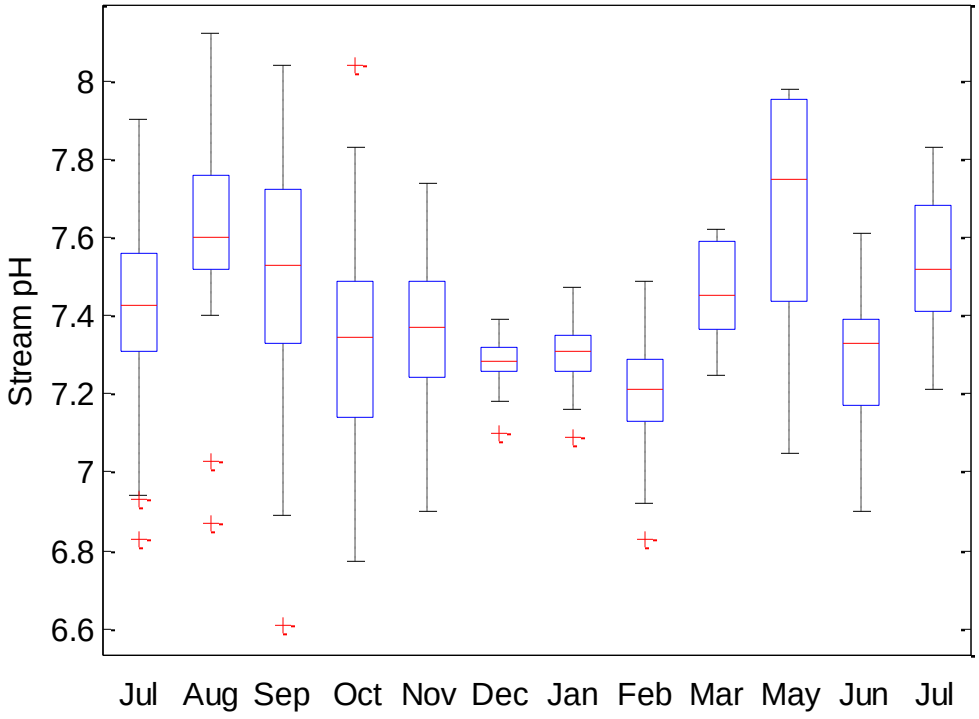

Figure D.9 - Annual variation in stream pH and from the Lookout Creek drainage network from July 2013 to July 2014. Box plots show medians (red lines), quartiles (boxes), 90 percent confidence intervals (whiskers) and range (red plus symbols) of measured pH.

Table D.1 - Time sensitivity error analysis in laboratory determination of carbonate alkalinity. 8 random samples from the February sampling round were selected and processed again 31 days later.

Sample Location	HCO_3-C (mg/L)	
	2/24/2014	3/27/2014
W203	3.62	3.59
W109	4.11	4.10
W1001	4.11	4.08
W110	4.09	4.05
W112	4.14	4.08
LO07	3.50	3.44
LO06	3.41	3.37
W108	4.14	4.10

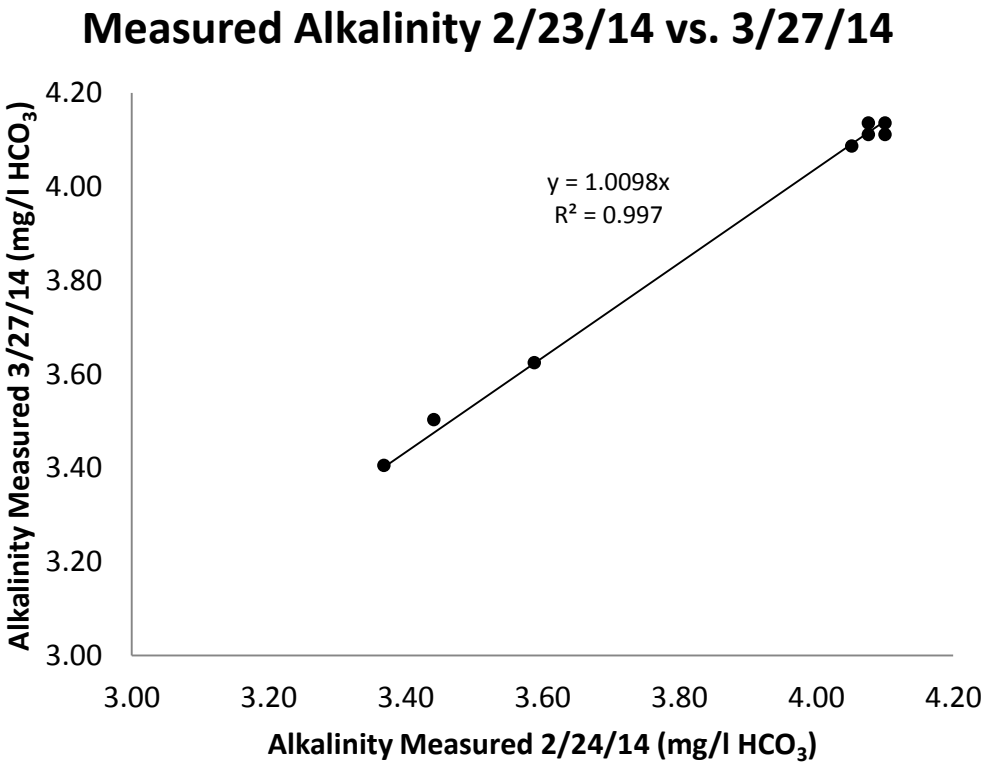

Figure D.10 - Alkalinity time sensitivity regression. Samples processed 31 days later show good agreement with samples processed according to standard procedure.

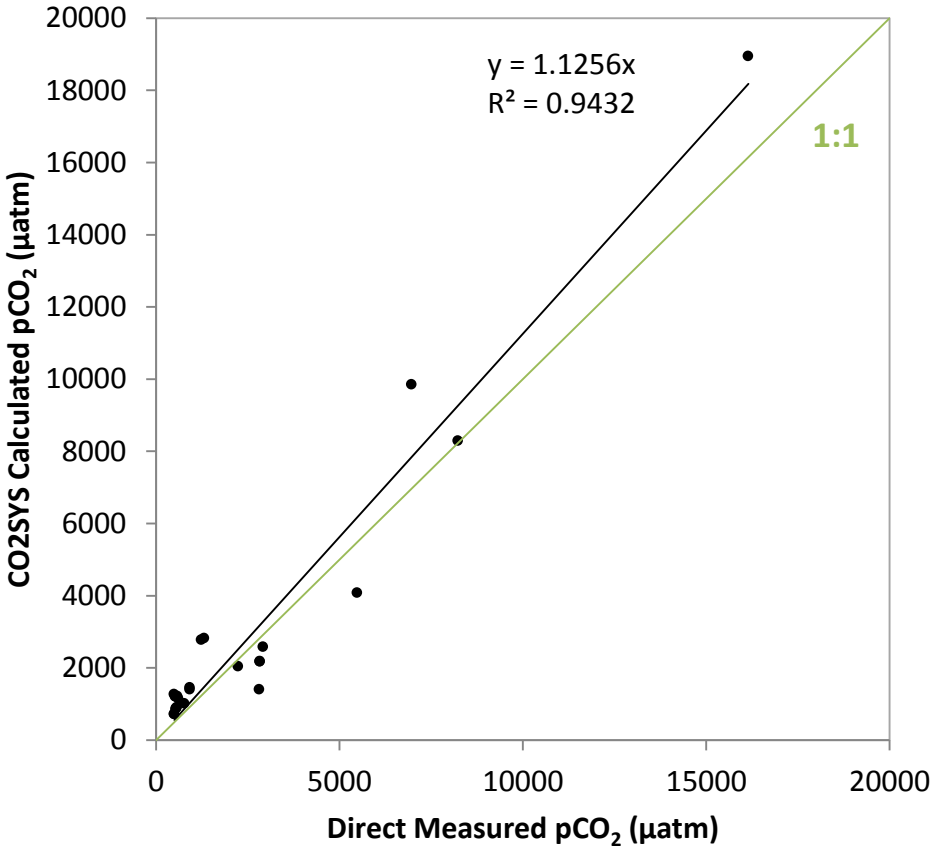

Figure D.11 - Directly measured pCO_2 and pCO_2 calculated with CO2SYS regression. The green line is the 1:1 line, simulating a perfect relationship. The regression indicates that calculated pCO_2 slightly over predicts direct measurements of pCO_2.